Comparing the Persistence of Inorganic Gunshot Residue (IGSR) on 3D-Printed Polymer and Metallic Surfaces

Charles Dennis James Wright



Submitted in fulfilment of the degree of

Master of Science by Research

School of Natural Sciences

August 2026

19538 words

i. Table of Contents

i. Table of Contents i
ii. List of Figures iii
iii. List of Tables vii
iv. List of Equations viii
1- Introduction 1
1.1 Gunshot residue within forensic science 1
1.2 Ammunition 2
1.3 The Propellant and GSR 3
1.4 The Primer and GSR 4
1.5 Why analyse IGSR over OGSR? 9
1.6 Current GSR Analysis Techniques 9
1.7 Ammunition Differentiation 12
1.8 Other Forms of Evidence on Textured Surfaces and Firearms 13
1.8.1 Finger marks 13
1.8.2 DNA 14
1.9 The Evolution Firearm Construction 15
1.9.1 The adoption of polymers 15
1.9.2 The incorporation of 3D-priniting 16
1.9.3 FDM surface texture and its effect on evidence 17
1.10 Aims and Objectives 20
2- Methodology 21
2.1 Method 21
2.1.1 Materials: Metallic firearm surface 21
2.1.2 Methodology: Metallic firearm surface 22
2.1.3 Materials: FDM polymer surface 24
2.1.4 Methodology: FDM polymer surface 25
2.2 Analysis 26
2.2.1 Scanning Electron Microscopy (SEM) - Theory 26
2.2.2 Energy Dispersive X-rays (EDX) - Theory 28
2.2.3 Settings and Practice 29
2.3 Statistics 31
2.3.1 General particle persistence 31
2.3.2 Particle size persistence 33
2.3.3 Particle composition persistence 33
3- Results 34
3.1 Total Population Loss 34

3.2 Population Loss in Relation to Particle Size 39
3.3 Population Loss in Relation to Particle Composition..... 44
4- Discussion..... 48
4.1 Sampling..... 48
4.2 Analysis 52
4.3 Results..... 54
5- Conclusions of this Study..... 55
6- Future works 57
7- References..... 58
Appendix 1: Data- Particle Size: Baseline i
Appendix 2: Data- Particle Size: Experimental ii
Appendix 3: Data- Particle Chemistry: Baseline iv
Appendix 4: Data- Particle Chemistry: Experimental iv

ii. List of Figures

1.1-Annotated picture of cutaways of ammunition. Including Berdan primer (Left & Right) and Boxer style primer (Centre) (Pearlman, 2015)……..…2

1.2-Berdan and Boxer primer and casing diagrams (Ammo.com, 2024)…….3

1.3-SEM images of (a) multiple particles adhered to a larger particle, (b) fragments of solid particles, and (c) a particle after fragmenting revealing a hollow. Modified from Brożek-Mucha (2011)…..…7

1.4- SEM images of large GSR particles found after longer intervals between shooting and sampling. Modified from Brożek-Mucha (2011)……..8

1.5-SEM images of irregular spheroid, bridged spheres, and regular spheres (left to right) IGSR particles, corresponding with a decreasing Sb-Ba composition ratio (Kara, et al., 2015)……...…8

1.6-SEM images of (a) hollow, (b) irregular, (c) spongey, and (d) half spheroid particles (Kara, et al., 2016)……9

1.7-Diagram showing the differing penetration of high and low accelerating voltage electrons into samples of high and low atomic weight (JEOL USA, Inc. , 2020)……11

1.8-“Schematic illustration of feed marks on a surface being turned (exaggerated)” (Kalpakjian, et al., 2021, p. 591)……18

1.9- Figure 1.9- Morphology of Machined surface taken with an Atomic Force Microscope (AFM) (Jasni & Lajis, 2013) ……..……..…18

1.10- Cross-section of FDM printed sample pictured by SEM (Glaskova-Kuzmina, et al., 2023)….19

2.1- 9 mm Ø x 19 mm Sydor barrel, length of 199 mm and a twist rate of 1:10” (model number: 911-2002)……..…21

2.2- Engineering drawing information for the housing including material, finish, and surface finish….22

2.3- (a) barrel retaining nut in situ on the universal receiver……22

2.4- Sampling pattern of the barrel retaining nut……..……23

2.5- 3D printed ‘basket’ (a) filled with lead and (b) with top/sleeve installed……24

2.6- First layer toolpath as shown on Cura……..24

2.7- 3D printed exhibit (a) drawing and (b) in situ on the receiver……..25

2.8- Sampling pattern used on the 3D printed exhibits depicting sampling of (1-5) the inner ring and (6-12) the outer ring……..26

2.9- Representation of the depth at which different signals are emitted within a sample (Zhou, et al., 2007)……..…….28

2.10- 6 pin stub holder and positions of the (a) calibration standard, (b & c) stubs for analysis, and (d) the reference stub……..…30

3.1- Metallic baseline study- Bar chart of particle population of side B as a proportion of side A (all particles) of a negative control and exhibits 1-3. Error bars calculated using 1st order standard deviation of results……..……..35

3.2- Metallic baseline- Bar chart of the particle population of side B as a proportion of side A (GSR only) of exhibits 1-3. Error bars calculated using 1st order standard deviation of results…….. …36

3.3-Metallic experimental- Bar chart of the particle population of side B (wiped) as a proportion side A (unwiped) (GSR only) with observed baseline and standard deviation. Error bars calculated using 1st order standard deviation of results……...…..37

3.4-Polymer baseline- Bar chart of the particle population of side B as a proportion of side A (all particles) of exhibits 1-6. Error bars calculated using 1st order standard deviation of results……37

3.5-Polymer baseline- Bar chart of the particle population of side B as a proportion of side A (just GSR) of exhibits 1-6. Error bars calculated using 1st order standard deviation of results……..38

3.6-Polymer experimental- Bar chart of the particle populations of side B (wiped) as a proportion of side A sides (unwiped) (GSR only) with observed baseline and standard deviation. Error bars calculated using 1st order standard deviation of results……..38

3.7-Metallic experimental v. Polymer experimental- Box and whisker chart of the % loss of GSR particles……..39

3.8-Polymer experimental- Bar charts showing average distribution of particle sizes of a) sides ‘A’, b) sides ‘B’, and c) the total of the exhibits. Error bars calculated using 1st order standard deviation of results..……40

3.9-Polymer baseline- Bar charts showing average distribution of particle sizes of a) sides ‘A’, b) sides ‘B’, and c) the total of the exhibits. Error bars calculated using 1st order standard deviation of results……...40

3.10- Polymer baseline- Bar chart showing distribution of particle sizes of exhibits1-6 (A & B) and their average……..41

3.11- Polymer baseline- Bar chart showing the average distribution of particle sizes between sides ‘A’ and sides ‘B’ of exhibits 1-6. Error bars calculated using 1st order standard deviation of results……42

3.12- Polymer experimental- Bar chart showing the average distribution of particle sizes between sides ‘A’ (unwiped) and sides ‘B’ (wiped) of exhibits 1-8. Error bars calculated using 1st order standard deviation of results..……..42

3.13- Metallic baseline- Bar chart showing the average distribution of particle sizes between sides ‘A’ and sides ‘B’ of exhibits 1-3. Error bars calculated using 1st order standard deviation of results……..43

3.14- Metallic experimental- Bar chart showing the average distribution of particle sizes between sizes ‘A’ and sides ‘B’ of exhibits 1-5. Error bars calculated using 1st order standard deviation of results……44

3.15- Polymer baseline- Bar charts showing the average distribution of particle composition of a) sides ‘A’, b) sides ‘B’, and c) the total of the exhibits. Error bars calculated using 1st order standard deviation of results……..45

3.16- Polymer baseline- Bar chart showing distribution of particle composition of exhibits 1-6 (A & B) and the average of all exhibits……..45

3.17- Polymer baseline- Bar chart showing the average distribution of particle composition between sides ‘A’ and sides ‘B’ of exhibits 1-6. Error bars calculated using 1st order standard deviation of results……46

3.18- Polymer experimental- Bar chart showing the average distribution of particle composition between sides ‘A’ and sides ‘B’ of exhibits 1-8. Error bars calculated using 1st order standard deviation of results……...46

3.19- Metallic baseline- Bar chart showing the average distribution of particle composition between sides ‘A’ and sides ‘B’ of exhibits 1-5. Error bars calculated using 1st order standard deviation of results……47

3.20- Metallic experimental- Bar chart showing the average distribution of particle composition between sides ‘A’ and sides ‘B’ of exhibits 1-3. Error bars calculated using 1st order standard deviation of results ……..……..48

4.1-a) The distribution of particles on exhibit before changes to slicing (2034 particles) and b) after (2433 particles)……..49

4.2- a) The tool path before slicing changes (authors own), b) rectilinear tool path (Saniman, et al., 2020), and c) concentric tool path (Saniman, et al., 2020)……49

4.3- Light microscope image of sampling surface of FDM polymer surface (x135) showing the grooves caused by the toolpath step-over and nozzle aperture……51

iii. List of Tables

1.1- Contents of characteristic and consistent IGSR particles from SINOXID primers (Organisation of Scientific Area Committees (OSAC) for Forensic Science, 2020)……..……...6

1.2-Table showing the lower limit of detection (LOD) for NAA, GF-AAS, ICP-OES, and ICP-MS……11

1.3- Number of repeats for the ‘Baseline’ and ‘Experimental’ experiments for both metallic and polymer exhibits……..26

2.1- Print settings for tough PLA ……...24

2.2- Number of repeats for the ‘Baseline’ and ‘Experimental’ experiments for both metallic and polymer exhibits……..26

2.3- Depth of penetration of incident electron beam, calculated using the Kayana- Okayama equation (equation 2.1) ……...29

3.1- Table of the composition of characteristic and consistent GSR particles……35

iv. List of Equations

2.1- Kanaya-Okayama Equation (Kanaya & Okayama, 1972)…….…….29

2.2-One-sample t-test equations…….……...31

2.3- Permutation test equation (Good, 2004)…….……..32

2.4-F-test equation…….……..32

2.5-Chi-square goodness of fit (Rahman, et al., 2025)…….……..33

2.6-- Cramér's V equation (Press, et al., 1993)……..……33

1- Introduction

1.1 Gunshot residue within forensic science

Forensic science is the application of scientific methods to aid in a criminal investigation, helping to reconstruct crime scenes and discern what the crime was and how it was committed. This can be via the use of chemistry, biology, and physics to help extract investigative value from evidence through research into the interactions between said evidence and their environments (Morgan, 2019). Forensic science is not limited to work performed on criminal exhibits and can include work done to further knowledge into evidence retrieval and analysis. Research into materials, for example, can inform the forensic scientist about what mediums lend themselves to finger marks development, extraction of DNA samples, or particulate retention.

Utilising techniques grounded in forensic science, associative evidence can be used to link locations, objects, or persons to each other (De Forest, 2001). These evidence types can be obtained from just about anything (Houck, 2018) which can include unassuming sources such as household dust (Petraco, 2020). Evidence like dust or particulates fall under the category of trace evidence and can provide physical or chemical fingerprints as it can be very easy to transfer from the environment to the criminal, for example. The usage of trace evidence stems from Locard's principle of exchange which states any contact, between persons or items, leaves a trace on one another (Saferstein, 2015). Once on an exhibit, permanence and ability to develop different trace evidence differs based on interactions between the evidence and mediums' physical and chemical characteristics (Moule, 2017; Amaral, 2022). Due to its latent nature, another advantage of trace evidence is that it can be difficult for the criminal to ensure adequate disposal of. The very complexity that provides trace evidence with its unique signature and therefore it's value as evidence, also brings an equal level of complexity to its analysis (Stoney, 2015). This high level of complexity is reflected in its cost to analyse. Therefore, investigators must also weigh up whether the value of the evidence justifies the cost of analysis (Roux, 2015).

An important trace evidence type is that of gunshot residue (GSR) or cartridge discharge residue (CDR). This evidence type has been leant on by forensic scientists to reach several conclusions about a scene or case including, but not limited to, bullet trajectory, number of shots, distance to target, and even the time of firing (Minzière, 2022, Organisation of Scientific Area Committees (OSAC) for Forensic Science, 2022). Despite the possible value, GSR is very easy to overlook as a source of evidence on exhibits. For one, GSR's latent nature makes it difficult to see with the human eye and may be passed up for more patent forms of evidence such as finger marks or bodily fluids such as blood spatter. Even one method for visualising GSR, utilising the luminescence of unburnt propellant under UV light, also elicits a similar luminescent response to other evidence types such as fibres, hairs, and some biological material (Houck, 2018). When using infrared (IR) photography to improve contrast, where GSR appears dark and textiles light (Houck, 2016), blood stains will also interfere with this visualisation (Sterzik, 2016). This demonstrates that, even when searching specifically for GSR, it can be overlooked as being other evidence types. The subsequent extraction of these alternative evidence types can contaminate or

remove possible GSR samples on the source object. Finger mark development, for example, can introduce both metallic and organic particles (Houck, 2016) or can brush away the existing metallic particles. The latter is especially a problem when considering the poor persistence of inorganic GSR (IGSR) (Kara, 2017).

1.2 Ammunition

Ammunition typically consists of four constituent parts: a casing which itself houses, a primer, propellant, and a projectile as shown in figure 1.1.



Figure 1.1- Annotated picture of cutaways of centrefire ammunition. Including Berdan primer (left & right) and Boxer style primer (centre). (Pearlman, 2015)

The primary explosive, with regard to centrefire ammunition, is usually a small cup that contains extremely sensitive explosive compounds. Under normal operation, the primer is first struck by a firing pin. Due to the content's sensitive and volatile nature, this causes a detonation of the material characterised by a flame front travelling through the medium at supersonic speeds (Grossel, 2002; Marshall, 2009). This detonation produces a jet of hot gas and material to flow through the flash holes in the primer to the propellant. Casings with multiple flash holes take Berdan style primers whereas those that take Boxer primers tend to have just one flash hole with the main difference between primer types is the anvil construction. As shown in figure 1.2, the anvil is a part of the primer or casing which aids in concentrating pressure on the mixture from the firing pin striking the back side. In Berdan style primers, the anvil is part of the casing which makes Berdan primers cheaper but much more difficult to

replace in the case of reloading ammunition. Whereas Boxer primers include the anvil in their construction making them more expensive to produce, but also easier to punch out and replace due to the larger, single, straight-through port within the casing. The distinction is necessary as the shape and size of these flash holes will determine flow characteristics of the jet(s) and therefore the pressure and absolute temperature achieved by the material which, in turn, may alter the production of GSR (Dalby, 2010).

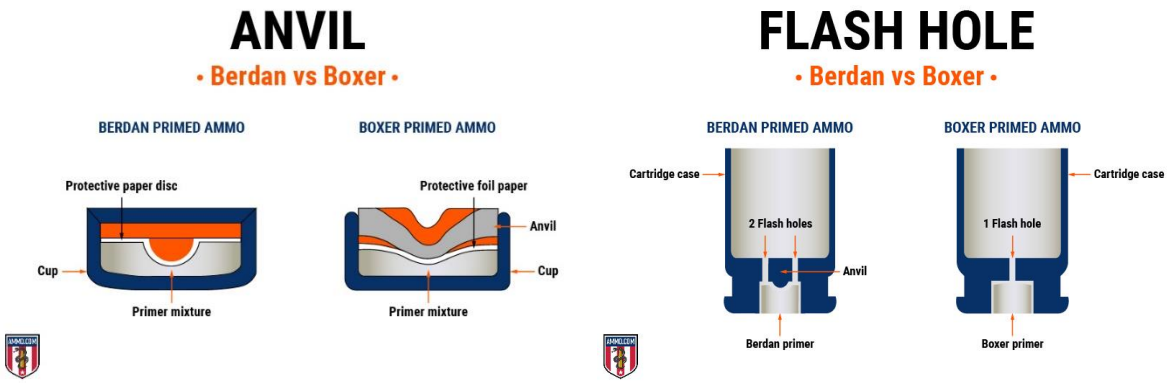


Figure 1.2- Berdan and Boxer primer and casing diagrams (Ammo.com, 2024)

The primer compound itself is not only far too sensitive for practical use as the main propellant (Akhavan, 2004) but it also but does not contain a lot of energy (Tariq, 2022). Therefore, a small amount of these compounds are used to activate the larger, more stable, main charge known as the propellant. The propellant is a secondary explosive which, due to its stability, requires more energy to initiate combustion than the percussive shock that detonates the primer. After the primer is detonated, the jet it produces provides adequate energy to initiate the deflagration of the propellant. This process differs from detonation as it is characterised by the combustion of the substance where the flame front moves through the propellant at sub-sonic speeds (Grossel, 2002; M. Marshall, 2009). The propellant is contained within the main body of the casing and provides the gas production (Yolhamid, 2018) that creates high pressure and thus, unseats and accelerates the projectile.

1.3 The Propellant and GSR

Gunshot residue can be separated into two subsets; organic GSR (OGSR) and inorganic GSR (IGSR). Although OGSR can be produced by primers from compounds used as binding agents such as gum Arabic (Oyler, et al., 2015), it is mainly produced by the propellant mixtures (Goudsmits, et al., 2015). These propellant mixtures consist primarily of nitrocellulose for single base propellants (Defanti, et al., 2020) or a mixture of nitrocellulose and nitro-glycerine for double base propellants (Crawford, et al., 1950; Urbanski, 1964; Vogelsanger, et al., 2011). These propellants decompose releasing NO_x molecules causing further decomposition in a positive feedback loop (Defanti, et al., 2020). The addition

of stabilisers is necessary to bond with the NO_x molecules and reduce the degradation of the propellant (Bohn, 2018). The stabilisers employed can come from one of two groups: the aromatic, amine-based group, or the urea-based group. The aromatic amine-based group includes chemicals such as diphenylamine (Apatoff & Norwitz, 1973; Rusly, et al., 2024), whereas the urea-based group includes akardite-II (Rusly, et al., 2024). Calcium carbonate can also be added to prevent ageing related degradation of propellants (Wallace, 2018), all of which would contribute to OGSR signatures. It is not, however, just the contents of the propellant or primers that can provide OGSR. Even any oils or lubricants used to clean and maintain a firearm would contribute to these findings (Feeney, et al., 2020). Fairly exhaustive lists for typical compounds seen in OGSR do exist; however, a great variation is seen between experiments (Goudsmits, et al., 2015) which could be due to the brand or batch of the ammunition. With the introduction and production of less toxic ammunition, constant changes to both the primer and propellant formulation (Dalby, et al., 2010) in favour of more organic compounds have been seen and are anticipated as development continues. Organic GSR does have the advantage of a low possibility of transference along with reported persistence of up to 24 hours after deposition (Moran & Bell, 2014), however, some have reported as low as 4 hours (Arndt, et al., 2012). For organic GSR, persistence on the body is dependent on the skin's absorption of certain compounds as well as the volatility of the compound (Moran & Bell, 2014; Minzière, et al., 2023). This possibly indicates that temperature fluctuations could have a great effect on the collected evidential sample if not taken in a timely manner. Other advantages, however, consist of the low environmental background levels of these compounds allowing for more sensitive analysis without background 'noise' affecting readings. As well as this, the high number of different compounds detectable would give higher fidelity of the chemical 'fingerprint' for comparison (Black, et al., 2017).

1.4 The Primer and GSR

Primers themselves consist of five components and have a firing progression akin to the round as a whole. These compounds consist of sensitisers, primary explosives, fuels, oxidisers, and binders (Oyler, et al., 2015).

Sensitisers- These work to amplify the energy given to the system by the firing pin to trigger the detonation of the higher energy compounds. In the case of extremely sensitive explosives, for sensitisers such as tetracene, the energy comes from an exothermic reaction. Whereas, using crystalline substances such as ground glass will increase the internal friction (Oyler, et al., 2015) and therefore the heat produced when deformed.

Primary explosives- In the widely used SINOXID primers (Brede, et al., 1996), the primary explosive in primers is lead azide or lead styphnate. Eastern bloc countries still manufacture primers using Mercury fulminate/potassium chlorate, a predecessor to SINOXID primers, allowing limited differentiation between the origins of the ammunition (Zeichner, et al., 1992; Wallace, 2018). The

primary explosive works as another amplifier, taking the energy from the sensitiser, using it to break its own bonds, thus releasing enough energy to initiate the combustion of the fuel.

Fuels- These are compounds that contain stored chemical energy which react with oxygen during combustion to release more energy in the form of heat (Daéid, 2004). In the case of primers, these flammable compounds tend to be aluminium powder (ThermoFisher Scientific, 2023) or antimony sulphide (CHEMOS, 2023) and combust utilising the oxygen stored in oxidisers.

Oxidisers- These are the compounds that provide the fuel with immediate access to oxygen within the substrate. These allow and promote combustion within a solid state and in primers are typically, barium nitrate (Hueske, 2009).

Binders- These are compounds, typically of organic nature, that aid in holding the aforementioned compounds together and stabilising the primary explosive and fuel. Not only for production, containment, and transport purposes, but also to ensure an even and complete detonation (Frihart & Beecher, 2022). This is primarily gum Arabic, but alternatives are utilised instead and sometimes as well as.

When primers are detonated, the organic binding agents produce a portion of the OGSR found in gunshot residue. While the majority of this GSR is composed of metallic compounds or metals from within the primer contents (Minzière, et al., 2023), it is also possible that these particles contain organic compounds. As OGSR analysis is not currently compatible with residue imaging techniques and is not detectable with IGSR analysis, the different analysis methods mean it is difficult to comment on their relationship. The ability to extract and detect OGSR compounds without altering IGSR counts significantly (Minzière, et al., 2023) suggests these GSR types do not coexist within particles but rather that the OGSR may exist as a film. To be certain, extraction and then analysis of whether this alters the IGSR's morphology would need to be conducted. These metal particles can also originate from the casing, the firearm's barrel, or the projectile itself and include a wide variety of elements including, but not limited to, copper (Cu); iron (Fe); zinc (Zn); and lead (Pb) (Dalby, et al., 2010). Differentiation of origin may be possible due to the suggestion that particles of pure elemental composition would originate from the bullet, gun, or casing. Whereas particles originating from the primer would melt and form in close proximity to other elements, making it unlikely for these particles to be of homogenous composition (Nesbitt & Wolten, 1980).

Lead, barium, and antimony are the elements of concern in chemical analysis of IGSR as these come from the primary explosive, the oxidiser, and the fuel respectively (Brożek-Mucha, 2017). This is, however, only true of the most common form of primer (SINOXID) (Kara, et al., 2015; Brożek-Mucha, 2017; Goudsmits, et al., 2019) as other primer residues will produce IGSR with a different composition. Particles containing all three of these elements are considered to be 'characteristic' of GSR as particles with similar compositions are rarely found from any other source. Particles considered to be 'consistent' with IGSR are particles said to have compositions that are produced by cartridges and other sources (table 1.1).

Table 1.1- Contents of characteristic and consistent IGSR particles from SINOXID primers (Organisation of Scientific Area Committees (OSAC) for Forensic Science, 2020)

	Composition			
Classification	**Lead** (Pb)	**Barium** (Ba)	**Antimony** (Sb)	**Additional Elements**
Characteristic	☒	☒	☒	
Consistent	☒	☐	☐	Calcium, Silicon
	☐	☒	☐	Calcium, Silicon
	☐	☒	☒	
	☒	☐	☒	
	☐	☒	☐	Aluminium
	☒	☒	☐	

Worth noting, however, is that in circumstances where non-toxic or organic primers are utilised, antimony may still be observed as it is used to harden lead in the projectile to increase penetration (Lucas, 1923).

There are, however, instances in everyday activities which produce chemically similar particles to IGSR. Particles containing Pb, Ba, and Sb have been found from automobile-related sources, exposing anyone who works on these cars to high concentrations of these particles (Garofano, 1999; Torre, 2002). It is worth noting that some particles were observed containing all three elements consistent with GSR but, were also accompanied by elements thought not to. For instance, brake linings will be accompanied by copious amounts of iron (Fe) (Torre, et al., 2002) and particles from airbag deployment will come with elements such as copper (Cu), cobalt (Co), or zirconium (Zr) (Berk, 2009). Despite these sources of particles that are chemically characteristic to GSR, the probability of finding such particles are no higher on mechanics than on the general population (Stamouli, et al., 2021). Efforts to phase lead out of brake pads and shoes are in place (Tucker, et al., 2017), removing one such source of contamination, but will surely lag due to the higher rate of ownership of cars ten years or older in the UK (GOV.UK, 2020).

Another source from which chemically similar particles are produced is that of fireworks where particles considered consistent with GSR particles are produced in similar, explosive, conditions as firearms. However, these consistent particulates were accompanied by magnesium (Mg) and Sodium (Na) (Grima, et al., 2012). In the case of automobile-originating particles, the included large concentration of iron is argued to be enough to determine non-firearm origins for these particles (Cardinetti, et al., 2004). It is, however, widely accepted that quantities of iron will be observed in IGSR due to the prevalence of the use of steel in firearm manufacturing including the barrel (Nesbitt & Wolten, 1980). Unlike in the case of automobile particles, the presence of Mg and Na makes it possible to rule out particles originating from this source (Grima, et al., 2012).

While sources producing chemically similar particles to that of GSR are important to be aware of, it is also important to be aware of the possible contamination of actual GSR on the general public due to its ease of transference. Studies have shown varying values for the probability of the mean presence of a characteristic particle, a particle containing all three components for SINOXID GSR, has been reported to be as high as 2% in Northern Ireland when sampling the clothes (Hannigan, et al., 2015). However, some studies which sample the hands claim a rate of occurrence as low as is 0.3% (Lucas, et al., 2016). A study by A. Stamouli in 2021 for populations both inside and outside of europe saw a probability of 0.4%, close to the previously mentioned value corroborating its validity. However, this study further differentiated the general population by those with and those without a relationship to firearms. When accounting for this, the mean rate of presence of characteristic GSR particles drops to 0.15% for those without and rises to 15.8% for those with a relationship to firearms, an increase of over 100-fold with this same paper reporting a worst-case scenario rate of 7.2% (Stamouli, et al., 2021). From these figures, a picture is born that speaks to the unlikeliness of the lay person having one, let alone a population, of GSR particles residing on them. Also represented in the difference between the aforementioned studies is a clear indication of GSR's poor persistence on skin and increased retention on more porous mediums.

The chemical composition of IGSR is not the only characteristic of interest for analysis. It is also the morphology of the particles that contribute to GSR's perceived uniqueness (Kara, et al., 2015). The surface texture of the particles is said to originate because of the high pressure and temperature conditions in which they are formed (Dalby, et al., 2010). This includes the vaporised mixture of elements (Kara, et al., 2015) at 2,000 °C (Heard, 2008) to c.2,800 °C (Kara, 2022), pressures of c.10^4 kPa (Romolo, 2001), and the subsequent rapid cooling as the particles transfer their heat to surfaces or the atmosphere (Brożek-Mucha, 2014). As such, a variety of morphologies have been observed in gunshot residue including variations in the surface texture, size, shape, and apparent completeness. F. Romolo, in 2001, described spherical particles with textured surfaces. Either displaying a smooth appearance or likened to a peeled orange (Romolo & Margot, 2001). These findings align with a study on explosive residues that found contained explosions produced smaller, more spherical, and more homogenous particulates when confinement was higher (Vermeij, et al., 2009). This evolved in 2011 with Brożek-Mucha observing physically traditional particles of GSR, consisting of spheroids with occasionally textured surfaces. However, these were accompanied by fragments of or fragmented particles that appear to show hollow spaces as seen in figure 1.3.

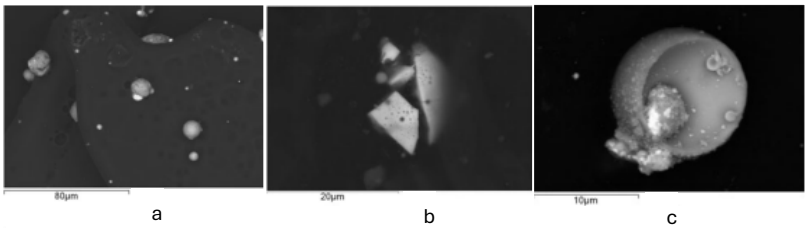


Figure 1.3- SEM images of (a) multiple particles adhered to a larger particle, (b) fragments of solid particles, and (c) a particle after fragmenting revealing a hollow. Modified from Brożek-Mucha (2011).

Within Brożek-Mucha's 2011 paper, as shown in figure 1.4, more irregularly shaped GSR particles were observed after longer periods between shooting and sampling (Brożek-Mucha, 2011). It is worth noting, however, that these particles were found at the upper size ranges the American Society for Testing and Materials (ATSM) defines typical of GSR particles. This is defined as between 0.5 µm and 5.0 µm, but the ATSM does concede that particles can reach 100+ µm in size and particles can be of an irregular shape (American Society for Testing and Materials, 2020).

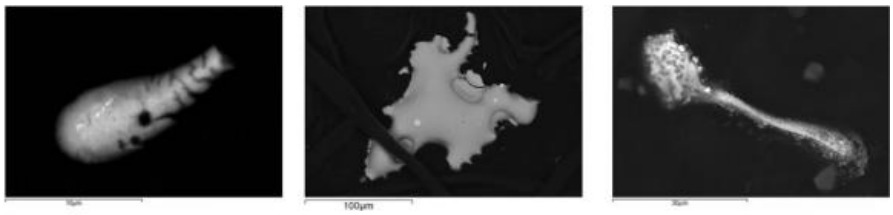


Figure 1.4- SEM images of large GSR particles found after longer intervals between shooting and sampling. Modified from Brożek-Mucha (2011).

In 2015, Kara categorised three particle shapes: the regular sphere, irregular sphere, and bridged spheres as seen in figure 1.5 which related to the ratios of the elemental composition (Kara, et al., 2015). They also describe the possibility of particles displaying partial expression or combinations of these shapes.

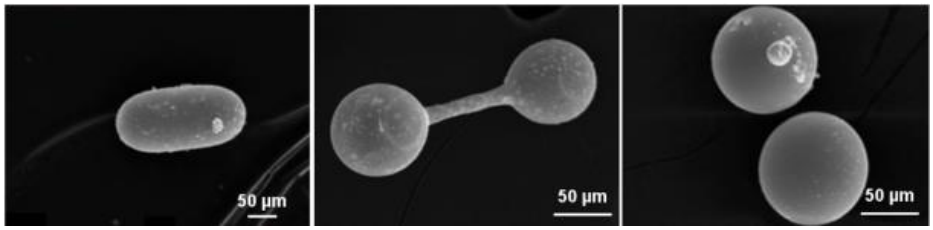


Figure 1.5- SEM images of irregular spheroid, bridged spheres, and regular spheres (left to right) IGSR particles, corresponding with a decreasing Sb-Ba composition ratio (Kara, et al., 2015).

Following this, in 2016, Kara describes the presence of more irregularly shaped particles other than that of the irregular spheroid described the previous year consisting of hollow, irregular, spongey, and half spheroid particles (Kara, et al., 2016). The observed hollow and much more irregularly shaped particles in figure 1.6 echoed those of figure 1.4 from Brożek-Mucha in 2011. Worth noting, however, is that these particles were well above the aforementioned 0.1 µm - 5 µm range. The spongey description, of particle (c) in figure 1.6, also added to the descriptors used for the surface texture for IGSR particles defined in 2001.

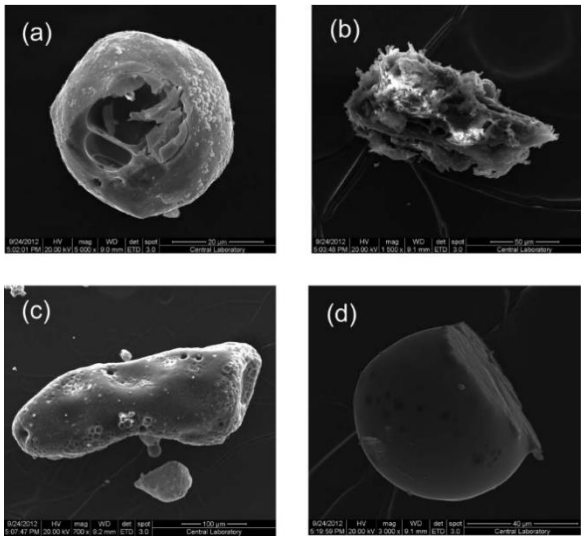


Figure 1.6- SEM images of (a) hollow, (b) irregular, (c) *spongey*, and (d) half spheroid particles (Kara, et al., 2016)

1.5 Why analyse IGSR over OGSR?

Although crystalline morphology is not indicative of IGSR (Organisation of Scientific Area Committees, 2020), particles that appear far more broken and sharp are reported in several studies. This disparity harms the narrative that morphology can be used as an indicator for IGSR as, despite the similar and violent conditions produced during discharge of various cartridges, a variety of morphologies have been observed. This variance could, perhaps, be explained by the number of factors that contribute to the formation of GSR particles which includes the rate of cooling (Basu, 1982) which, by definition, is affected by the difference in temperature of the detonating material and the ambient or barrel temperature. Therefore, physical properties of the particles are not basis enough to rule a particle as GSR and other evidence must be used to identify a particle as IGSR (Organisation of Scientific Area Committees, 2020). However, due to the presence of argued chemical and morphological characteristics, IGSR proves the stronger evidence type and is the industry standard for evidence for use in forensic investigations (Chang, et al., 2013).

The permanence of IGSR also betters that of OGSR despite the similar times of transference of as little as 4 hours (Arndt, et al., 2012). IGSR does have the advantage that, while in storage, the sample contents remain the same despite the high reactivity of the independent metals whereas the time between sampling and analysis of OGSR can have a marked effect on the results (Sauzier, et al., 2016).

1.6 Current GSR Analysis Techniques

Although the industry standard for analysis of IGSR is and has been scanning electron microscopy with energy dispersive x-rays (SEM-EDX) since circa 1977 (Schwoeble & Exline, 2000; Charles, et al.,

2020), several other methods exist that surpass SEM-EDX regarding chemical analysis accuracy and available sampling methods.

One such alternative analysis method is that of Neutron Activation Analysis (NAA) (Rudzitis & Wahlgren, 1975). This method allows for analysis of elements from $1.5x10^{-5}$ parts per billion (ppb) to 10 parts per million (ppm) (Pollard, et al., 2007), thus allowing for the sensitive analysis of Sb and Ba but has the drawback of having a poor detection limit for Pb. This is due to part of the analysis procedure involving the irradiation of the sample (Dalby, et al., 2010) using radioactive materials typically at large national/central facilities. This is, however, a known resistant property of lead, resulting in detection limits unsuitable for most applications (Greenberg, et al., 2011). With a large proportion of primers using lead azide or styphnate, instruments utilising this are less than desirable for the analysis of IGSR.

Atomic Absorption Spectroscopy (AAS), namely flameless AAS (Romolo & Margot, 2001), however, does not require the exhibit to be irradiated and is also able to detect the Pb within the sample. Graphite Furnace AAS (GF-AAS) even has a sampling advantage over SEM-EDX allowing for a longer time between shooting and sampling, leading to Policía de Investigaciones de Chile assigning an allowed 8-hour lag time over SEM's 6 hours (Aliste & Chávez, 2016). It is for these reasons AAS succeeded NAA as a method for GSR analysis.

For more sensitive analysis, the use of Inductively Coupled Plasma with Optical Emission Spectroscopy (ICP-OES) is a viable option with the exception Sb where it displays a higher limit of detection. This is due to analytical interference (Nash, et al., 2000), a shortfall not associated with the Mass Spectroscopy variant of this analysis (ICP-MS). reigns supreme when analysing trace elements (table 1.2). One advantage of ICP-OES analysis is the ability to create standards of certain concentrations which, when analysed to create the concentration gradient, can provide a higher fidelity around the expected concentration of the samples. A practical example of the use of ICP-OES's accuracy is that of being able to determine the number of shots fired in a scene (Vanini, et al., 2014). ICP-MS, however, has the edge when it comes to ultra trace analysis as it suffers from fewer interferences which are easier to eliminate (Tyler & Yvon, 2003). This method of analysis has been shown to provide data that can be used to determine firing distances (Santos, et al., 2015). However, interference issues caused by iron (Fe) (Tyler & Yvon, 2003) can be especially difficult to avoid during the analysis of GSR as it is often observed in GSR samples from the firearm itself (Dalby, et al., 2010). OES and MS analysis have equal but opposite issues that arise with concentration levels in the sample. ICP-MS does not cope well with high concentration samples and should be reserved for lower concentration samples whereas OES has a similar issue with low concentration samples. Hence, it is recommended that ICP-MS be reserved for trace/ultra trace analysis or used in combination with an ICP-OES for analysis of higher concentration samples (Tyler & Yvon, 2003). ICP-OES has proven value as, with appropriate setup, it can be easier to operate (Leikin & Phillips, 2023), have lower running costs (Leikin & Phillips, 2023), and have faster analysis times (Tyler & Yvon, 2003) all while achieving decently low LOD and high fidelity of the sample. The main value of these methods is that they allow for more accurate and sensitive (Table 1.2) analysis, but they also give a more complete chemical analysis of the sample.

Table 1.2- Table showing the lower limit of detection (LOD) for NAA, GF-AAS, ICP-OES, and ICP-MS

	Analysis Method				
Element	**NAA** (mg Kg^{-1})	**GF-AAS** (µg L^{-1})	**ICP-OES** (µg L^{-1})	**ICP-MS** (µg L^{-1})	
Pb	$4400_{(1)}$	$52.22_{(3)}$	$1.49_{(4)}$	$0.003_{(5)}$	
Ba	$10_{(2)}$	$11.94_{(3)}$	$0.15_{(4)}$	$0.001_{(5)}$	
Sb	$0.02_{(2)}$	$3.30_{(3)}$	$4.79_{(4)}$	Sb^{121}	Sb^{123}
				$0.001_{(5)}$	$0.001_{(5)}$
	1- (Dulloo, et al., 1998) 2- (Greenberg, et al., 2011)	3- (Yüksel, et al., 2016)	4- (Vanini, et al., 2015)	5- (Costa, et al., 2016)	

EDX can only analyse the sample as deeply as the electron beam can penetrate which is dependent on multiple variables (figure 1.7) whereas the dissolution of a sample, typically in nitric acid (Yüksel, et al., 2016), allows for the complete analysis of samples. This is useful in situations such as detecting GSR within blood stains (Li, et al., 2024) or other exhibits that may cover or contain GSR as EDX analysis is reliant on line of sight to the analysed particle and low penetration depth of the beam. This also means fibres and other particles may cover and prevent analysis of GSR particles (Romolo, et al., 2001). Of course, during the digestion of theses samples, the particles will lose any morphological features. Therefore, this removes the ability to analyse what particles are made up of which combination of elements as they become a homogenous solution.

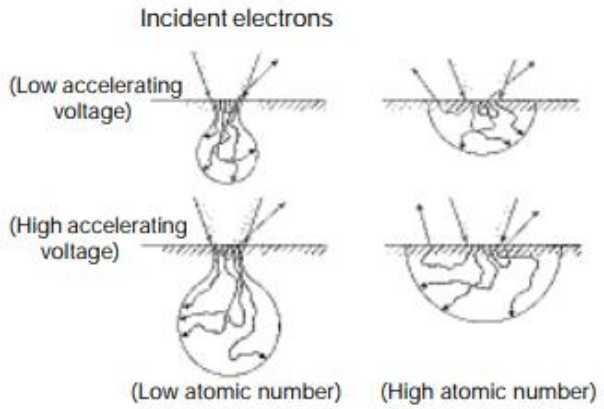


fig 1.7- Diagram showing the differing penetration of high and low accelerating voltage electrons into samples of high and low atomic weight (JEOL USA, Inc. , 2020)

IGSR's chemical composition, as discussed in section 1.5, can be replicated to some extent from non-firearm environmental sources and therefore more differentiation is needed to rule a particle's origin as coming from firearms. Although methods can be employed to use SEM-EDX as a quantitative means

of analysis (Newbury & Ritchie, 2013), it is generally only used in a qualitative manor with regards to the chemical composition (Nasrazadani & Hassani, 2016). Despite this, it is the combination of the ability to analyse both the distinctive features (section 1.4) and this limited chemical composition which proves this method of analysis an invaluable tool (Shrivastava, et al., 2021). In a forensic context, verification is one of the highest priorities when selecting analysis methods. Conducting two forms of analysis simultaneously and knowing it is from the same particle is incredibly important. Even further, is the ability of SEM-EDX samples to be analysed by another machine or lab as, unlike the aforementioned methods of chemical analysis, this process is considered a non-destructive technique (Acquafredda, et al., 1999; Romolo, et al., 2001; Olivella, et al., 2002) allowing for samples (such as GSR) to be retested and verified by other laboratories. SEM-EDX analysis does have some disadvantages which include the presence of a large number of fields as a result of the high magnification which adds to the high run times associated with this method of analysis. A further addition to the overall time is that of manual rejection and authentication before IGSR are to be reported (Ritchie, et al., 2020).

1.7 Ammunition Differentiation

Developing on from the idea that the chemical composition of IGSR gives it a certain level of uniqueness, there is an argument to be made that further differentiation can be made based on elemental constitution. Based on the assumption of manufacturers having slightly different formulations for the primer contents (Dalby, et al., 2010), it would be possible to identify the specific ammunition using observed ratios of lead, barium, and antimony in the GSR. Even the morphology of the GSR can be altered due to the differing composition of the primers (Serol, et al., 2023) which, ideally, would differentiate GSR not only between manufacturers but also individual batches.

Unfortunately, the differences in primer compositions between brands is simply not that significant (Zeichner & Eldar, 2004). Even if they were, inaccuracies of mass production would cause inevitable overlap between manufacturers and indeed batches (Blakey, et al., 2018). Even regarding the morphological properties of the particles, with the countless factors affecting the formation of GSR, means that predicting manufacturer or batch would require a vast wealth of data. As the rate of cooling of the particles influences the morphology (Basu, 1982), one would need to know the ambient temperature, the temperature of the firearm and of the ammunition. Just knowing the temperature inside the barrel would require knowing the temperature change caused by firing that specific ammunition, the heat absorption and dissipation coefficients of the barrel and firearm, the time in between shots, the movement of the air around the firearm, to name but a few variables.

The differing primer flash hole profiles would cause similar changes to combustion efficiency to jet profiles seen in pre-ignition chambers within internal combustion engines (ICE) (Zhu, et al., 2022). Therefore, changing the maximum pressure and temperature reached (Ritter, 2014), having an impact on the morphology of the particles (Basu, 1982). However, no studies could be found comparing any

performance differences between primer styles nor any effects on GSR profile. Although, forums have stated that performance effects are “nearly undetectable” (Ammo.com, 2024).

To aid in identification, however, some companies are producing ‘marked’ ammunition containing other uncommon elements which would have little to no effect on the performance on the primer. Currently, ‘marked’ ammunition is laced with gadolinium and/or gallium (Polovková, et al., 2015). However, for widespread adoption of these additions to be useful regarding identification, different ratios of these ingredients between manufacturers would need to be standardised to give an expected value within the GSR resulting from analysis. Here, however, the issue with mass producing errors arises once again and therefore brings its usefulness into question.

1.8 Other Forms of Evidence on Textured Surfaces and Firearms

Firearms present certain challenges to evidence retrieval which are themselves dependent on the evidence types likely to be obtained from a firearm related scene. One such genre of evidence is that of physical markers which result from standard operation of a firearm. This includes tool marks from the firing pin on the primer (or casing on rimfire ammunition) and on the projectile itself from the barrel. Casings from automatic loading or ejecting firearms may also have additional tool marks present from associated mechanisms. Trace evidence, on the other hand, may consist of DNA from cells in bodily fluids (Abraham, et al., 2012) or touch DNA (Tozzo, et al., 2022), latent finger marks, and GSR. These evidence types can be used to attest to contact between a person or environment and a weapon. An issue that comes with this plethora of evidence types is the collection of one type of evidence without contamination of another. For example, aluminium powders for developing finger marks will contaminate GSR samples and affect subsequent attempts at ammunition association. Not only this, but the cost of exhibit examination and evidence development also requires a careful consideration when deciding the forensic strategy and what evidence will provide the most value to the case (House of Commons- Science and Technology Comittee, 2005). It is for these reasons that other forms of evidence must be considered in the same context as GSR and the effectiveness of their collection be evaluated to inform the decisions of those overseeing this strategy.

1.8.1 Finger marks

Finger marks on firearms can be deposited from a variety of interactions with a firearm and on a variety of surface types. When loading a magazine, one can deposit finger marks on the ammunition (Bond, et al., 2009) that are then ejected and can be left at a scene of crime. This as well as the loading of the magazine into the firearm itself can leave finger marks on the magazine’s surfaces while general handling of the weapon will deposit prints on the external surfaces of the firearm. Despite these opportunities for finger mark deposition, the likelihood of such instances are very low (Hueske, 2008). This is replicated during one study that reported a success rate of the development of viable prints at just 3.4%-13.6% on firearms and 0.5% on casings or cartridges (Nunn, 2013). One of the saving graces

of finger marks is that, once developed, they can be strong evidence of the contact of one individual to the exhibit (Hueske, 2008).

Finger marks are resilient to external stimulus when compared to most other evidence types, being able to withstand relatively high temperatures, humidity, and other environmental conditions they may be exposed to (Barnett & Berger, 1976). In the case of firearms, however, finger marks can be exposed to temperatures of c. 90 °C (Gashi, et al., 2010) which has been reported to have detrimental effects on the fidelity of the developed marks (Bond, et al., 2009). This is mostly applicable to the casings whereas finger marks on the external surfaces of a firearm are unlikely to experience such extreme temperatures but will encounter more locomotive disturbance. In fact, for both internal and external surfaces of a firearm, the movement of the firearm and resulting abrasive action applied to the finger mark poses the greatest threat to their permanence (Bond, et al., 2009). Even passive characteristics of firearms such as the presence of textured surfaces can also have detrimental effects on the deposition and development (Hueske, 2008, Girod, et al., 2012). This seems to correlate with the proportion of smooth surfaces found on handguns with pistols at 3.4% and revolvers at 4.7% whereas the development rate for long guns (rifles and shotguns) are significantly higher at 13.6% (Nunn, 2013). Although this may be seen to correlate with the total surface area instead, even the finger mark development rate of 10% on magazines (Nunn, 2013) indicates an association with the proportion of flat and untextured surfaces. Worth noting, however, is the lack of specificity in current literature regarding surfaces characteristics from which evidence was recovered. Whether it be from the slide or lower receiver, from a smooth or textured area, if the medium was metal or plastic, and what roughness or finish said surface has. These are all factors which affect evidence retrieval, a concept which will be developed later, and are vital to our understanding of evidence retrieval.

1.8.2 DNA

Although the public opinion of DNA is easily swayed (Neumann, et al., 2016), especially by media (Brewer & Ley, 2010), DNA is a well-known and well-respected source of evidence (Koehler, 2001) with its reliability bolstered by its use in exonerations (West & Meterko, 2015-16). On firearms, however, it's accuracy in identification is somewhat lacking. Touch DNA, a form of trace DNA as a result of direct contact of a subject with an exhibit, can deposit anywhere from 0-169 ng of DNA depending on time of contact, pressure applied, and surface type (Burrill, et al., 2019). For example, touch DNA could be found on stainless steel for as long as 7 days, compared to the 24 hours it remains viable on cloth, and is further degraded by UV-B exposure (Ramsey, 2022). One reason for the difficulty of developing usable DNA profiles (Nunn, 2013) may be due to the property of DNA to bind to metal surfaces, making extraction on larger, metallic items more difficult (Bonsu, et al., 2020). This could be due to the positive charge of some metal ions and the negative charge of certain areas of DNA's double helix. Smaller items such as casings, however, may provide more value when analysed due to their size allowing for use of the Bardole DNA collection method. A method which involves encasing and part or fully submerging the item in a buffer solution (M-Vac Systems, Inc., 2017). In the example of casings, this may make DNA more viable considering the 0.5% rate of viable print development on casings (Nunn,

2013). DNA's persistence characteristics on metals also depends on where in the double helix a binding occurs. In cases where the metal binds to the bases, destabilisation occurs, negatively impacting the value of the data gained from development whereas in cases where binding occurs at the excessively negative phosphate groups, DNA will have an increased stability (Anastassopoulou, 2003). When considering the proliferation of polymers and the medium's disposition to become negatively charged due to friction (Tao & Chen, 2025), the current knowledge regarding interactions between DNA and firearms (traditionally mostly metallic objects) is limited.

One study comparing TriggerPro touch DNA swabs to finger marks in the production of positive identifications (ID's) found no difference despite DNA providing a markedly higher production of profiles (Nunn, 2013). This could be due to contamination issues or even interpretation inaccuracies (Butler, 2015) but regardless, it could be argued that when a finger mark is successfully developed it is more likely to provide a positive ID. The value of DNA, however, may go beyond the identification of a perpetrator. Of course, a full DNA profile would provide significant value to a forensic strategy, but even the presence and amount of retrievable DNA may also provide information on the distance of the firearm to the target. For example, Schyma found some correlation between the presence of blood staining, DNA, and RNA and the distance of the firearm relative to the target. They did, however, advise against relying solely on this data for shot distance estimation (Schyma, et al., 2024). Another study, however, concluded there was no significant correlation between target distance and DNA or RNA presence, but the presence of biological material could be utilised (Grabmüller, et al., 2016).

1.9 The Evolution Firearm Construction

1.9.1 The adoption of polymers

While firearms throughout history have mostly been made from metals, with the occasional use of wood or plastics for ergonomic parts, the use of polymers in the construction of firearms has proliferated through the industry in recent years (United Nations General Assembly, 2014). Polymer frames are not an uncommon sight on firearms available straight from the factory, especially on pistols. Glock, for example, are well known for their polymer frames, boasting the materials recoil absorbing properties (Glock inc., 2025). Even where polymer frames are not supplied by the manufacturer, aftermarket suppliers make it possible to purchase polymer receivers even for larger firearms such as 5.56 mm chambered rifles (Brownells UK, 2025). The manufacturing processes used for polymers, such as injection moulding, allows for texture to be included on the part without much additional processing time and without needing post processing procedures or auxiliary parts. This has resulted in textured surfaces being continued across the external surfaces of the receiver, thus reducing the available space for deposition of identifiable finger marks.

Injection moulding is not the only method of manufacturing available to the firearm industry, however. Additive manufacturing (AM), also known as 3D-printing, has been a staple in economical prototyping by reducing the amount of scrap material produced, its ability to edit and share designs globally, and its consistent reproduction of complex geometries (Jenzen-Jones, 2015, Kalpakjian, et al., 2021). As 3D printing technologies, including equipment and materials, have become more advanced, efficient, and cheaper, the use of 3D printers to produce viable, final products is becoming more common (Wong, 2015). 3D printing has three popular forms: Selective Laser Sintering (SLS); Stereolithography (SLA); and Fused Deposition Material (FDM), all with their own benefits and drawbacks. Choosing a suitable process comes down, mostly, to the materials which the product is to be made from (Kafle, et al., 2021). The cheapest by far is that of FDM as a result of its range of printable materials, simplicity, speed, and customisation all while offering results of comparable accuracy to SLS for, at least, a fraction of the price.

Despite this, these advancements and options change very little for the commercial sector, as injection moulding is still favoured for high output rates and the economy of scale seen in large batches keeps the cost per part low. However, in line with Harvey Firestone's phrase of "Win on Sunday, sell on Monday", advancements in the technology made in the industrial market have trickled down into the domestic.

1.9.2 The incorporation of 3D-priniting

The combination of prices of entry level models being c. £200, a large selection of materials, a selection of Computer Aided Design (CAD) and slicing programmes, and a plethora of online courses/tutorials make the world of 3D-printing a beginner friendly environment. This accessibility is reflected in its reported adoption into homes irrespective of age, profession, or level of education (Mavri, 2023). This broad domestic access to CAD and Computer Aided Manufacture (CAM) programs, and online training gives the public the ability to create complex, relatively strong, and precise parts. This includes criminals, who would be attracted to this process due to its decentralisation ethos (Daly, et al., 2020) and lack of traceability. 3D-printing has also proven its viability for crimes other than just firearms related, as shown by its use in a 2014 fraud case where perpetrators used FDM 3D-printed card slot bezels to allow the skimming of bank cards (O'Neal, 2014). This issue has become apparent in the United States of America (US) where, the citizens see firearms so routinely, they are desensitised to their ownership (Sheptycki & Edwards, 2009; Cukier & Sheptycki, 2012). The comparably more liberal gun laws in the US relative to the UK reflect this, allowing the purchase of many of the mechanical components of a firearm without a license or background check. The only part that requires serial number markings and a licence is the lower receiver or frame (Bureau of Alcohol, Tobacco, Firearms and Explosives, 2023) which groups of individuals have taken to 3D-printing. These communities have not necessarily been nefarious in nature, focusing on the customisation of firearms, the quality of the prints, and exercising their interpretation of the constitution privately (Hays & Jenzen-Jones, 2018; Dent, et al., 2023). Companies such as Sig Sauer have recognised this market for customisation and are set to introduce Fire Control Units (FCUs). These would be the only serialised part of the firearm with custom combinations of "grip modules", barrels, guides, and slides available for separate purchase (Sig Sauer,

2025). However, it is unclear if this commercial availability of this customisation would retire the need for these communities or if they would simply adopt these FCUs and, instead, make the grip modules for themselves.

1.9.3 FDM surface texture and its effect on evidence

The FDM process itself produces parts with several nuances compared to using traditionally manufactured parts. The layer-by-layer process produces recessed ‘layer lines’ dependent on z-axis offsets and material temperature and extrusion rates at intervals specified by the slicing program used and the machines limitations. This is inherent to the process as a ‘slicer’ cuts the object into individual layers at user specified intervals on the z axis, and the programme then maps out a toolpath for the printer head to follow on that specific layer before moving up at the set interval and following the toolpath for that layer’s geometry. Industrial grade FDM 3D printers, such as the Fortus 900mc, have minimum layer heights of c. 0.127 mm (Tri-Tech 3D, 2025) whereas a domestic market targeted machine, the Ender3, has a minimum layer height of 0.1 mm (Creality, 2025) with some forums claiming the Ender3’s layer height is more accurately 0.12 mm due to limitations of the stepper motors used. Not only does the limitation of the hardware that produces a part impact the final surface finish of the part, but also the user specified settings appropriate to their goals. For instance, the prevailing sentiment within 3D printed US 2nd amendment communities such as r/fosscad on Reddit is to aim to attain a near flawless surface finish utilising smaller layer lines. Although this does have the desired effect of improving aesthetics, it also has the added effect of improving the stiffness of the part in exchange for a decrease in the overall tensile strength and a lowering in the flexural fracture point depending on print orientation (Chacón, et al., 2017). This has been supported by resonance testing which saw not only layer height to have a noticeable effect on the stiffness of the sample, but also the nozzle diameter (Beníček, et al., 2025). The subsequently affected surface characteristics of lower layer heights, such as surface roughness, can have marked effects on the deposition, persistence, and development of trace evidence that are be found on parts exhibits (Hughes, et al., 2021).

Milling, a prevalent process in the manufacture of firearms (Werner, et al., 2021), creates different surface morphology to FDM printing. This is not just referring to the depth and prevalence of deviations to the target dimensions, but the shape as well. For machined surfaces, cutting tools will have a described radius of the cutting edge, meaning the surface has sharp peaks and curved troughs as shown in figure. 1.8 and 1.9.

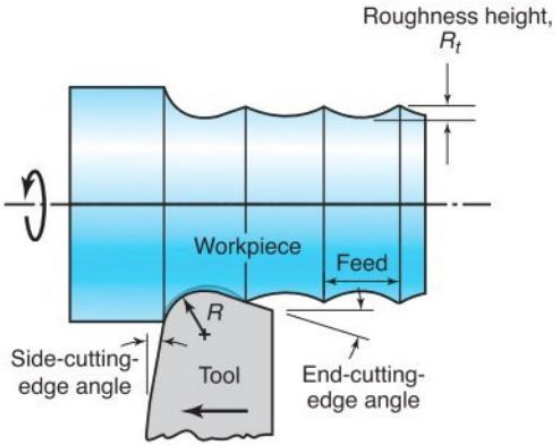


Figure 1.8- "Schematic illustration of feed marks on a surface being turned (exaggerated)" (Kalpakjian, 2021, p. 591)

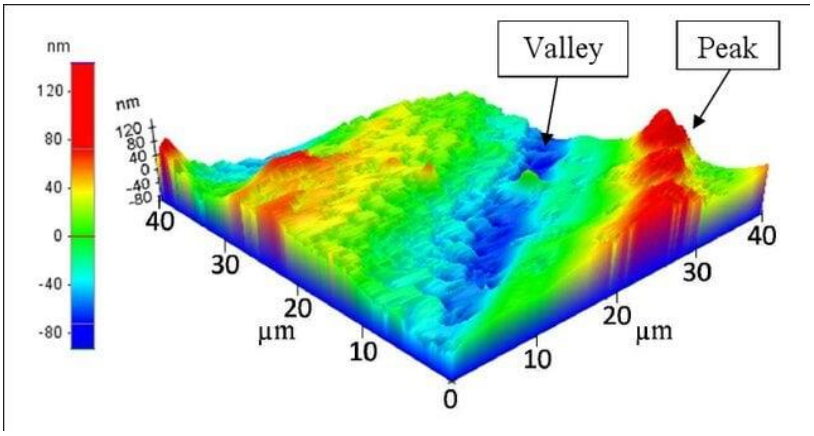


Figure 1.9- Morphology of Machined surface taken with an Atomic Force Microscope (AFM) (Jasni & Lajis, 2013)

Conversely, an FDM 3D print will contain rounded peaks and sharp troughs due to the material flowing and layers compressing each other (known as 'squishing', see figure 1.10). The extent to which this occurs will change depending on the extrusion settings in the slicer software and the printer, the material and temperature of the nozzle, and the layer heights chosen by the user and dictated by the hardware as previously mentioned.

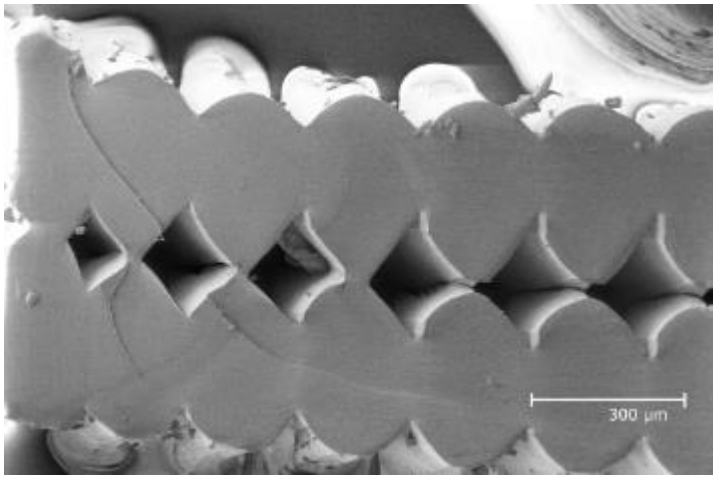


Figure 1.10- Cross-section of FDM printed sample pictured by SEM (Glaskova-Kuzmina, et al., 2023)

A further complication of this topography is the introduction of non-planar slicing which creates irregular layer lines. Although non-planar slicing as a concept has been around for many years (Batchelder, 1997) it has recently been developed to a standard where it might be not only be seen from specialist software and equipment (Yoon, et al., 2019), but also from domestic machines as a 'brick layer' option is available in modded versions of slicing software (O'Connell, 2021). However, the implementation of 'bricklayer' versions do not affect the outer wall of prints and true non-planar slicing sees undulations of each layer in the x and y directions but expected 'layer lines' are still observed in the z axis.

Although these features pose an issue for finger mark development, this textured polymer medium may provide the ideal surface for the deposition and retention of other evidence types such as DNA or GSR which have been documented as having poorer persistence. Regardless of surface texture, the material itself has marked effects on the retention and development processes. Preparation of ninhydrin for finger mark development on paper, for example, is affected by the type of paper the finger mark was deposited on (Margo, et al., 2015). In the case of DNA, polymer substrates have been shown to retain this evidence for longer periods when comparing organic versus inorganic fabrics (Chen, et al.,

2019). The development of DNA may also be easier as sampling does not have to contend with the previously mentioned affinity for metallic surfaces (Bonsu, et al., 2020). With these shifts in evidence substrate interactions of these evidence types, it stands to reason there is a need to study the interactions of GSR with 3D printed mediums. More research would ensure the decisions made by examiners and investigators are educated ones based on scientific findings.

This shift in firearm manufacturing towards polymer firearms, as well as the newfound capability of the general public to produce their own receivers or 'grip modules', requires the police and forensic services to be aware of how the medium affects what evidence can be extracted from the surface. This includes alterations to its perceived value to the forensic strategy. Also to be considered is what knowledge would be pertinent to a crime in the event of changes to current legislation. For instance, the 1982 amendment to the Firearms Act 1968 is already under threat as it states a gun shall be considered readily convertible if it can be converted without specialist tools or equipment (Gov.uk, 1982). The increased accessibility of these advanced tools clearly raises the level of alteration the general public

is capable of. Therefore, what was once considered not readily convertible will soon be easily so. This is to emphasise the prevalence of these materials and processes, the subsequent increased likelihood to see crimes involving these substrates, and the need for better understanding of the interactions between these non-traditional surfaces and trace evidence such as GSR.

1.10 Aims and Objectives

While persistence studies have been undertaken with regards to IGSR on skin, specifically hands, very little has been done in comparing one medium's retention of IGSR to another. A study in 2024 by D. Demircioğlu compared several surface types in the context of a secondary transfer experiment. The results were that, in descending order, paper, plastic, ceramic, metal, and then glass were observed to have notably different acceptance of IGSR particles from a shooters hand (Demircioğlu, et al., 2024). This did not, however, cover the retention of IGSR on those surfaces after a tertiary transfer or an initial transfer from to the surface in question. While X-ray imaging techniques can be employed, such as microtomography in cases where the usability of a weapon must be proven (Goia, et al., 2024), high levels of retention may allow IGSR to be used to link a firearm to a scene through its chemical fingerprint. Despite this and the fact 3D-printed weapons are not as far-fetched as they once seemed, there is currently no research into the effects 3D printed parts have on the trace evidence deposited on them and even the study of trace evidence produced by 3D prints and 3D printed weapons is in its infancy. This gap in current intelligence is vital to fill as well as the apparent short comings of existing research regarding generic polymer surfaces and textured surfaces effects on evidence retrieval from firearms. As such, this study aims to detail the effects that FDM 3D printed surfaces have on gunshot residue and the persistence of this evidence type on surfaces produced by FDM printers. The presence of the internet and the adoption of 3D printing in more households is ensuring the days of strategic ignorance about what is possible with domestic manufacturing is coming to an end. With the increased possibility of 3D printed materials at crime scenes and the decision of which evidence types to prioritise ultimately being down to the investigator, it is imperative to understand the interactions between trace evidence and this emerging medium. Care needs to be taken as the development or processing techniques for one type of evidence may risk the contamination of another or interfere with its viability. This study aims to determine if an FDM 3D print has a higher likelihood of retaining gunshot residue than on a metal surface akin to that of traditional firearm materials. If this is the case, it is possible that GSR could provide significant value to investigations involving 3D printed firearm components. This knowledge can then be compared to similar features of different materials in future studies or to develop methods that could be used in the field to inform the investigator of a typical number range of GSR particles that one might expect to find under such conditions.

To achieve this, this study will utilise FDM printed parts to provide a sampling surface which will first have the topography characterised. These exhibits will then be contaminated with GSR by attaching

each one to the muzzle of a gun and performing a live firing to achieve more realist results. The plume of gasses will deposit GSR as the Coandă effect (Reba, 1966) and pressure differential causes the gases to wrap back onto the exhibits. To do this, whilst ensuring both the method of deposition best replicates real world applications and providing controlled populations of particles, each exhibit will be exposed to the same number of shots in a controlled environment within a set time to allow for settling of airborne GSR. A standardised GSR collection procedure will be applied to half the contaminated exhibit for analysis of the of GSR population present using a scanning electron microscope and energy dispersive x-ray analysis to detect the particles of inorganic gunshot residue. These same experiments will also be conducted on a surface more similar to traditional firearms and the results compared to determine whether FDM printed parts have an inherently higher affinity to GSR.

2- Methodology

2.1 Method

2.1.1 Materials: Metallic firearm surface

To gather samples of the GSR population, 12.5 mm aluminium pin stubs from Agar Scientific (SEM Specimen Stubs- Short Pin 12.5 mm Ø, 3.2 mm Ø x 6 mm pin, AGG301F) were used with carbon adhesive tabs (Agar Scientific - AGG3347N 12 mm Ø) applied. These were then dubbed on the surface multiple times to gather particles from an area. To take samples from a surface similar to that found on firearms, samples were taken from a universal receiver. The universal receiver and stand utilised were from the brand “Sydor” (model number: HPD 11114 435-2001 & HDR/OSA HPD 11665) and using the Sydor barrel (see figure 2.1).

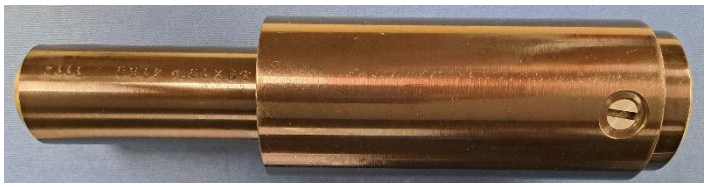


Figure 2.1- 9 mm Ø x19 mm Sydor barrel, length of 199 mm and a twist rate of 1:10” (model number: 911-2002)

The universal receiver was machined from EN8M steel to a surface roughness (Ra) of 1.6 µm (an N7 standard) before having a phosphate and oil treatment applied (figure 2.2). This process used includes acid cleaning of the surface before immersing the part in a phosphate bath (Burduhos-Nergis, 2023). The acid cleaning and the phosphate layer itself is likely to have affected the roughness to some extent. The resultant micro-voids allow the surface to retain oil and improve the part’s wear resistance (Sivakumaran, 2012). It is the barrel retaining nut of the universal receiver (see figure 2.3) which was used as the sampling surface.

MATERIAL	FINISH	DIM'S IN MM	SCALE 1–1	SABRE COMPUTERS INTL. LTD
EN8M ——	PHOSPHATE & OIL	TOLERANCES:– One decimal place (.0) ± 0.25 Two decimal places (.00) ± Three decimal places (.000) ± Unless otherwise stated		TITLE A1/B1 TEST GUN 0.5" HOUSING
EST.WT.		SURFACE ROUGHNESS 1.6		

Figure 2.2- Engineering drawing information for the housing including material, finish, and surface finish

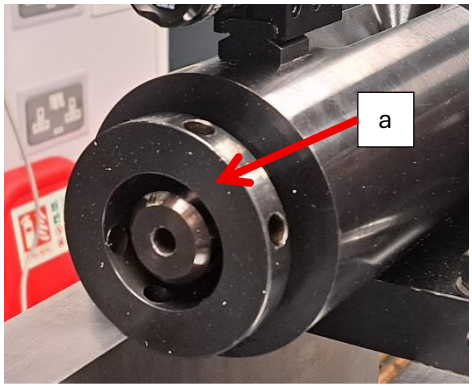


Figure 2.3- Barrel retaining nut (a) *in situ* on the universal receiver

2.1.2 Methodology: Metallic firearm surface

Negative control:

As the same surface was to be used for each set of shots, a cleaning protocol for the metallic surface was developed to ensure no cross contamination occurred. This consisted of donning a new pair of nitrile gloves and cleaning the sampling surface thoroughly with 70% industrial methylated spirit (IMS) and a new, clean cloth. The face of the nut was then sampled with a stub using a concentric pattern (pin stub with carbon adhesive disk applied) and the results analysed along with the baseline (see below) to determine the populations of IGSR that might remain on the surface after the cleaning protocol. Doing this just with the baseline allowed run times to be kept low which was important to maintain the accuracy of the SEM-EDX analysis.

Baseline:

After cleaning, a vertical line was drawn in situ with a marker pen to separate two sampling areas on the surface later referred to as side 'A' and side 'B'. A 'dot' drawn on the outer face of the nut denoted the right side to ensure orientation of the nut is known once it is unscrewed and removed for sampling. Three Magtech 9 x 19 mm (Luger/Parabellum), 115 gr, Jacketed Hollow Point (JHP) (model number: 9C) rounds were then fired from the universal receiver in a climate-controlled range with consistent windspeed. The shots were conducted horizontally with the direction being perpendicular to the sampling surfaces with a period of 1 minute between shots observed to allow airborne GSR to settle or be carried away from the gun by the airflow in the firing range. To get a baseline for the distribution of GSR particles between the sides, the nut was first removed and placed face up on a bench which was possible without contacting the front/sampling surface. Five dubs of a stub were performed without overlap on one half before a second stub was used to sample the remaining half as shown in figure 2.4.

This was repeated three times and gives context as to the expected distribution of particles between both halves/sides of the sampling surface.

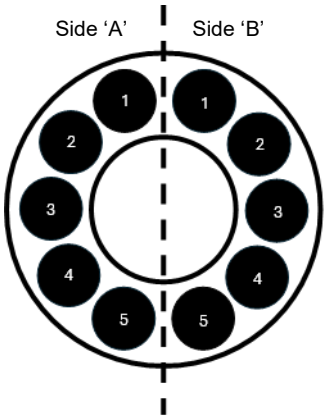


Figure 2.4- Sampling pattern of the barrel retaining nut

Experimental:

As with the baseline, the nut was cleaned, three shots fired, and the nut then removed for sampling. After removal, a set of nitrile gloves were donned to ensure no cross contamination occurred. The surface was then sampled, during which no overlapping areas between dubs was ensured. Side ‘A’, or the ‘control’ side, of the marked line was then dubbed with 5 placements of a stub and named as “non-wiped” samples. New gloves were put on before the right side was wiped once with a new, single layer piece of Tissum cotton towel using a lead filled basket (see figure 2.5) to ensure constant force is applied downward onto the surface. A standard weight in the basket and thus a standard force applied to the exhibit reduced the effects of additional variables and the weight helped the user to maintain a consistent motion both during the wipe and between wipes. Wiping was done after the ‘control’ dubbings to ensure no accidental wiping of the ‘control’ side occurred before sampling. A symmetrical sampling procedure was then conducted with a fresh stub on this other side to produce the “wiped” samples. This was repeated six times, the results of which are expected to display the material’s resistance to particle loss after active contact.

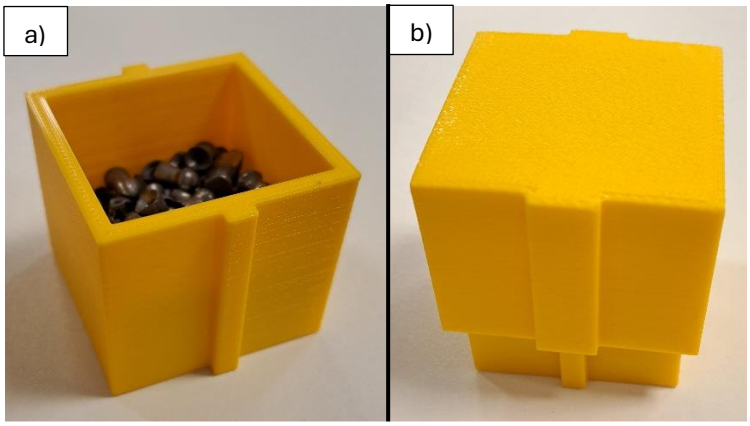


Figure 2.5- 3D printed ‘basket’ (a) filled with lead and (b) with top/sleeve

2.1.3 Materials: FDM polymer surface

A part was designed in Fusion360 to fit over the retaining nut of the universal receiver to provide a sampling surface. This was then transferred into Cura slicer to generate toolpaths in the form of G-code for the printer (an Ultimaker 2+) to follow. To attain a consistent surface as shown in figure 2.6 the “Initial layer pattern” setting was set to “concentric”. The G-code generated was tailored towards and uploaded to an Ultimaker 2+ equipped with a 0.4 mm nozzle. Once a print was completed it was placed in a new, clean petri dish and the dish labelled with the identifying experiment code (dd/mm - ‘n’). These exhibits were printed using a PLA based filament (Ultrafuse PLA pro, natural white, 7503B075) which, when not in use, was stored in dry conditions using silica beads to control the humidity in an airtight container. Key print settings are specified in table 2.1.

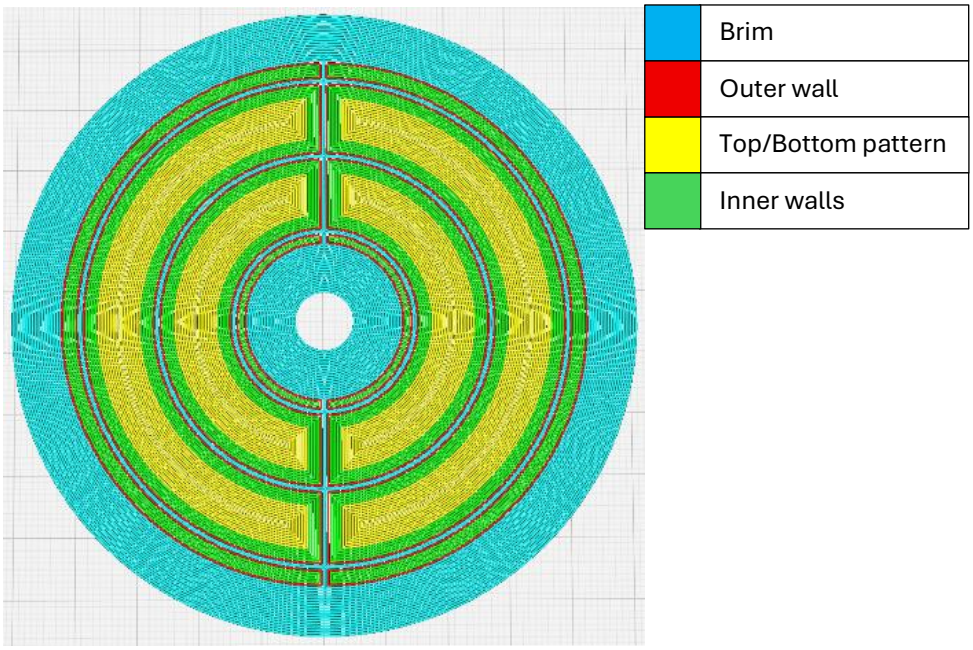


Figure 2.6- First layer tool path as shown on Cura (authors own)

(*Table 2.1*) Print settings for tough PLA

Print setting	Value
	Tough PLA (7503B075- Ultrafuse PLA pro, natural white, 2.85 mm Ø)
Initial layer height	0.1 mm
Layer height	0.15 mm
Bed temperature	60 °C
Temperature	215 °C
Initial fan speed	0 %
Regular fan speed (init. @ layer 4)	50 %
Nozzle diameter	0.4 mm
Line width	0.4 mm

2.1.4 Methodology: FDM polymer surface

Control:
Unlike the retaining nut, no cleaning of the exhibits was conducted before figure 2.6

hand due to the printer being far removed from the firing range. Still, several exhibits were tested before experimentation and no IGSR particles were identified by the SEM-EDX. No negative control stubs were utilised, again to reduce run times and thus improve accuracy of the results.

Baseline:
The exhibits were then taken into the firing range where, as needed, they were removed from the petri dish with a fresh nitrile glove, mounted onto the receiver with the central division vertical, and knocked into place with the clean, gloved hand (see figure 2.7). The right side was, again, marked with a dot to ensure awareness of orientation remained.

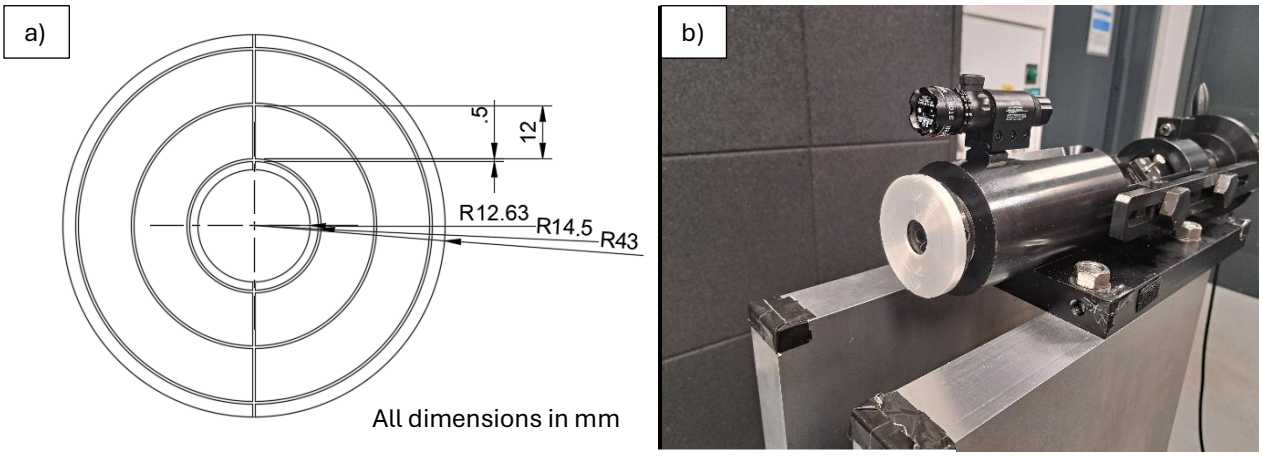


Figure 2.7- 3D printed exhibit (a) drawing and (b) in situ on the receiver

Three 9 x 19 mm rounds were then fired from the universal receiver with a minute in between each shot, as before. The exhibit was then removed from the universal receiver and placed in the petri dish which can be done without contact with the sampling surface due to the taper in the petri dishes. Once in the lab, each exhibit was removed from the petri dish, sampling side up, and placed on a clean and covered bench. Each side was sampled utilising five dubbings on the inner area and seven on the outer, without overlap (figure 2.8). The dead spaces on the very inner and outer portions of the exhibit were designed to allow for a margin of error when handling each exhibit and the positioning of tweezers to hold the exhibits in place during said sampling to be constrained to these areas. These tweezers were cleaned with 70% IMS in between each exhibit as a precaution. Only one exhibit was removed from its petri dish at a time to reduce risk of cross contamination and losing track of exhibits. This was repeated with six exhibits.

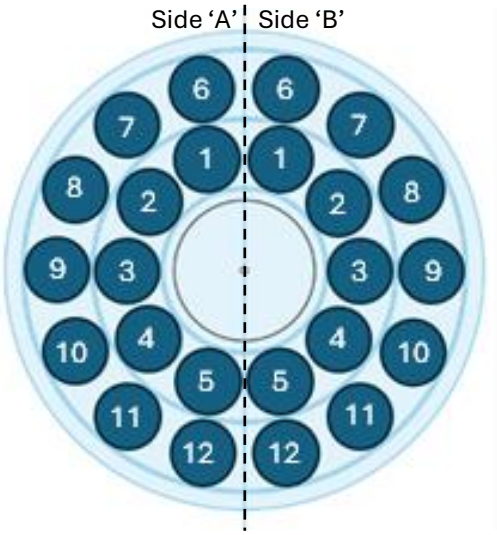


Figure 2.8- Sampling pattern used on the 3D printed exhibits depicting sampling of (1-5) the inner ring and (6-12) the outer ring

Experimental:

Again, one-by-one, the exhibits were removed from the petri dish and placed and secured to the retaining nut in the correct orientation. Orientation was then marked and three 9 x 19 mm rounds were fired with the same time observed between shots. Each exhibit was returned to the petri dish and taken to the lab where it was then removed from the petri dish, sampling side up, and placed on a clean and covered bench. Firstly, side 'A' of an exhibit was sampled utilising the same five and seven, inner-outer pattern as in the 'baseline' experiment. As in the metallic surface experiments, these samples are referred to as "non-wiped". The other side was then wiped once with the lead filled basket and a new, single layer piece of towel, akin to the 'metallic experimental' exhibits, before being sampled in the same manner as the previous side to produce the "wiped" samples. This was repeated with eight exhibits.

(*Table 2.2*) Number of repeats for the 'Baseline' and 'Experimental' experiments for both metallic and polymer exhibits

	Metallic	Polymer
Baseline	3	6
Experimental	6	8

2.2 Analysis

2.2.1 Scanning Electron Microscopy (SEM) - Theory

SEM is concerned with the morphological properties of the samples. This allows the observation of shape, size, and surface texture utilising electrons rather than photons as would be used in traditional light microscopes (Mohammed & Abdullah, 2018). In SEMs that utilise thermionic emission guns, such as the Hitachi S3400 used in this study, the source of electrons come from a tungsten filament heated

to temperatures in excess of 2,500 °C (Vernon-Parry, 2000). These electrons are accelerated by the gun between 0.1 and 30 keV by a potential difference created between the filament and an anode plate (Zhou, 2007), and are then focused into a beam by a series of apertures (Zhou, et al., 2007) and electromagnetic lenses (Khursheed, 2010). This beam is then deflected to scan across the surface of the sample in a raster pattern scan (Vernon-Parry, 2000) to achieve an image of the observed area. The resolution of the resulting image is a direct result of the diameter of the electron beam as it incidents the sample (Crewe, et al., 1969) or the 'spot size'.

One form of this imagery comes from the secondary electrons (SE) which are produced from the sample after the incidence of electrons from the beam resulting in inelastic collisions (Nanakoudis, 2019). They originate from the surface and, therefore, provide more accurate information of the topography (Goldstein, et al., 2003). A lower accelerating voltage (<5 keV) is advantageous when utilising this form of imagery as it reduces the penetration of the beam (Vernon-Parry, 2000) which favours the production of SEs (Joy & Newbury, 2002) and which limits noise from other types of signals generated from deeper within samples (Butler, 1995). Lower accelerating voltages are also less likely to affect the samples stability due to a decreased intensity of radiation, that is unless you localise the scanned area too severely (Joy & Newbury, 2002). This method of imaging can also be utilised on electrically insulating materials despite their reluctance to release energy through diffusion through the sample and out via the stage or through the emission electrons. This would normally result in charging but, due to the low energy of the beam, this is not so much of an issue. (Liu, 2000).

Back scattered electron (BSE) imagery, on the other hand, benefits from increased keV as the proportion of signals generated that come from unwanted sources (SEs) decreases. This is due to the deeper origins of these signals within the sample. Therefore, a greater depth of penetration by the electron beam is advantageous (see figure 2.9). This form of imagery is higher energy, in part due to the higher keV values required for adequate penetration, but also due to the process of emittance being elastic (Ohring, 2015). Although topography detail in this form of imagery is weak, BSE benefits from the fact the strength of the signal is, in part, dependent on atomic mass of the element from which it emanates. This gives it the unique advantage of being able to instantly, albeit approximately, differentiate between particles of divergent compositions just from the image (Kim, et al., 2010; Thermo Fisher Scientific Inc., 2025).

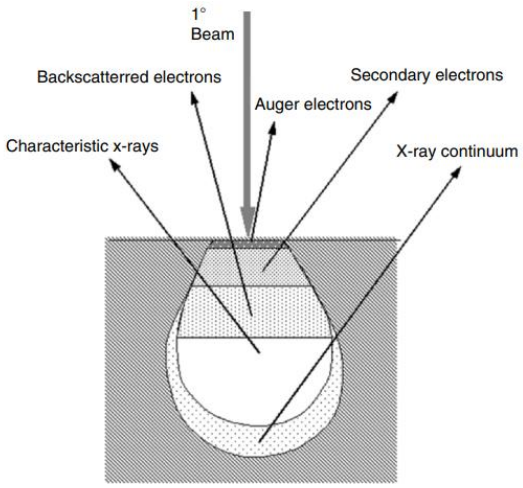


Figure 2.9- Representation of the depth at which different signals are emitted within a sample (Zhou, et al., 2007)

It is for these reasons BSE imagery is utilised, aiding to eliminate particles of non-interest with just an image. This reduces waste in the form of filaments, due to their finite life, and man hours as it results in lower runtimes by ignoring certain particles which are unlikely to be GSR. This negates the need for further imaging and analysis as well as time taken to manually discard particles for not meeting the criterion to label them as GSR.

2.2.2 Energy Dispersive X-rays (EDX) - Theory

The second phase of analysis was the use of Energy Dispersive X-rays (EDX), also referred to as Energy Dispersive Spectroscopy (EDS). The instrument involved was an Oxford instruments X-Max 80 mm^2 paired with the Hitachi S-3400N SEM to chemically analyse specific areas or particles within each sample. The signals utilised for this are emitted at depths just greater than that of BSE imagery (see figure 2.7) which makes utilising a combination of both BSE and X-ray signals advantageous. Programmes, such as Oxford Instruments' AZtec GSR software, were utilised to automate the identification process by 'ignoring' particles that are under or over a certain white value in the image (an indication of chemical composition as mentioned in the previous section), avoiding administering unnecessary, time consuming EDX analysis.

Although this method of spectroscopy allows for the differentiation of the chemical composition across a particle as the user sees it (X and Y axis), it cannot give a complete 'image' of the composition (limited range in the Z axis). The maximum depth at which signals are produced, and therefore the maximum depth at which information is gathered, is instead dependent on the beam's penetration, as mentioned in section 1.6, which itself can be calculated using the accelerating voltage and the atomic density using

the Kanaya-Okayama equation (see equation 2.1). This can range between 4.6 µm and 14 µm for the elements of interest in GSR (see table 2.1) at the aforementioned accelerating voltage of 20 keV.

(*Equation 2.1*) Kanaya-Okayama Equation (Kanaya & Okayama, 1972)

$$R = \frac{0.0276 * A * E^{1.67}}{Z^{0.89} * \rho}$$

Where:

R = Depth of penetration

A = Atomic weight

E^n = Beam energy, ^{n} = 1.67 when beam energy is over 5 keV

Z = Atomic number

P = Density (g/cm^3)

(*Table 2.3*) Depth of Penetration of Incident Electron Beam, calculated using the Kanaya-Okayama equation (*equation 2.1*)

Depth of Penetration of Incident Beam at 20 KeV (µm)		
Lead (Pb)	Barium (Ba)	Antimony (Sb)
4.6	14	7.4

2.2.3 Settings and Practice

The Hitachi S-3400N was setup with respect to the alignment, beam shift and tilt, and stigma at 20 keV accelerating voltage. Higher keV values have been used in current literature such as by Goudsmits who used 25 keV in 2019 (Goudsmits, et al., 2019) however, to preserve the filament and to reduce beam drift or fluctuations in the beam current, 20 keV was deemed suitable. After this, the areas for automation were defined using 120x magnification with the working distance set to focus on a reference stub. The working distance varied between runs due to the physical set up but was typically between 10.4 mm - 10.8 mm. With the automation area defined as area of the carbon tab and “inside area” option selected with 10% overlap, 137 separate fields were defined which themselves were aligned using SE data. With the previously mentioned area settings, the resulting coverage totalled 95.74 mm^2 of the total stub. Using a calibration standard of Cobalt, Gold, and Rhodium, the contrast and brightness of the image were set according to the AZtec GSR protocol and its step notes. Regarding image settings, the image scan size was 2048 with a dwell time of 5 µs leading to a frame time of 15.729 seconds. For the feature detection, the smallest feature size was set to 1 pixel and a lower limit of detection (L.O.D) of 3,000 units was implemented. This often gave a highest rate of detection with very little variation reducing the lower L.O.D further. However, during runs where a high population of particles are seen, this lower

L.O.D was increased to 4,000. This was done as high GSR population runs would result in an impractical run time which, given the aforementioned issues, would make it difficult to gather reliable results.

A calibration of the feature acquisition and analysis of a reference stub as a positive control was carried out before each run, utilising the same reference stub for each run. The reference stub allowed for the setting of working distance, as previously mentioned, but acted as a positive control to allow for the calibration of the software prior to each run. During the run, automatic brightness and contrast was employed with a 10% deviation of the standards grey levels allowed with this being checked every 120 minutes. This worked out to once per stub as well as being checked before moving onto the next stub, well in line with the standards set out in 2020 by OSAC of once per batch (Organisation of Scientific Area Committees, 2020). Automated analysis on each stub and was performed across the whole surface of each stub divided into 137 fields covering 95.74mm^2. The sample stubs were placed in a stub holder along with the reference stub and the SEM calibration stub, see figure 2.10.

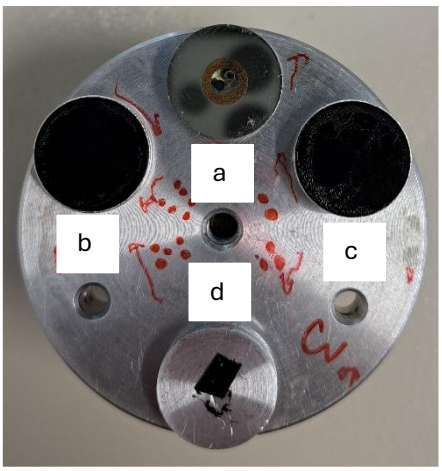


Figure 2.10- 6 pin stub holder and positions of the (a) calibration standard, (b & c) stubs for analysis, and (d) the reference stub

For the EDX analysis, within the AZtec software most options remained in line with the default GSR profile with the first pass dwell time for analysis set to 5 µs with second pass imaging enabled and set to 50 µs with 10 leading and trailing pixels. The scan mode was “scan feature” at 20 keV and number of channels set to 2048 and process time of “4”. The exception to the defaults was that of acquisition mode which, by default, was listed as 30,000 counts but was changed to live time with 2 seconds. This was done as the runs were taking an unreasonable amount of time due to the high populations of GSR observed. This also caused run failure due to the time the beam was on causing aforementioned beam drift. Therefore, as the data observed during EDX analysis stabilised after c. 1 second, 2 seconds of live time was chosen to ensure the data was representative of the sample while improving efficiency. After EDX analysis of the particles present within this examination area, those determined to be environmental particles were discounted. This left particles described by AST 1588-20 as being

characteristic and consistent (table 1.1) of IGSR which could be counted and undergo statistical analysis.

2.3 Statistics

2.3.1 General particle persistence

Total particle population data where both sides of either the metallic barrel retaining nut or 3D printed component were contaminated with GSR but neither had been wiped was converted to a relative proportion of particles found on side B when compared to side A. Under ideal conditions, this would be expected to take a value of 1, suggesting an even distribution of particles on each side of the sample surface. Comparison of an expected and the observed dataset was done using a one-sample t-test (Equation 2.2) to confirm if the values were close enough to be determined normal and justify future comparisons to this observed data set. This was done as one tailed t-tests are prone to missing significance if the difference occurs in the other direction than expected but is more sensitive to significance in that one direction, unlike two tailed t-tests which can detect significance in both directions but are not as sensitive. All statistical tests were carried out using by coding the equations into MATLAB R2025a.

(*Equation 2.2*) One sample t-test equations

$$t=X-\mu o\sigma/n$$

Where:

t = Observed test result

X = the mean of the observed population

μo = the expected mean

σ = the variance

n = the number of data points in the observed data set

and

$$p= Px\leqslant t$$

$$pvalue=2\cdot\min(p, 1-p)$$

Where:

p = probability value

P = Probability of…

x = t-test statistic

t = Observed t-test statistic

p_{value} = p-value to compare against α-value

Once the values were determined to be statistically equal, the proportional values of exhibits which had one side wiped were compared to the baseline data. This was done using a permutation test as shown in *Equation 2.*3

(*Equation 2.3*) Permutation test equation (Good, 2004)

$$T_{observed} = \overline{X} - \overline{Y} = \frac{1}{n_1}\sum_{i=1}^{n_1} x_i - \frac{1}{n_2}\sum_{j=1}^{n_2} y_j$$

Where:

$\bar{X}$ = mean of dataset 1

$\bar{Y}$ = mean of dataset 2

x_i = the value of observation i in dataset 1

y_j= the value of observation j in dataset 2

n_1 = the number of observations for dataset 1

n_2 = the number of observations for dataset 2

A permutation test was then employed again to determine the significance in the difference of values given by the wiping of the polymer against metallic surfaces.

Determination of significance in variance between FDM polymer and metallic surfaces was conducted using an F-test (*Equation 2.4*)

(*Equation 2.4*) F-test equation

$$F_{(df_1, df_2)} = \frac{{S_1}^2}{{S_2}^2}$$

Where:

df_X = degrees of freedom (as calculated using number of data points in dataset (x) -1)

S_X^2 = the variance of each dataset

2.3.2 Particle size persistence

Data regarding the sizes of the particles that make up the total population were analysed to determine if wiping affects certain sizes of particles disproportionately. To do so, a chi squared goodness of fit test (*equation 2.5*) was used to determine if the proportion of each size range differed between the unwiped and wiped side and the results then verified using Cramér's V (*equation 2.*6). Due to the large range datapoints, these tests were done on the particle proportions as a percentage of the total population.

(*Equation 2.5*) Chi-square goodness of fit (Rahman, et al., 2025)

$$X^2 = \sum \frac{(O_i - E_i)^2}{E_i}$$

Where:

x^2 = the Chi-square statistic

O_i = the observed value for data point i

E_i = the expected value for data point i

(*Equation 2.6*) Cramér's V equation (Press, et al., 1993)

$$V = \sqrt{\frac{X^2}{N \cdot \min(k-1)}}$$

Where:

V = the test value

X^2 = The Chi-square statistic

N = The number of values

k = The number of rows or columns

2.3.3 Particle composition persistence

Analysis of the particles for population data involved the chemical analysis of said particles for confirmatory purposes. As a result, data on the composition could also be analysed without rerunning the samples. This data was handled in an identical method to the particle sizes as both datasets were categorical and the large range between exhibits meant the values must be converted into proportions to create a useful dataset.

3- Results

3.1 Total Population Loss

The range of total populations between exhibits used to set the base line proportion of just the metallic surface ranged from 20 IGSR particles to 1187. Even the polymer surface samples had a large divergence from one another with the total population of IGSR particles on baseline exhibit samples (both sides ‘A’ and ‘B’) ranging from over 14,000 IGSR particles down to just <1,800. The large ranges of values present for both mediums are representative of the huge number of variables affecting IGSR production and deposition, as mentioned in section 1.7, and variability seen in factory loaded ammunition (McTee, et al., 2025). Especially as other environmental factors that contribute to the deposition, such as wind speed, temperature, and surface, were consistent throughout the experiments. Therefore, for comparison purposes, the population data of particles was converted into proportions of side ‘A’ in relation to side ‘B’ due to the extreme variation seen in these GSR populations. For example, For the determination of the significance of the divergence seen in the observed base line and the expected, one-sample t-tests were used. The observed data set was tested against an expected value of 1 as an identical distribution of particles between sides should result in this value.

Subsequently, significance of the deviation between wiped proportions and the baseline itself was calculated using a permutation test. While Welch’s variation of the unpaired t-test may also have been appropriate, in cases where ‘n’ is low it creates extremely strict parameters which the P-value needs to achieve before significance is determined. If more samples were taken and analysed, Welch’s test would have been preferred due to the ratio of variances (Sinscow, 1997). These tests were performed using an alpha (α) of 0.1 which, although increases the chances of false positives, gives the tests more power which is required due to the low number of repeats (n). The number of repeats (see *Table 2.2*) was a result of time limitations due to the significant efforts required to refine the SEM methodology alongside the collection and analysis of the samples. Reducing the α-value to the standard 0.05 should be considered in further, more refined research with more repeats, but 0.1 was decided to be sufficient for this study due to its more exploratory nature (Noymer, 2008).

The use of particles listed as ‘*characteristic of*’ and ‘*consistent with*’ GSR according to ASTM-1588 (Oxford Instruments, 2026) (*Table 3.1*), with the exclusion of particles listed as ‘*commonly associated with*’ or environmental, was applied as a result of a high variability within the A/B proportions both above and below the expected 1:1 during base line testing (see *figure 3.1*). Perhaps more notably, a high variability still occurred within a negative control test, where the whole surface was cleaned and then sampled, despite containing no IGSR consistent or characteristic particles. This may be due to the SEM working distance being more ideal for the SEM stub on the left or right side of the holder (see *figure 2.10*). This would most likely be due to any variance in the level of the pin stub holder, something that would need to be checked with a dial indicator. Any difference in elevation and, thus, working distance of the beam to the sample directly affects the focus resulting in a change of the intensity and white level of particles. This would have certainly skewed the results as a majority of these particles were at the

limit of detection, being just 1 pixel with an area of 0.269 μm^2. This may indicate a significant flaw in the general methodology; however, a high proportion of these particles contained iron and were labelled as "environmental" suggesting their origin could be contamination from the metallic collection surface and more specifically the EN8 steel used in the construction of the part.

Table 3.1- Table of the composition of characteristic and consistent GSR particles as recorded by the default Aztec GSR software settings

Particle Class	Particle Composition
Characteristic	Sb Ba Pb
Consistent	Ba
Consistent	Ba Al
Consistent	Ba Sb
Consistent	Ba Si Ca
Consistent	Cu Zn
Consistent	Pb
Consistent	Pb Ba
Consistent	Pb Sb
Consistent	Sb
Consistent	Sb Ba Pb Sn
Consistent	Ti Zn Cu
Consistent	Sr

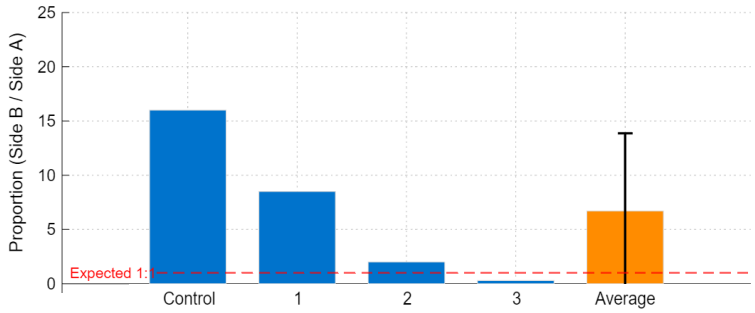


Figure 3.1- Metallic baseline study- Bar chart of particle population of side B as a proportion of side A (all particles) of a negative control and exhibits 1-3. Error bars calculated using 1st order standard deviation of results.

Due to the difficulty in differentiating particles originating from the environment or medium from those produced by the firing of the gun or originating from the primer, those considered environmental by the AZtec GSR were disregarded. This left only particles considered consistent or characteristic of GSR and, therefore, known to be unlikely to come from a source other than the ammunition were counted for both surfaces to ensure equal treatment. This led to proportions much closer to the 1:1 ratio expected as shown in *figure 3.2* (data in appendix 1). This amended data set showed values of 0.54, 1.29, and 0.47 for the baseline exhibits of the metallic surfaces. The control was found to have no GSR particles on either side, attesting to the efficacy of the data cleaning protocol, and as a result was not included on *figure 3.2*. It could be inferred that, because the ideal proportion is within the error bars of the average,

it is possible that further results would only serve to bring the average closer to this expected. The one-sample t-test gives a P-value of 0.4615 which, being larger than 0.1, results in the hypothesis that datasets are equal, not being rejected. Despite this, due to the small sample sizes, further comparison was done using the observed average from *figure 3.*2 (a value of $0.76\dot{6}$) as a base line from hereon as the 'expected' line to weight the tests against the experiment to dispel any bias for future analysis.

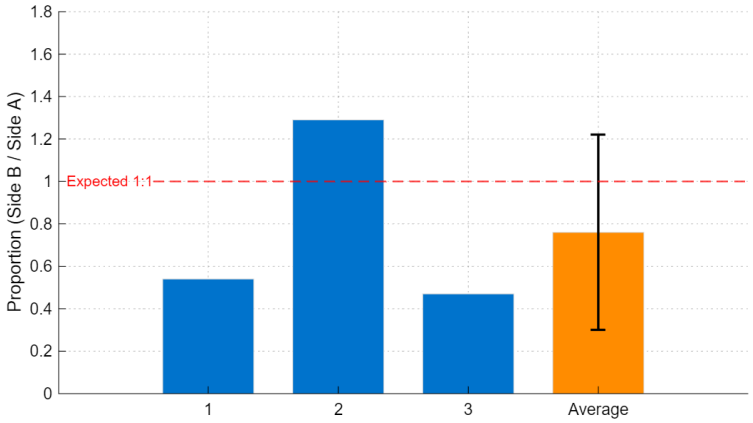


Figure 3.2- Metallic baseline- Bar chart of the particle population of side B as a proportion of side A (GSR only) of exhibits 1-3. Error bars calculated using 1st order standard deviation of results.

Despite this lower 'expected' line, *figure 3.3* (data in appendix 2) shows all the results gathered after wiping the metallic surface displaying a proportion of less than the lower range of standard deviation of 0.3 with an average of 0.073 and a standard deviation of just 0.06. We would expect 68% of the results to fall within 1st order of standard deviation if the loss was due to natural variance in the GSR populations (Montgomery & Runger, 2003), but as 100% of these results were outside of this range it can be determined these losses were of direct result of the wiping process. Due to the vastly different variances, a permutation test was performed and saw a P-value of just 0.0179 in both one- and two-sided tests. As the P-value < α-value, significance in the difference between values was indicated, thus remarking on the significance of the effect wiping has on GSR present on machined, metallic surfaces. This serves as a good comparator with which to compare the results of experiments on polymer exhibits as it demonstrates the poor persistence GSR has had on traditionally made firearms surfaces.

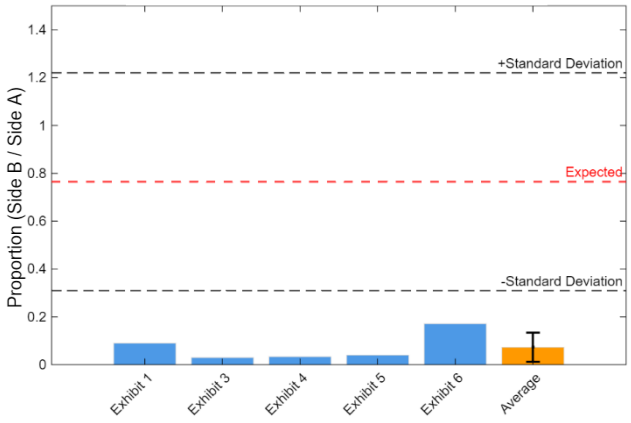


fig. 3.3- Metallic experimental- Bar chart of the particle population of side B (wiped) as a proportion side A (unwiped) (GSR only) with observed baseline and standard deviation. Error bars calculated using 1st order standard deviation of results.

For FDM polymer surfaces, the same contamination was not as much of an issue due to the obvious difference in material and even when counting all particles, deviation from the expected 1:1 proportion was shown to be much lower in *figure 3.4* than it was for the metallic baseline data in *figure 3.1*. Despite this, it was thought reasonable to discount particles listed as environmental or unclassified due to the high likelihood of these being iron particles originating from the barrel itself. Even though these would be the product of wear, not the surface itself, it still brings more variance to the data as shown by the tighter distribution in *figure 3.5* (data in appendix 1). Discounting these particles saw the 1st order standard deviation value drop by 10%, from ±0.40 to ±0.36. Performing a one-sample t-test on the GSR data against the expected mean of 1, a P-value of 0.9484 is observed. This indicates no statistically significant deviation when testing with the same 0.1 α-value.

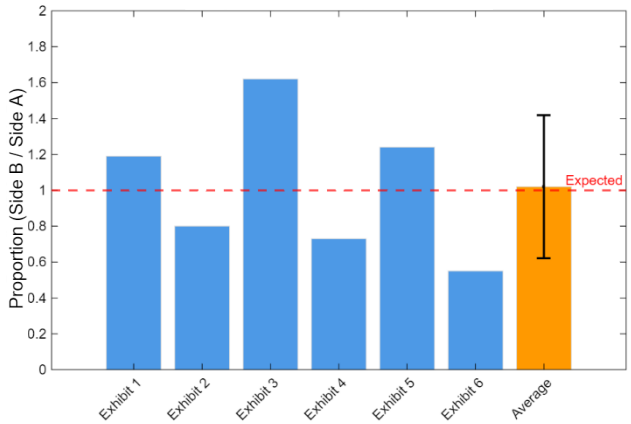


fig. 3.4- Polymer baseline- Bar chart of the particle population of side B as a proportion of side A (all particles) of exhibits 1-6. Error bars calculated using 1st order standard deviation of results.

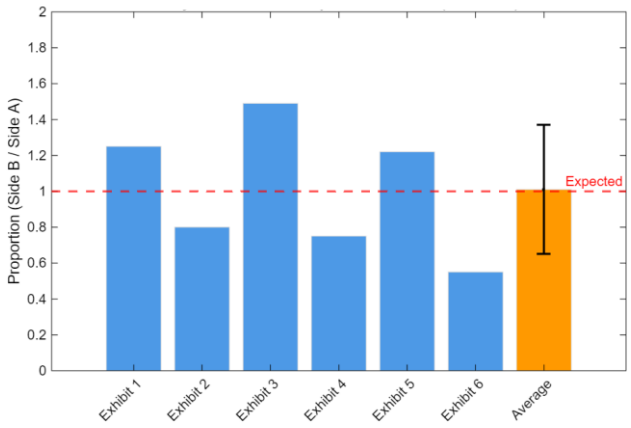


fig. 3.5- Polymer baseline- Bar chart of the particle population of side B as a proportion of side A (just GSR) of exhibits 1-6. Error bars calculated using 1st order standard deviation of results.

With this baseline for the distribution between both sides of the FDM polymer surface established, a graph was plotted to compare the expected distribution to the distribution seen after wiping to determine if wiping had a significant effect on the particle population. *Figure 3.6* (data in appendix 2) shows a marked reduction in these populations with an average just 0.42 of the expected population remaining. Although one data point sits within the 1st order of standard deviation of the typical distribution, it makes up 12.5% of the sample size which is well below the 68% threshold that would be expected if non-significance was the case. Performing a permutation test of the polymer baseline against the polymer experimental data returned a P-value of just 0.0021 for the two sided and 0.0019 for the one sided, both cases providing values lower than $\alpha = 0.1$ supports the conclusion of a significant difference between the means.

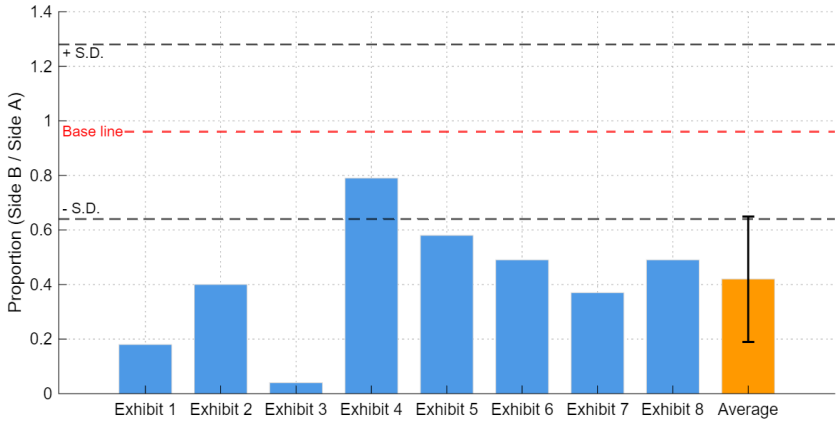
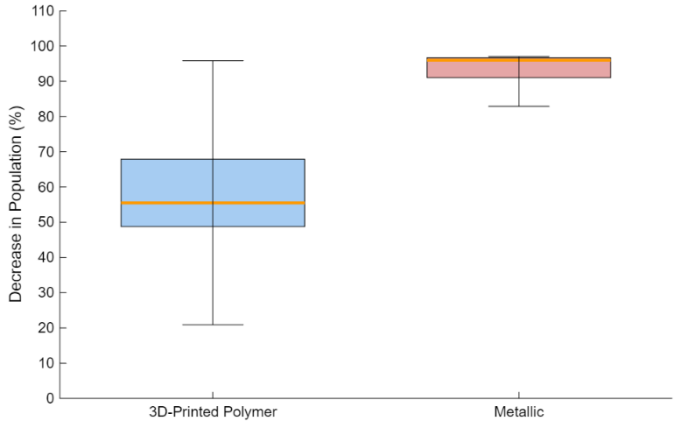


fig. 3.6- Polymer experimental- Bar chart of the particle populations of side B (wiped) as a proportion of side A sides (unwiped) (GSR only) with observed baseline and standard deviation. Error bars calculated using 1st order standard deviation of results.

As both metallic and FDM polymer surfaces show significant reductions in populations after just one wipe, the extent to which these reductions occur can be compared. *Figure 3.7* shows variance in observed losses was much higher for FDM polymer surfaces at a standard deviation of 0.23 versus that

of metallic surfaces at just 0.05. An F-test was performed to verify the use of an unequal variance test, a permutation test in this case, in order to properly compare the population losses of IGSR populations on polymer vs. metallic surfaces after one wipe. The F-test returns a P-value of just 0.021 which, being below 0.1 and even 0.05, shows statistically significant variance. The permutation test returned a two-sided P-value of just 0.00729 which, again, being lower than α = 0.10 or even 0.05 corroborates the hypothesis that FDM polymer surfaces displayed a higher average rate of retention of 42 % compared to the 7 % of the metallic surface. That is to say, the FDM surfaces lost just 58% of the total population of IGSR particles after one wipe while the metallic surface lost 93% of IGSR particles.



	Polymer experimental (% loss)	Metallic experimental (% loss)
Max.	95.84	97.01
3rd quartile	67.89	96.69
Median	55.49	95.99
1st quartile	48.76	91.02
Min.	20.89	82.89

fig. 3.7- Metallic experimental v. Polymer experimental- Box and whisker chart of the % loss of GSR particles

3.2 Population Loss in Relation to Particle Size

With the differences and variation of the overall GSR populations being deemed significant, the differences of the persistence between size ranges were evaluated. In order to do so, the results of the baseline and experimental results were grouped together. However, as shown by the averages (graph 'c' in *figures 3.8* and *3.9*), the 'profiles' created by one set of exhibits are drastically different to another despite correspondence between sides of the same exhibit (graphs 'a' and 'b' within *figures 3.8* and *3.9)*. This indicates the proportion of each size range of GSR being specific to that combination of shots to create a 'profile' of the distribution of particle sizes.

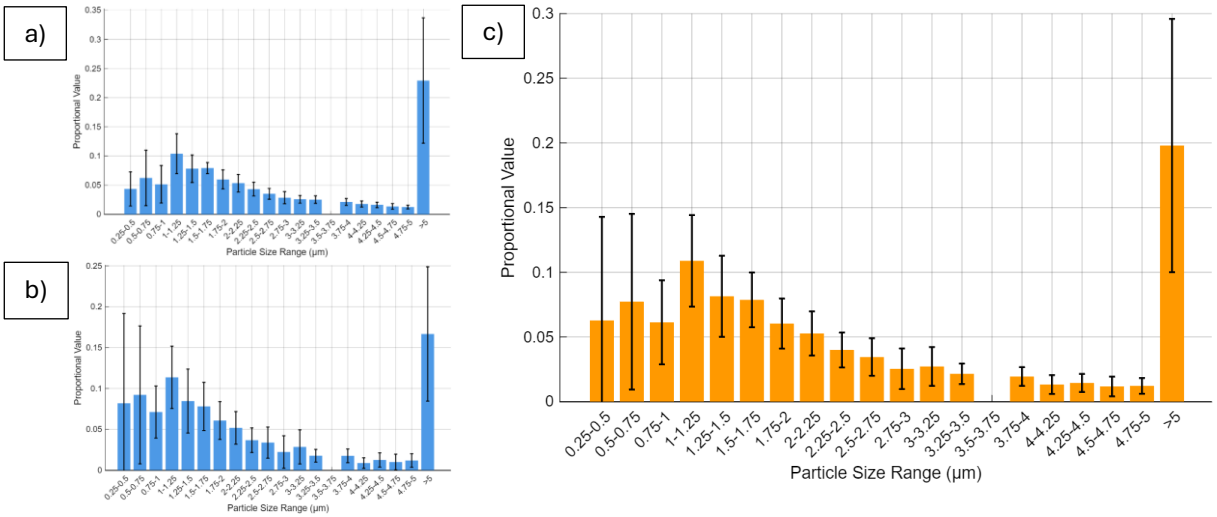


fig. 3.8- Polymer experimental- Bar charts showing average distribution of particle sizes of a) sides 'A', b) sides 'B', and c) the total of the exhibits. Error bars calculated using 1st order standard deviation of results.

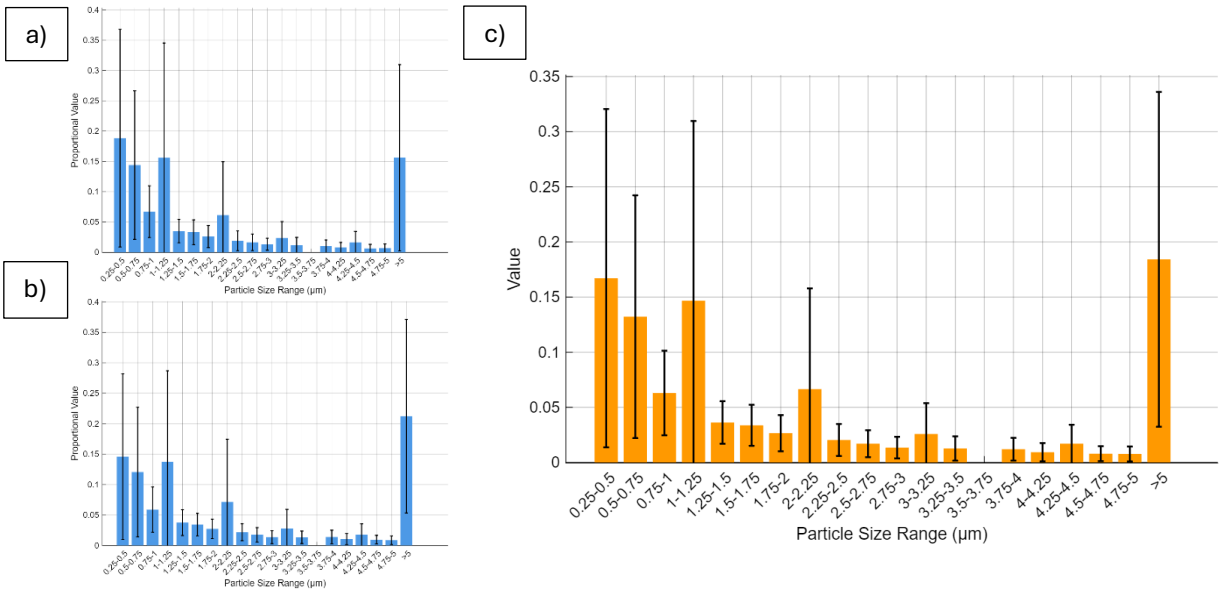


fig. 3.9- Polymer baseline- Bar charts showing average distribution of particle sizes of a) sides 'A', b) sides 'B', and c) the total of the exhibits. Error bars calculated using 1st order standard deviation of results.

The uniqueness of these profiles is corroborated by observing a bar chart of proportions produced by each exhibit individually (*figure 3.10*). As each set of shots can produce such a different profile from the last, each of these 'profiles' contribute towards the average 'profile' of the proportion distribution.

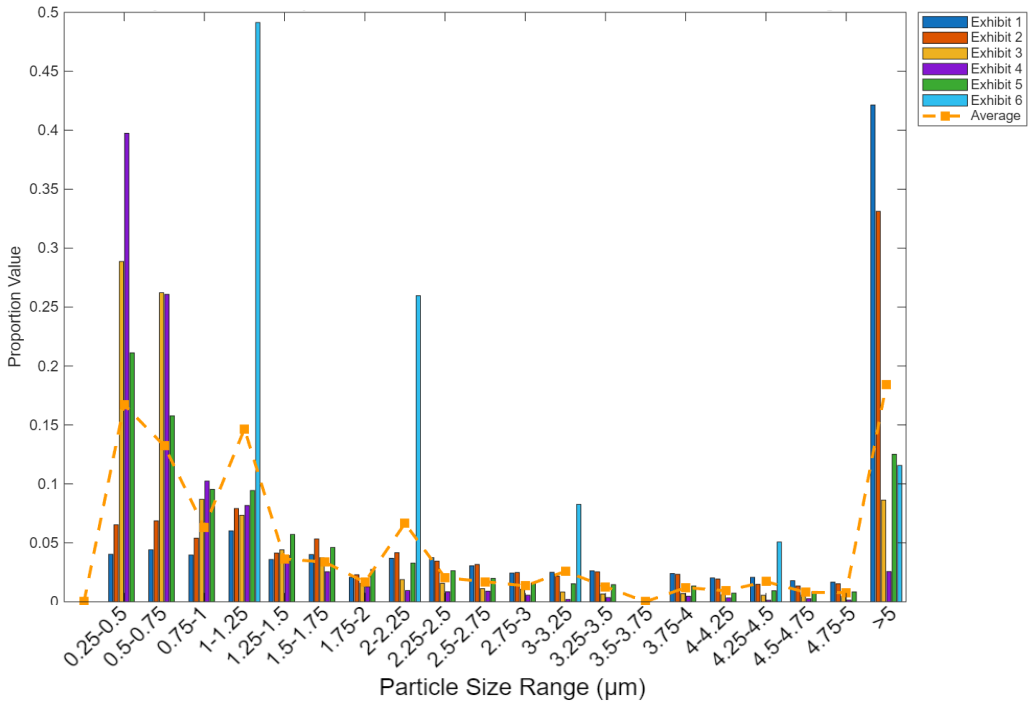


fig. 3.10- Polymer baseline- Bar chart showing distribution of particle sizes of Exhibits 1-6 (A & B) and their average.

Due to the categorical nature of the data set and the need to compare proportions of these categories between the two data sets, a Chi-square test was applied. As the Chi square test suffers when analysing large and small numbers within the same table, the data ranges were narrowed by defining the value of each size range as a percentage of the total population of the respective side of the exhibits. Despite the difference in the profile of the exhibits, these tests were performed on the baseline exhibits to gauge how data between unaltered sides differs. Performing this test returns a P-value of 0.9999 which, being higher than 0.1, show there is no statistical significance in the difference of the profiles at any points when both sides are handled equally. As the Chi-squared test is more of a binary test, a Cramér's V test was performed to determine the strength of the relationship. This provided a value of this of 0.1294 which indicates the *difference* is very weak and therefore the conclusion of the Chi-square test itself is upheld. *Figure 3.11* shows the profiles for side A and B visually appear as though the particles were affected by the wipe evenly regardless of size and that both sides should display near identical proportions of particle sizes.

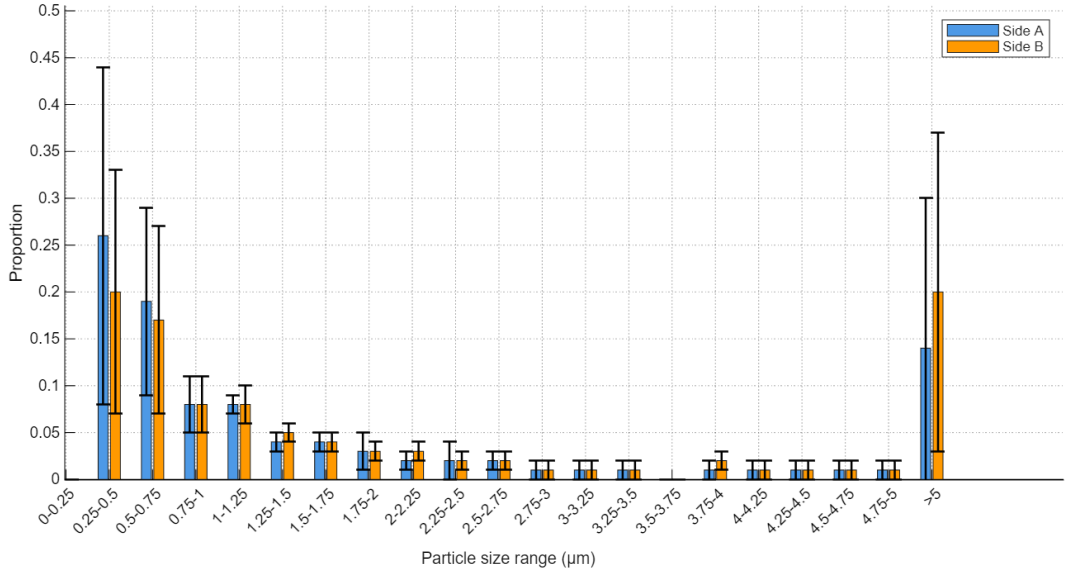


fig. 3.11- Polymer baseline- Bar chart showing the average distribution of particle sizes between sides 'A' and sides 'B' of exhibits 1-6. Error bars calculated using 1st order standard deviation of results.

Performing these tests for the data produced by the wiped experimental polymer exhibits (*figure 3.12*) returns a P-value of 1.0000 and a Cramer's V value of just 0.1043. The former concludes that the proportions are equal, but the latter also bolsters the strength of that conclusion which is to say the particles of wiped populations are representative of those of an unwiped exhibit provided both experiencing the same shots.

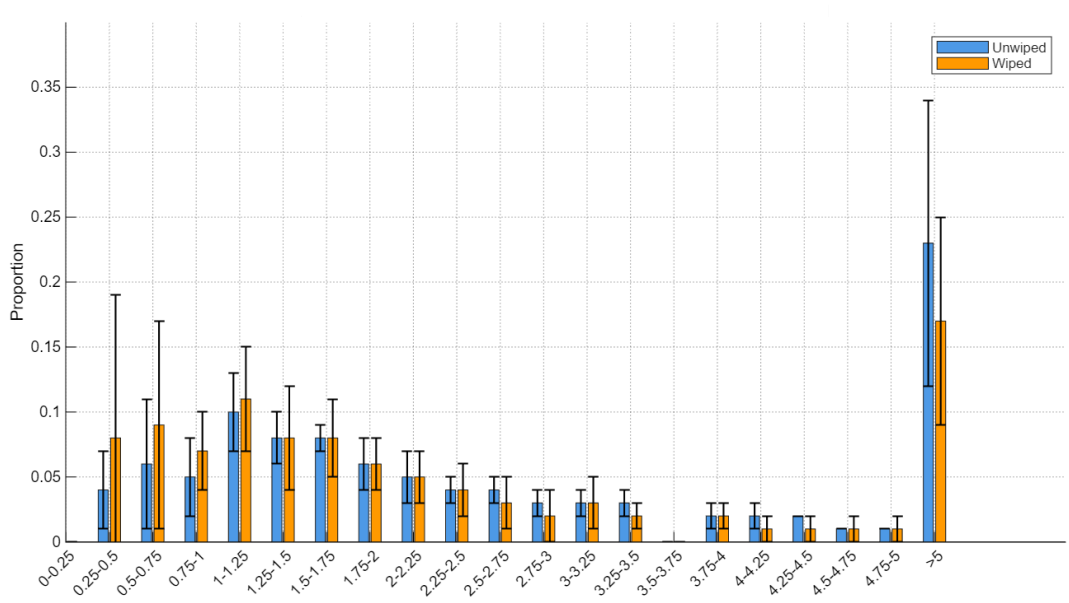


fig. 3.12- Polymer experimental- Bar chart showing the average distribution of particle sizes between sides 'A' (unwiped) and sides 'B' (wiped) of exhibits 1-8. Error bars calculated using 1st order standard deviation of results.

Chi-square and Cramér's V were utilised to again to determine if there was any significant difference in the proportions of particle sizes before and after wiping for the metallic surface. As with the FDM polymer surfaces, the baseline where both sides of each exhibit were left unaltered (*figure 3.13*) showed no statistically significant difference with a P-value of 0.7645. The Cramér's V test concluded that although the difference was weak to moderate it still supports the Chi-square tests conclusion (a higher value of 0.2508 is noted). Now it is also determined the proportions of each size range should be equal across sides, the experimental metallic exhibits can be analysed.

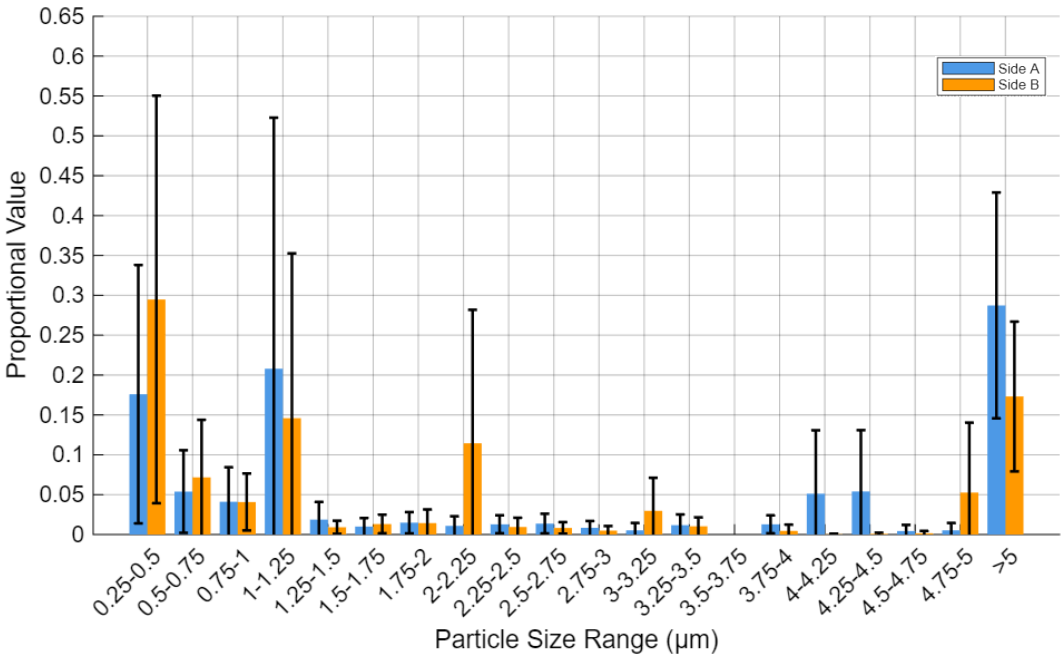


fig. 3.13- Metallic baseline- Bar chart showing the average distribution of particle sizes between sides 'A' and sides 'B' of exhibits 1-3. Error bars calculated using 1st order standard deviation of results.

Testing the results of the metallic experimental exhibits, a P-value of 1.0 and a Cramér's V value of 0.0895 are obtained. These, again, both support a lack of statistical difference between the profiles at any point, which confirms all particles experienced the same degradation of population regardless of size (see *figure 3.14*).

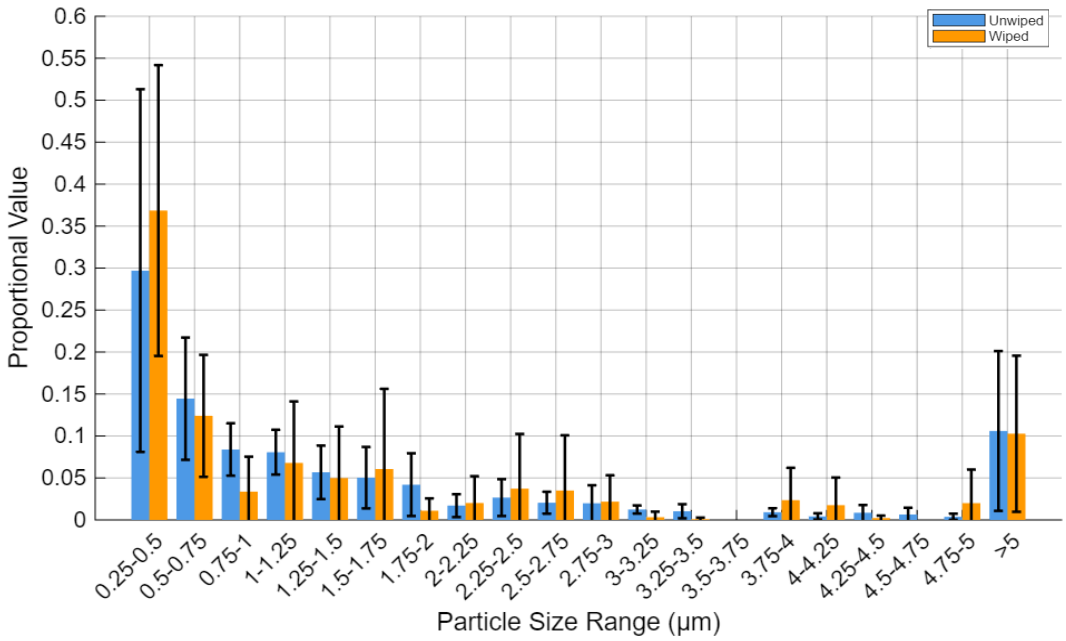


fig. 3.14- Metallic experimental- Bar chart showing the average distribution of particle sizes between sides 'A' and sides 'B' of exhibits 1-5. Error bars calculated using 1st order standard deviation of results.

The higher P-values returned by the experimental exhibits of both polymer and metallic exhibits indicates something about wiping process causes a lower rate variance between sides and brings the proportions of the wiped side to be more representative of that of the unwiped side.

3.3 Population Loss in Relation to Particle Composition

The particle composition of IGSR particles (excluding environmental particles for the same reasons as before) was also explored. Similar to the particle size distributions, the average distribution of particle composition between sides 'A' and 'B' are very close to one another as seen in *figure 3.15* (data in appendix 3).

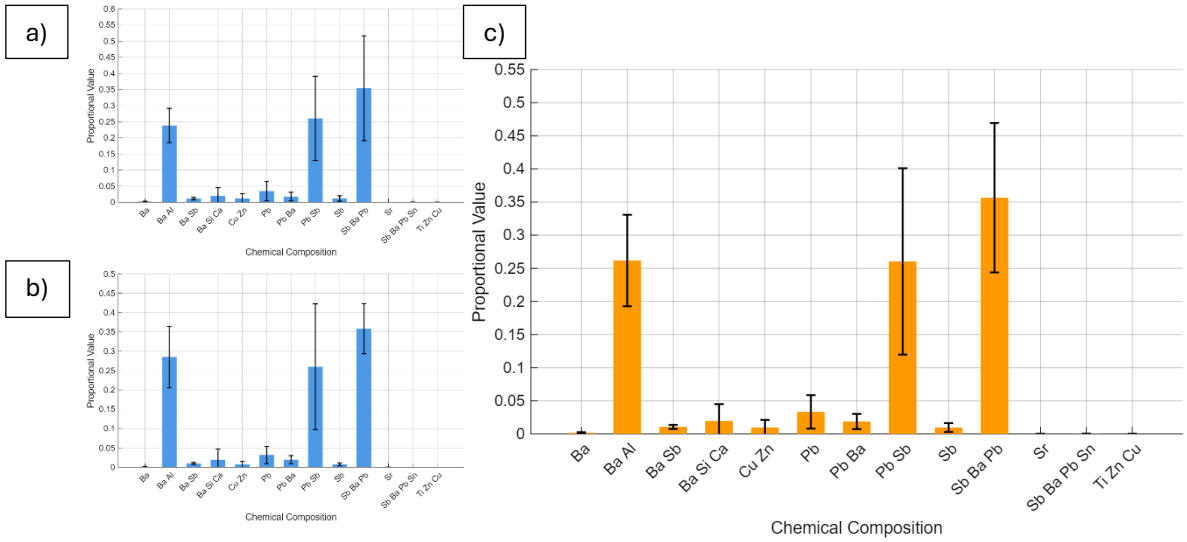


fig. 3.15- Polymer baseline- Bar charts showing average distribution of particle compositions of a) sides 'A', b) sides 'B', and c) the total of the exhibits. Error bars calculated using 1st order standard deviation of results.

As with the particle size distribution, these average profiles seem to be a result of extremely variable individual profiles (*figure 3.16*). It is due to these variables to which a certain level of uniqueness of the average profile can be attributed.

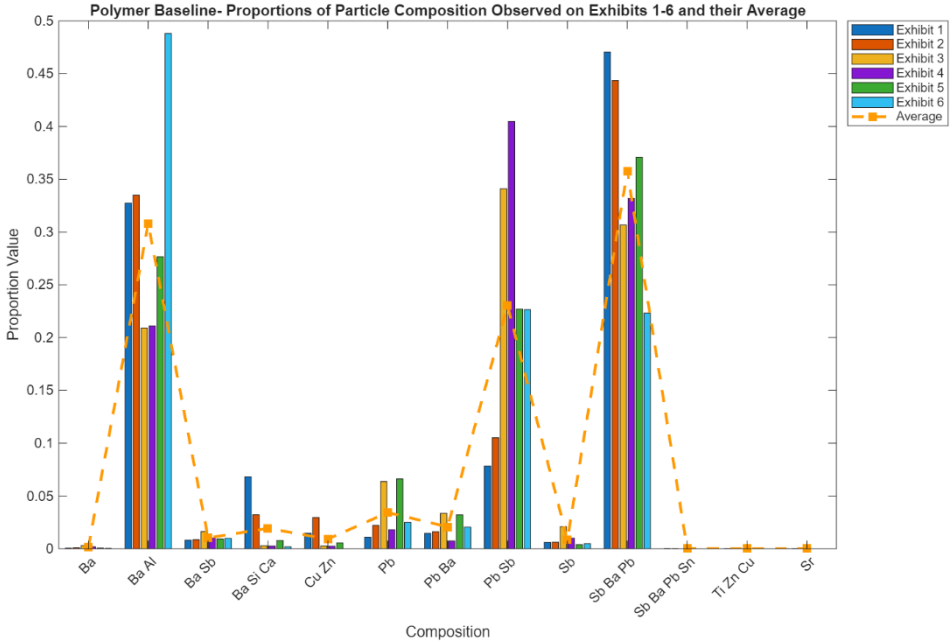


fig. 3.16- Polymer baseline- Bar chart showing distribution of particle composition of exhibits 1-6 (A & B) and the average of all exhibits.

Chi-square and Cramér's V tests were employed again using the same method of converting each category (this time being elemental composition instead of size range) into percentages of the total population for that respective side of all exhibits.

Performing the Chi-square test for the FDM polymer baseline exhibits (*figure 3.17* -data in appendix 3) returns a P-value of 0.9993 which, being higher than 0.1, show that there is no statistical significance in the difference of the profiles at any point. Cramér's V test provided a value of 0.1013, supporting the lack of significance in differences and bolstering the conclusion that both sides naturally display an identical proportion of elements.

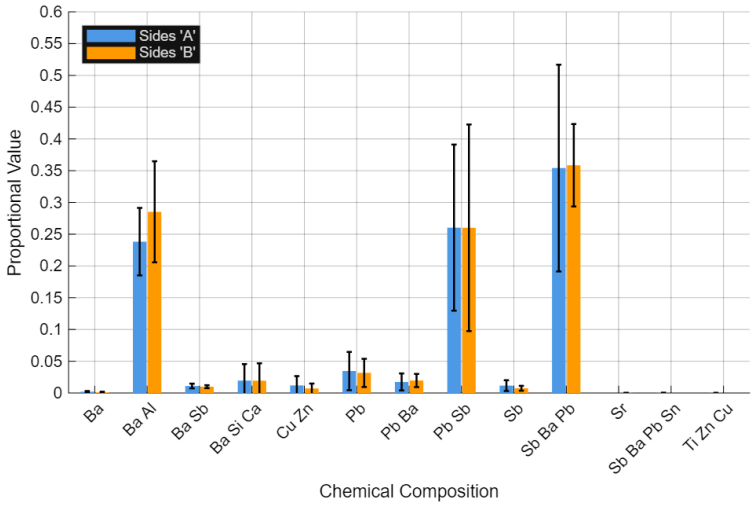


fig. 3.17- Polymer baseline- Bar chart showing the average distribution of particle composition between sides 'A' and sides 'B' of exhibits 1-6. Error bars calculated using 1st order standard deviation of results.

With the expected proportions between sides established as equal, the Chi-square and Cramér's tests were performed using the data from the FDM polymer experimental exhibits (*figure 3.18*- data in

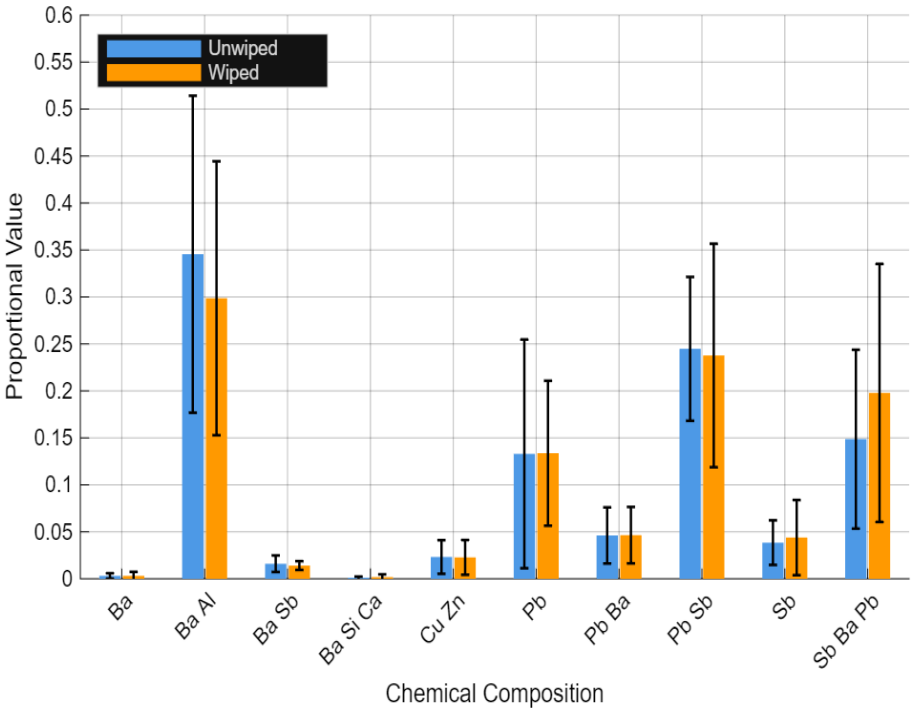


fig. 3.18- Polymer experimental- Bar chart showing the average distribution of particle composition between sides 'A' and sides 'B' of exhibits 1-8. Error bars calculated using 1st order standard deviation of results.

appendix 4). Values of 1.0 for the former and 0.1043 for the latter indicate a lack of significance between the profiles produced by the chemical composition of these particles and support this conclusion respectively.

Applying this methodology to the baseline metallic surface data (*figure 3.19*- data in appendix 3) to gauge the natural deviation, a p-value of just 0.0024 was returned. This suggests a statistically significant difference between the composition of the GSR particles found between the sides of the metallic exhibits. Therefore, not much can be gained by comparing this to the experimental data. A Cramér's V value of 0.3455 relays a moderate association between these values.

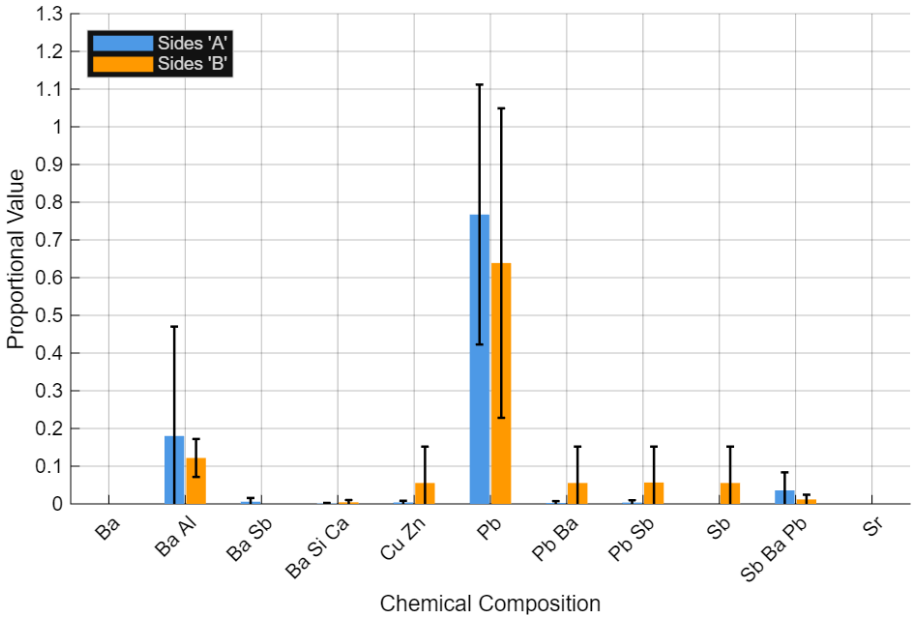


fig. 3.19- Metallic baseline- Bar chart showing the average distribution of particle composition between sides 'A' and sides 'B' of exhibits 1-5. Error bars calculated using 1st order standard deviation of results.

Subsequent testing of data obtained from the experimental metallic exhibits (*figure 3.20*- data in appendix 4) returned a p-value of 9.8410×10^{-10} indicating a stronger significance in the differences. A higher Cramér's V of 0.5612 was also returned indicating an even stronger practical difference between the sides than that found in the baseline data.

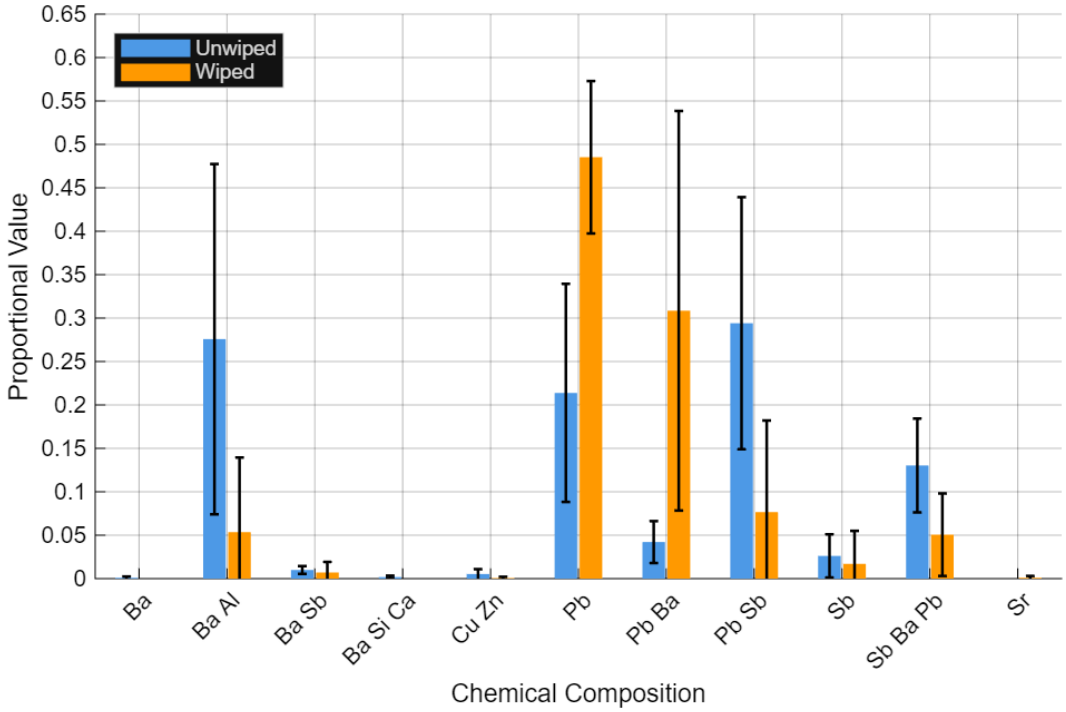


fig. 3.20- Metallic experimental- Bar chart showing the average distribution of particle composition between sides 'A' and sides 'B' of exhibits 1-3. Error bars calculated using 1st order standard deviation of results.

4- Discussion

4.1 Sampling

To keep variance due to random factors down, both substrates should be sampled in identical circumstances regarding orientation to the line of fire and distance from the barrel exit. For the metallic surface, the barrel retaining nut was chosen in part because it gave a surface on which to mount the FDM polymer surface. This kept the two surfaces in alignment and as close as possible to experiencing the same conditions during firing. Although the total particle populations saw great disparity between exhibits due to the randomness of the GSR production of the ammunition, the spread between sides of individual exhibits were equal enough such that conclusions could be drawn from proportional results. The shots were fired in a climate-controlled range with consistent windspeed so the randomness of GSR populations were likely due to the production of GSR by the ammunition which could be negated by increasing the number of shots.

For sampling, the use of stubs and carbon adhesive tabs was employed due to its prevalence in industry and the similarity in efficacy displayed by other methods such as tape lifts (Zeichner, 1993). This method has also been found to leave fewer traces of OGSR than swabbing indicating a higher affinity to the

other constituent parts of the sample (Gassner, 2016). Again, as long as both sides of the exhibit were sampled in the same manor with the same affinity to the sample, the proportional value should be reliable. During development of the sampling surface, a disparity in the distribution of GSR across the stub was seen. This showed as a bias of the particle population towards the outer edge of the SEM stub (see *figure* 4.1 a). This weighting coincided with the wall thickness and the rectilinear infill pattern of the FDM printed parts (*figure 4.2* a & b). Subsequently, settings were changed in the Cura software to achieve a concentric pattern (*figure 4.2 c)* for the bottom layers resulting in a consistent pattern as shown by the tool path in *figure 2.5*. This consistently provided visibly better distribution (*figure 3.1* b) and was adopted for the main body of the experiment.

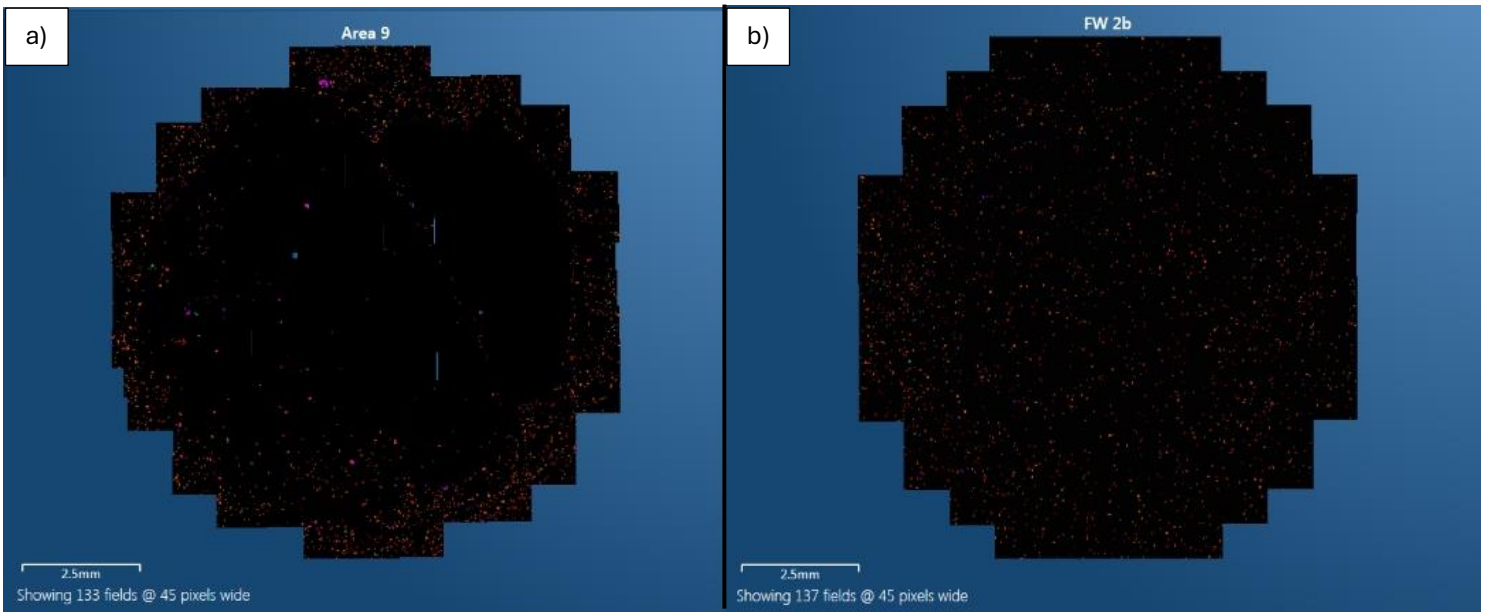


Figure 4.1- a) The distribution of particles on exhibit before changes to slicing (2034 particles) and b) after (2433 particles)

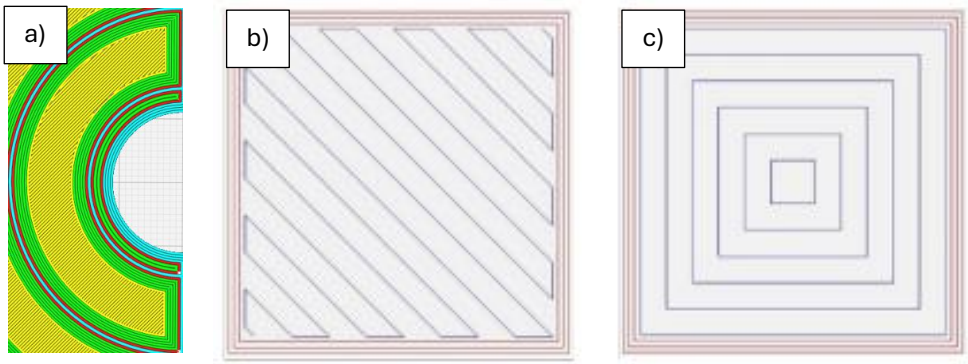


Figure 4.2- a) The tool path before slicing changes (authors own), b) rectilinear tool path (Saniman, et al., 2020), and c) concentric tool path (Saniman, et al., 2020)

To further combat any uneven stub contact, the stubs were sanded on a flat bench to remove a lip on the sampling face which was only visible when placing a straight edge on the sampling face and

observing light leaking in between the two objects in the middle. Although the carbon adhesive tab is compliant to some extent and able to take up differences in the surface, the surface inconsistencies had a notable effect on the results collected. The smooth, machined surface of the aluminium stub also provided limited grip to the carbon tab's adhesive, resulting in the carbon adhesive tabs regularly coming away from the stubs themselves and adhering to the rougher FDM printed surface during sampling. The keyed aluminium surface caused by the sanding process resulted in better adhesion between the stub and the tab. It is worth noting, this issue was still prevalent at times under warmer temperatures as the adhesive became tacky and displayed a higher affinity to even the machined and coated steel surface over the keyed stub. This was sufficient to combat the uneven contact of the stub to the sampling surface, although several other factors had to be mitigated to avoid the possible warping of the 3D-printed surfaces. These factors included the 3D-printer being unenclosed in a laboratory with traffic and temperature fluctuations, and the filament material also experiencing temperature cycles. To reduce the likelihood of 3D-printed sample collectors warping, a wide brim was implemented to aid in print bed adhesion. No cooling on the initial layer with fan speed slowly ramping up to a maximum of 50 % by layer 4 further improved layer adhesion and reduced warping. Preventing the warping of the exhibit as it cooled allowed for tighter tolerances which meant for a more secure fit on the universal receiver. This was advantageous as the print was prone to coming away from the receiver and the improved flatness would have also further improved stub contact. This resulted in fewer exhibits being wasted and more data collection for the same material, a saving of material, and a saving of electricity and time due to the 5-hour print time of each exhibit.

Regarding the surface roughness (Ra), an FDM 3D print can have a variety of surface roughness measurements depending on the orientation of the sampling surface with the build plate. Surfaces facing away from the build plate, which are typically the surfaces printed last and will have tool marks from the printer nozzle (Pavlovich & Garrison, 2023), have been found to have a surface roughness of 4.74 µm ± 2.19 S.D and 1.82 µm ± 0.79 S.D for 0.5 mm and 0.3 mm nozzles respectively (Alsoufi & Elsayed, 2017). The surface of sampling was not characterised directly, but we can assume surface roughness sits in between these values due to the use of a 0.4 mm nozzle. A company, Xometry, allows users to upload a model for manufacturing by them and lists the surface roughness of Acrylonitrile Styrene Acrylate (ASA) FDM printed parts. The roughest surface, "*perpendicular to the layering"*, was stated as having an Ra of 22.5 µm which is in line with the values found for 0.2 mm layer heights by Alsoufi in 2017. The company then states the Ra of the 0º measurement as being 0.9 µm although nozzle size is not mentioned. A low roughness for the printer materials in this study can be assumed due to the GSR sample collections occurring on the face of the print in direct contact with the untextured, glass build plate. This should put the surface roughness of the exhibits used below the values stated above and therefore closer to the 1.6 µm Ra value of the metallic surface. Worth noting, however, is the presence of regular imperfections ~0.4 mm apart (*Figure 4.3*) which coincides with the nozzle diameter and therefore the offset between deposited ribbons of polymer. The image in figure 4.3 was achieved by pouring a layer of resin on top of on the 3D-printed parts in this study. This allowed for the contrast between materials to be observed whilst preventing the formation of a bur which would have altered or obscured the topography of the print.

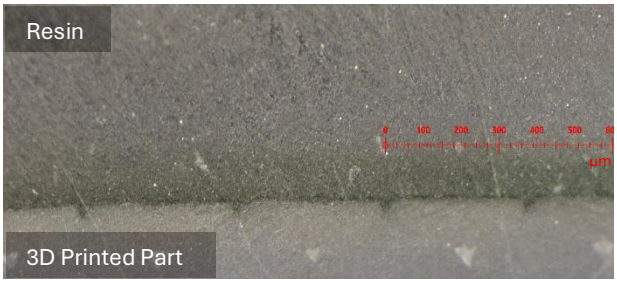


Figure 4.3- Light microscope image of sampling surface of FDM polymer surface (x135) showing the grooves caused by the toolpath step-over and nozzle aperture.

Also to be considered is the Ra of 1.6 µm listed as the surface finish in *figure 2.2* as the Ra of the machined surface. Although the surface features a phosphorous coating, this process has been found not to affect surface roughness (Podgornik, et al., 2020). A commonly featured coating on firearms, nitriding, has shown *increases* in Ra which can subsequently be knocked back down through polishing (Nitrera Technologies, Inc., 2025). As the surfaces will differ between firearms, it is still applicable to compare retention rates between the machined surface of the universal receiver to polymer as the value is in the difference in GSR retention regardless of surface roughness and has more to do with the material itself or the formation of these troughs.

A brief test of the number of shots required to produce enough GSR was done in an attempt to get an even coating of GSR on the exhibit. Due to the variability of the ammunition used to produce GSR, any attempt to create even deposition between exhibits would have been highly challenging. Instead, multiple shots for each surface type were performed to reduce the effect of uneven deposition due to unforeseen factors. Due to the high number of particles produced for five shots, which would have also dramatically increased the analysis time, three shots of ammunition were shown to produce an even coating across the exhibit while providing enough GSR particles that small variances between shots were eliminated. With less particles to analyse, this lead to a lower run time and meant more exhibits could be examined in the same time period. This also provided a greater accuracy during SEM analysis as a result of improved beam stability, and the wear on the SEM filament was dramatically reduced.

To measure any change in persistence between substrates, a variable that would affect the population of IGSR particles on a surface must be applied equally. In this case, contact was used to initiate transfer of GSR off the exhibit by wiping. To ensure consistency, an equal pressure and contact patch must be employed to perform the transfer. A 3D printed ‘basket’ (*figure 2.4*) was designed, the bottom of which would be covered with a disposable surface to avoid contamination between exhibits. To replicate a ‘wipe’ consistently, the basket was filled with lead (see *figure 2.3a*) and a top sleeve installed over it (see *figure 2.3b*). This was to allow lateral authority without affecting the force applied to the exhibit vertically. Of course, this meant wiping had to be done with the sampling surface facing upwards but, due to the ability to remove both types of sampling surfaces, this was a non-issue.

To predetermine a suitable mass of lead in the basket, a device created to measure the average maximum wipe force applied. Utilising a trigger force gauge (Lyman Electronic Digital Trigger Pull

Guage, 7832248) suspended perpendicular to the top surface, in a locating divot of the device. The top surface was then wiped and an average of the maximum weight measured was taken. Values for this were observed between 157 g and 208 g, with an average of 172.2 g. The lower portion of the *basket* was filled with lead until the basket *and* contents weighed 172.2g.

4.2 Analysis

In SEM BSE imaging, as much as the keV influences the distinction of features, the brightness of features between setups can be the effect of brightness, contrast, and threshold. These are all variables which have the propensity to change between runs as a result of human error or, in the case of brightness and contrast, even during a run due to physical limitations of the instrument. Thermionic emission SEMs utilise a sacrificial process to release electrons (Bloomer, 1957) which sees the tungsten filament life limited to around 100 hours (Khursheed, 2010). As a result of this heating process, these SEMs can suffer from a variety of drift errors caused by vibration or thermal expansion (Jin & Li, 2015). These drift errors can move the image or alter the brightness and contrast of the images. The image shift issue over time was compensated by including a 10% overlap in frames. This overlap provides a buffer which then allows the program to move the images to maintain alignment without losing detail. The brightness and contrast issues were overcome by the routine checking of the image against a calibration standard and automatic brightness and contrast alteration by the program. This, however, relies on initial set up and parameters used when performing these calibration checks.

This calibration check was where another issue with the AZtec software was encountered. Each automation area can be set with separate working distances as to achieve as near perfect focus. This is due to the possibility of the working distance on one sample being different on the other due to a height difference caused by the physical setup. The separate working distance setting makes itself an issue when analysing the calibration standard as in run checks will be done at the working distance set for the stub it is currently analysing, not of the calibration standard. As a result, the grey levels of each element might change due to them being slightly out of focus, the extent of which will differ between stubs due to the variation in working distance being applied to the standard. Not only this, but human error is brought into play again as the degree to which the first stub is in focus is near impossible to replicate for the second stub. As such, a reference stub known to contain GSR was employed to combat these discrepancies. This was an identical aluminium stub with a carbon adhesive which had been placed down range of the universal receiver, facing it, and shot at using the same ammunition as was used for the experiment. This ensures it has a high concentration of particles, representative to what is seen from that ammunition. Once focus is found on the reference stub, this same working distance is then applied to the calibration standard and sample stubs. This ensures the calibration standard will be at the same working distance during in-run checks for each stub and both sample stubs are treated equally in terms of focus. This is a limitation to this study as it may result in an unequal treatment of each stub as the reference stub may be closer to the correct working distance for one stub or the other. Despite this, this method was determined to be the fairest method and the method which achieved more

consistent results due to the calibration standard being in a consistent degree of focus throughout the run.

Another limitation to this study is the lack of repeated analysis on each stub. Ideally, a 90-degree rotation followed by re-analysis would allow for an estimation as to the error rates of the SEM and the process. This was not possible, however, due to the time associated with each run and limitations of this study's duration. Higher consistency of beam strength would allow for lower error rates and subsequent ability for longer run times. This would result in less time wasted due to failed runs, downtime due to filament replacement, and the improved reliability would allow for longer run times and an increased magnification. To achieve this, and as is currently used in the industry, an SEM with a field emmission gun would be more suitable for this or a similar study. Time was also the reason no manual review was conducted on larger particles that may have been a result of clustering. As such, this limitation of this study calls in to question the accuracy of the population results.

Due to the time allotted for the experiment in conjunction with the time for a run to complete, the number for repetitions was inconsistent. As the focus was on the persistance of IGSR on 3D-printed polymer surfaces, the highest number of repeats were conducted on the 3D-printed surfaces. This included the baseline experiment as to provide a solid foundation on which the expected proportions were based. Lower priority was given to the persistance on the metallic surface but inclusion was necessary to provide a reference point on traditional firearm materials due to the lack of information available on this specific subject. Ideally repeated would be pletiful and equal, but that was not the case for this study. Another issue that arose regarding repetitions was the subsequent need to discount an exhibit. This was due to dropping the exhibit within the laboratory. As the laboratory was used for heavy metal analysis the risk of contamination as well as an unquantifiable force having disrupted the IGSR particles was considered too great and analysis was not completed.

4.3 Results

A seemingly unique profile was created by each set of shots, regarding both particle size (*figure 3.10*) and composition (*figure 3.16*). This variance occurring between shots is more than likely a result of random chance. Of course, it might have simply been due to error caused by the instruments, for which repetition of the sample analysis would be the remedy. It may also be due to random chance and will differ just as greatly between every shot. On polymer FDM surfaces, these profiles were comparable between sides and indeed after wiping indicating value in GSR evidence even after tampering. This similarity is not replicated, in respect to the chemical composition, on the machined surfaces akin to traditional firearms. This may arise due to the different number of repeats, but the maintained proportions of particle size but not chemistry on the metallic baseline exhibits signals discrepancies in the interactions of particles and the substrate being dependent on their composition rather than the issue being the repeats. This would seem to discredit the ability to match GSR profiles between scenes or people and a firearm as it could be said the composition of the initial deposited population can change significantly depending on where on a machined metallic surface a sample is taken. However, a localised effect on an otherwise undisturbed population based on chemistry alone is unlikely. It may be the result of a static charge within the particles or the metallic surface itself but is more likely the result of the metallic surface being a harder material. One would expect this to still produce a repeatable effect seen across both sides, but this could instead be introducing another point of variability that just happened to be characterised in this way. This is attests to the need to then measure population persistence across a range materials of differing surface hardnesses with a constant Ra value or testing of the exhibits to ensure a hardness equal to that of the metallic sampling surface. Only then could persistence differences be attributed solely to the surface roughness.

It could be that the same mechanism that randomly inhibits adhesion of particles on the metallic surface is the same mechanism that allows the particles to embed and resist transfer on FDM polymer surfaces. In the case of polymer exhibits, this would allow more particles, and therefore a more representative sample, to adhere to the substrate. This interaction is difficult to quantify as PLA and EN8 steel differ so vastly regarding hardness properties, they appear on entirely different scales. Plastics appear on a Shore hardness scale (Smooth-On, Inc., 2019) with PLA appearing on the scale at Shore D with a value in the low 80s (Prusa Polymers, 2022, Ultimaker, 2022). The scale on which metals are measured, however, begins at a much higher hardness and can be in Rockwell or Brinell. EN8 steel forexample, has a Brinell score of 201-255 (Smiths Metal Centres, 2023). It is therefore incredibly difficult to accurately compare hardness as there is no practical need to publish such data. As a result, to obtain this comparison, hardness testing on the same machine would have needed to be completed alongside this study. Further testing of intermediate materials would also need to be undertaken to determine exactly the nature of the correlation between hardness and particle behaviour from a persistence and variability standpoint.

The difference in variance could be due to the method in which samples were taken. As FDM polymer samples were taken from a different exhibit each time (A & B samples for each exhibit), the surface roughness resulting from the temperature of the material and environment at the time of extrusion may

change. Even how level the bed is and backlash in the z-axis lead screw would affect the ‘squish’ of the first layer which, in this experiment, was also the sampling surface. The metallic surface samples, on the other hand, were all taken from the same surface which was merely cleaned between shots allowing for more consistency in interactions between the medium and the GSR or stubs. Of course, variation in IGSR produced by the ammunition itself could be to blame with factory ammunition having a higher level of pressure inconsistencies, displaying as inconsistent velocities, compared to home loaded ammunition.

5- Conclusions of this Study

In conclusion, the rate of retention of GSR particles on FDM polymer surfaces was a mean of 35% higher than on metallic surfaces showing a higher persistence. On polymer surfaces, the retention or loss was experienced equally by all particles regardless of size and composition. This may suggest that polymer surfaces not only retain a larger population of IGSR particles but also retain a group of particles more representative of the wider population produced by firing. This improves the likelihood of being able to match ammunition types or shot combinations if polymer surfaces are present in the scene and sampled. On the other hand, baseline testing of metallic exhibits indicated an unequal proportion of deposited particles between sides based on chemical composition despite equal proportions of size ranges. This non-significance found regarding particle size distribution combined with the significant difference of composition observed could also indicates particle size and composition are two unrelated characteristics of the IGSR population produced during shots.

A higher variance in the populations was also observed for the polymer exhibits when compared to the metallic surface. This variance was likely due to changes in the FDM polymer exhibits caused by differences in the surface characteristics between exhibits. An improvement to the experiment and a consideration for future studies would be the standardisation of the exhibits themselves. The use of a 3D printer that conducts a bed levelling procedure with a predetermined z-offset before each print as well as surface roughness characterisation using an atomic force microscope would be advantageous. Standardising or quantifying these variables that may affect the retention of IGSR particles may allow for variances in the retention between exhibits to be attributed to the surface roughness if a correlation is present.

As the retention of particles was not concentrated towards the range of sizes smaller than the troughs observed in the surface morphology of the medium, it can be inferred that retention was instead affected a property shared by the whole surface. This could be a product of the hardness of the substrate allowing particles of all sizes to impress themselves into the surface enough to resist a locomotive force, but not enough to resist sampling which applied force at a normal angle to the surface. A study on the retention of particles across a range of materials of differing hardnesses on the same scale may be necessary to make this conclusion. Not only this, but a range of surface roughnesses and shapes of these recessions could be tested to determine if surfaces have a critical value for the GSR retained dependent on these factors.

The results that the wiped sides more accurately represent the original population of GSR than when both sides were unwiped may indicate a certain level variance that is negated by the wiping. Although a stretch, it is possible the wiping sheds excess particles in a similar fashion to knocking off loose glitter which could support the theory of a critical value of GSR that a surface can hold. A test comparing the variance in proportions of particle size and composition would need to be conducted where both sides are wiped to determine if any difference in respective proportions is retained after wiping or if this process brings these profiles closer to agreement.

There is a long way to go before the behaviour of IGSR evidence on this new medium is understood and how forensic awareness of criminals affects the retention of the information contained by this evidence type. It is worth emphasising the idea that when discussing a new medium, all knowledge of *any* trace evidence and their interactions with surfaces are back at square one. Until the same tests are performed and results observed on these new substrates, standard operating procedures should not apply. Even the constant development by engineers to create “fingerprint” resistant coatings (Belhadjamor, 2018) may change our understanding of what is considered an ideal surface to develop finger marks from. A 2017 study by Kesmez found this to be the case even if the surface roughness is lower than that of the machined surfaces seen in the research conducted in this paper (Kesmez, et al., 2017). Thorough understanding of even development techniques and when their application is suitable is needed. Testing of previous and proposal of new techniques should include empirical information of the substrate it was tested upon including hardness and surface roughness measurements. Future studies would do well to test these techniques on unintended surfaces or a variety of surfaces which differ in surface roughness or hardness than that of the intended. The methodology employed in a 2020 study by H. Barros is a good example having included the testing of the new methods on non-porous surfaces despite an initial focus of efficacy on porous surfaces (Barros, et al., 2020).

Changes caused by developments in manufacturing processes as well as post processing will result in constant changes to the hierarchy of evidence types regarding the value they bring to an investigation. Therefore, before a forensic strategy is settled upon, careful consideration using information such as surface hardness, roughness, and coatings and their interactions with different trace evidence types must be exercised. 3D prints and their polymers unveil opportunities with which associations of exhibits to crime scenes may be made. Works such as Blacks’ study in 2017 investigated the analysis of polymers residue on the bullets themselves and the dyes within them allowing for the identification of the type, colour, and even brand of filament used to create a firearm (Black, et al., 2017). This was done using fully 3D printed firearms and required the bullet to make contact with the polymer itself which was uncommon as hybrid or rails-down prints are a much more popular option. However, the reemergence of fully printed firearms including print-in-place pistols and even 3D printed sound moderators may bring this method back into relevancy. Changes in legislation that occur constantly change what is a chargeable offence and may declassify or classify firearm accessories and parts (The National Archives, 2026). These changes would also alter what components the police would need to test in lower severity possession charges to prove use as a firearm part as opposed to use with airguns.

6- Future works

For future works, it is important to update standards as technology is made available. Therefore, for future studies, the use of a field emission gun SEM is advised to maintain a more stable beam and reduce errors that may have resulted from the equipment when analysing stubs of each exhibit. Being able to keep a beam stable for longer allows for the loading and running of more samples under each setup which would reduce the effect of human error on the results. Further reducing opportunities for variability to arise is recommended as well as identifying when variance is affecting the results. As such, repeat analysis of each stub would be suggested in any continued work.

Eliminating sources of variance would confirm or disprove the theory of each shot produces a unique profile. Due to the seemingly unique profiles produced by a specific set of shots, any future studies that wish to investigate the difference in profiles observed on metallic and polymer surfaces must be done by exposing metallic and polymer surfaces to the same shots before to produce the same proportions of sizes/compositions. Single shot testing between sides to determine the variability in profiles between shots should also be undertaken to verify the presence of these seemingly unique profiles. If these 'unique' individual and average profiles exist, it is likely to disrupt investigations aiming to differentiate GSR evidence between specific ammo brands. It may, however, indicate the ability to match two sources of GSR. This could be between firearm and a scene or the like, provided no contamination has occurred and enough particles are contained in the samples. This evidence may be extremely valuable on polymer exhibits given that these profiles did not differ significantly even after simulated evidence tampering (wiping), unlike as was seen on metallic surfaces. Further investigation conducted on the apparent discrepancies of proportions of composition observed between sampling areas on metallic exhibits should include whether variance changes between brands.

Further variables such as barrel length, grain values of the ammunition and size of the grains should also be investigated to assess the possible influence of these factors on the production of IGSR with regards to particle size and composition due to their effects on peak pressure and temperature.

7- References

Abraham, J. et al., 2012. Saliva Samples are a Viable Alternative to Blood Samples as a Source of DNA for Hight Throughput Genotyping. *BMC Medical Genomics,* 5(19), pp. 1-6.

Acquafredda, P., Andriani, T., Lorenzoni, S. & Zanettin, E., 1999. Chemical Characterization of Obsidians from Different Mediterranean Sources by Non-destructive SEM-EDS Analytical Method. *Journal of Archaeological Science,* 26(3), pp. 315-325.

Akhavan, J., 2004. *The Chemistry of Explosives.* 2nd ed. Cambridge: The Royal Society of Chemistry.

Aliste, M. & Chávez, L., 2016. Analysis of Gunshot Residues as Trace in Nasal Mucus by GFAAS. *Forensic Science International,* Volume 261, pp. 14-18.

Alsoufi, M. & Elsayed, A., 2017. How Surface Roughness Performance of Printed Parts Manufactures by Desktop FDM 3D Printer with PLA+ is Influenced by Measuring Direction. *American Journal of Mechanical Engineering,* 5(5), pp. 211-222.

Amaral, M., Gibson, A. & Morgan, R., 2022. Trace Evidence Dynamics of Cocaine on Banknotes: A comparison study of paper and polymer banknotes. *Science and Justice,* 62(2), pp. 221-228.

American Society for Testing and Materials, 2020. *iTeh, Inc.*. [Online]
Available at:
https://cdn.standards.iteh.ai/samples/107250/b45a9f3054a148dc9d35d53cece01a50/ASTM-E1588-20.pdf
[Accessed 1st December 2024].

Ammo.com, 2024. *Berdan vs Boxer Primed Ammo:*. [Online]
Available at: https://ammo.com/primer-type/berdan-vs-boxer
[Accessed 28th 10 2024].

Ammo.com, 2024. *Berdan vs Boxer Primed Ammo: What's the Difference.* [Online]
Available at: https://ammo.com/primer-type/berdan-vs-boxer
[Accessed 29th 10 2024].

Anastassopoulou, J., 2003. Metal-DNA Interactions. *Journal of Molecular Structure,* Volume 651-653, pp. 19-26.

Apatoff, J. & Norwitz, G., 1973. *Role of Diphenylamine as a Stabiliser in Propellants; Analytical Chemistry of Diphenylamine in Propellants (A Survey Report),* Philadelphia (US): U.S. Army Armament Command.

Arndt, J. et al., 2012. Preliminary Evaluation of the Persistence of Organis Gunshot Residue. *Forensic Science International,* Volume 222, pp. 137-145.

Barnett, P. & Berger, R., 1976. The Effects of Temperature and Humidity on the Permeanency of Latent Fingerprints. *Journal of the Forensic Science Society,* 16(3), pp. 249-254.

Barros, H., Tavares, L. & V., S., 2020. Dye-doped Starch Microparticles as a Novel Fluorescent Agent for the Visualization of Latent Fingermarks on Porous and Non-porous Substrates. *Forensic Chemistry,* Volume 100264, pp. 1-13.

Basu, S., 1982. Formation of Gunshot Residue. *Journal of Forensic Sciences,* 27(1), pp. 72-91.

Batchelder, J., 1997. *Method for Controlled Porosity Three-Dimensional Modeling.* United States, Patent No. 5,653,925.

Belhadjamor, M., El Mansori, M., Belghith, S. & Mezlini, S., 2018. Anti-fingerprint Properties of Engineering Surfaces: A review. *Surface Engineering,* 34(2), pp. 85-120.

Beníček, L., Vašina, M. & Hrbáček, P., 2025. Influence of 3D Printeng Conditions on Physical-Mechanical Properties of Polymer Materials. *Polymers,* 17(43), pp. 1-21.

Berk, R., 2009. Automated SEM/EDS Analysis of Airbag Residue. II: Airbag residue as a source of percussion primer residue particles. *Journal of Forensic Sciences,* 54(1), pp. 69-76.

Black, O., Cody, R., Edwards, D. & Cizdziel, J., 2017. Identification of Polymers and Organic Gunshot Residue in Evidence from 3D-Printed Firearms using DART-Mass Spectrometry: A feasibility study. *Forensic Chemistry,* Volume 5, pp. 26-32.

Blakey, L., Sharples, G., Chana, K. & Birkett, J., 2018. Fate and Behaviour of Gunshot Residue- A Review. *Journal of Forensic Sciences,* 63(1), pp. 9-19.

Bloomer, R., 1957. The Lives fo Electron Microscope Filaments. *British Journal of Applied Physics,* 8(83), pp. 83-85.

Bohn, M., 2018. *Principles of Ageing of Double Base Propellants and its Assessment by Several Methods Following Propellant Properties.* Fraunhofer, NATO Science and Technology Organisation.

Bond, J., Phil, D. & Heidel, C., 2009. Visualisation of Latent Fingerprint Corrosion on a Discharged Brass Shell Casing. *Journal of Forensic Science,* 54(4), pp. 892-894.

Bonsu, D., Higins, D. & Austin, J., 2020. Forensic Touch DNA Recovery from Metal Surfaces- A review. *Science & Justice,* 60(3), pp. 206-215.

Brede, U., Hagel, R., Redecker, K. & Weuter, W., 1996. Primer Compositions in the Course of Time: From Black Powder and SINOXID to SINTOX Compositions and SINCO Booster. *Propellants, Explosives, Pyrotechnics,* Volume 21, pp. 113-117.

Brewer, P. & Ley, B., 2010. Media Use and Public Perceptions of DNA Evidence. *Science Communication,* 32(1), pp. 93-117.

Brownells UK, 2025. *AR-15 KP-15 STRIPPED LOWER RECEIVERS POLYMER - KE ARMS KP-15 STRIPPED LOWER RECEIVER POLYMER BLACK.* [Online]
Available at: https://www.brownells.co.uk/AR-15-MK-3-STRIPPED-LOWER-RECEIVERS-POLYMER
[Accessed 23rd January 2025].

Brożek-Mucha, Z., 2011. Chemical and Morphological Study of Gunshot Residue Persisting on the Shooter by Means of Scanning Electron Microscopy and Energy Dispersive X-Ray Spectrometry. *Microscopy and Microanalysis,* Volume 17, pp. 972-982.

Brożek-Mucha, Z., 2014. Scanning Electron Microscopy and X-Ray Microanalysis for Chemical and Morphological Characterisation of the Inorganic Component of Gunshot Residue: Selected Problems. *BioMed Research International,* Volume 428038, pp. 1-11.

Brożek-Mucha, Z., 2017. Trends in Analysis of Gunshot Residue for Forensic Purposes. *Analytical and Bioanalytical Chemistry,* 409(25), pp. 5803-5811.

Burduhos-Nergis, D.-P.et al., 2023. Phosphate Conversion Coating- A short review. *Archives of Metallurgy and Materials,* 68(3), pp. 1029-1034.

Bureau of Alcohol, Tobacco, Firearms and Explosives, 2023. *ATF Publications Library.* [Online]
Available at: https://www.atf.gov/file/177016/download
[Accessed 29th January 2025].

Burrill, J., Daniel, B. & Frascione, N., 2019. A Review of Trace "Touch DNA" Deposits: Variability factors and an exploration of cellular composition. *Forensic Science International: Genetics,* Volume 39, pp. 8-18.

Butler, J., 2015. The Future of Forensic DNA Analysis. *Philosophical Transactions B,* 370(1674), pp. 1-10.

Butler, J., Joy, D., Bradley, G. & Krause, S., 1995. Low-voltage Sacnning Electron Microscopy of Polymers. *Polymer,* 36(9), pp. 1781-1790.

Cardinetti, B. et al., 2004. X-Ray Mapping Technique: a preliminary study discriminating gunshot residue particles from aggregates of environmental occupational origin. *Forensic Science International,* Volume 143, pp. 27-46.

Chacón, J., Caminero, M., García-Plaza, E. & Núñez, P., 2017. Additive Manufacturing of PLA Structures using Fused Deposition Modelling: Effect of process parameters on mechanical properties and their optimal selection. *Materials and Design,* Volume 124, pp. 143-157.

Chang, K., Jayaprakash, P., Yew, C. & Abdullah, A., 2013. Gunshot Residue Analysis and its Evidential Values: a review. *Australian Journal of Forensic Sciences,* 45(1), pp. 3-23.

Charles, S., Geusens, N., Vergalito, E. & Nys, B., 2020. Interpol Review of Gunshot REsidue 2016-2019. *Forensic Science International: Synergy,* Volume 2, pp. 416-428.

CHEMOS, 2023. *Safety Data Sheet: Antimony(V) sulfide*. [Online]
Available at: https://www.chemos.de/import/data/msds/GB_en/1315-04-4-A0287757-GB-en.pdf
[Accessed 27th November 2024].

Chen, C. et al., 2019. The Effect of Climatic Simulations on DNA Persistence on Glass, Cotton, and Polyester. *Forensic Science International: Genetic supplement series,* 7(1), pp. 274-276.

Costa, R. et al., 2016. Gunshot Residues (GSR) Analysis of Clean Range Ammunition Using SEM/EDX, Colorimetric Test, and ICP-MS: A comparitive approach between the analytical techniques. *Microchemical Journal,* Volume 129, pp. 339-347.

Crawford, B., Huggett, C. & McBrady, J., 1950. The Mechanism of the Burning of Double Base Propellants. *Journal of Physical and Colloid Chemistry,* 54(6), pp. 854-862.

Creality, 2025. *Creality Ender 3 3D Printer*. [Online]
Available at: https://www.crealityofficial.co.uk/products/official-creality-ender-3-3d-printer
[Accessed 7th February 2025].

Crewe, A., Isaacson, M. & D., J., 1969. A Simple Scanning Electron Microscope. *Review of Scientific Instruments,* 40(2), pp. 241-246.

Cukier, W. & Sheptycki, J., 2012. Globalization of Gun Culture Transnational Reflections on Pistolization and Masculinity, Flows and Resistance. *International Journal of Law, Crime and Justice,* Volume 40, pp. 3-19.

Curtis, C., 2009. Public Perceptions and Expectations of the Forensic Used of DNA. *Bulletin of Science, Technology & Society,* 29(4), pp. 313-324.

Daéid, N., 2004. An Introduction to Fires and Fire Investigation. In: N. Daéid, ed. *Fire Investigation.* Boca Raton (US), London (GB), New York (US), Washington D.C. (US): CRC Press, pp. 1-12.

Dalby, O., Butler, D. & Birkett, J., 2010. Analysis of Gunshot Residue and Associated Materials- A Review. *Journal of Forensic Sciences,* 55(4), pp. 924-943.

Daly, A., Mann, M., Squires, P. & Walters, R., 2020. 3D Printing, Policing and Crime. *Policing and Society,* 31(1), pp. 37-51.

De Forest, P., 2001. What is Trace Evidence?. In: B. Caddy, ed. *Forensic Examination of Glass and Paint: Analysis and Interpretation.* London (GB), New York (US): Taylor and Francis, pp. 1-24.

Defanti, B., Mendonça-Filho, L. & Nichele, J., 2020. Effect of Aging on the Combustion of Single Base Propellants. *Combustion and Flame,* Volume 221, pp. 212-218.

Demircioğlu, D. et al., 2024. Beyond the Shot: Exploring secondary transfer of gunshot residue on common surfaces and the impact of hand cleaning methods. *Foresnic Science International,* 361(112135), pp. 1-13.

Dent, K., Veilleux-Lepage, Y. & Zuppello, M., 2023. *Global Internet Forum to Counter Terrorism.* [Online] Available at: https://gifct.org/wp-content/uploads/2023/09/GIFCT-23WG-0823-3DPrinting-1.1.pdf [Accessed 28th May 2025].

Dulloo, A. et al., 1998. Detection Limits of a Laboratory Pulsed Gamma Neutron Activation Analysis System for the Nondestructive Assay of Mercury, Cadmium, and Lead. *Nuclear Technology,* 123(1), pp. 103-112.

Feeney, W., Pyl, C., Bell, S. & Trejos, T., 2020. Trends in Composition, Collection, Persistence, and Analysis of IGSR and OGSR: A review. *Forensic Chemistry,* 19(100250), pp. 1-16.

Frihart, C. & Beecher, J., 2022. *Binders for Small-Caliber Gun Primers: Understanding Gum Arabic and Exploring Possible Synthetic Replacements,* Madison (US): U.S. Department of Agriculture.

Garofano, L. et al., 1999. Gunshot Residue Further Studies on Particles of Environmental and Occupational Origin. *Forensic Science International,* Volume 103, pp. 1-21.

Gashi, B. et al., 2010. Measurement of 9 mm Cartridge Case External Temperatures and its Forensic Application. *Forensic Science International,* Volume 200, pp. 21-27.

Gassner, A.-L.et al., 2016. Organic Gunshot Residues: Observations about sampling and transfer mechanisms. *Forensic Science International,* Volume 266, pp. 369-378.

Girod, A., Ramotowski, R. & Weyermann, C., 2012. Composition of Fingermark Residue: A qualitative and quantitative review. *Forensic Science International,* 223(1-3), pp. 10-24.

Glaskova-Kuzmina, T. et al., 2023. Effect of Post-Printing Cooling Conditions on the Properties of ULTEM Printed Parts. *Polymers,* 15(324), pp. 1-14.

Glock inc., 2025. *Glock Technology.* [Online]
Available at: https://us.glock.com/en/learn/glock-pistols/technology
[Accessed 23rd January 2025].

Goia, S. et al., 2024. The Use of Micro-CT in the Investigation of a Case Involving 3D Printed Weapons. *Forensic Science International,* 363(112157), pp. 1-11.

Goldstein, J. et al., 2003. *Scanning Electron Microscopy and X-Ray Microanalysis.* 3rd ed. New York (US): Springer Science + Business Media.

Good, P., 2004. *Permutation, Parametric, and Bootstrap Tests of Hypotheses.* 3rd ed. New York (US): Springer.

Goudsmits, E. et al., 2019. The Analysis of Organic and Inorganic Gunshot Residue from a Single Sample. *Forensic Science International,* Volume 299, pp. 168-173.

Goudsmits, E., Sharples, G. & Birkett, J., 2015. Recent Trends in Organic Gunshot Residue Analysis. *TrAC- Trends in Analytical Chemistry,* Volume 74, pp. 46-57.

Gov.uk, 1982. *Firearms Act 1982.* [Online]
Available at: https://www.legislation.gov.uk/ukpga/1982/31
[Accessed 12th May 2025].

GOV.UK, 2020. *GOV.UK.* [Online]
Available at: https://www.google.com/url?sa=t&rct=j&q=&esrc=s&source=web&cd=&ved=2ahUKEwi-lZefrf-JAxVVQ0EAHXMqJuMQFnoECAwQAQ&url=https%3A%2F%2Fassets.publishing.service.gov.uk%2Fmedia%2F5e1f3439e5274a4f08f3c5ed%2Fntsq02001.ods&usg=AOvVaw1_KMODYZHfX7DteXgXI04Y&opi=89978
[Accessed 28th November 2024].

Grabmüller, M., Cachée, P., Madea, B. & Courts, C., 2016. How Far Does It Get?- The effect of shooting distance and type of firearm on the simultaneous analysis of DNA and RNA from backspatter recovered from inside and outside surfaces of firearms. *Forensic Science International,* Volume 258, pp. 11-18.

Greenberg, R., Bode, P. & De Nadai Fernandes, E., 2011. Neutron Activation Analysis: A primary method of measurement. *Spectrochimia Acta Part B: Atomic Spectroscopy,* 66(3-4), pp. 193-241.

Grima, M., Butler, M., Hanson, R. & Mohameden, A., 2012. Firework Displays as Sources of Particles Similar to Gunshot Residue. *Science and Justice,* Volume 52, pp. 49-57.

Grossel, S., 2002. *Deflagration and Detonation Flame Arresters.* New York (US): American Institute of Chemical Engineers.

Hannigan, T. et al., 2015. Evaluation of Gunshot Residue (GSR) Evidence: Surveys of prevalence of GSR on clothing and frequency of residue types. *Forensic Science International,* Volume 257, pp. 177-181.

Hays, G. & Jenzen-Jones, N., 2018. *Beyond State Control: Improvised and craft-produced small arms and light weapons,* Geneva (CH): Small Arms Survey.

Heard, B., 2008. *Handbook of Firearms and Ballistics.* 2nd ed. Chichester (GB), Oxford (GB), New Jersey (US): John Wiley & Sons, LTD..

Houck, M., Crispino, F. & McAdam, T., 2018. *The Science of Crime Scenes.* 2nd ed. London (GB), San Diego (US), Cambridge (US), Oxford (GB): Academic Press.

Houck, M. & Siegel, J., 2016. *Fundamentals of Forensic Science.* 3rd ed. Oxford (GB), San Diego (US): Academic Press.

House of Commons- Science and Technology Comittee, 2005. *Forensic Science on Trial- Seventh report of session 2004-05,* London: The House of Commons.

Hueske, E., 2008. *Firearms and Fingerprints.* New York (US): Facts on File.

Hueske, E., 2009. *Essentials of Forensic Science: Firearms and Fingerprints.* New York: Facts On File, Inc..

Hughes, D. et al., 2021. Impact of Surface Roughness on the Deposition of Saliva and Fingerprint Residue on Non-porous Substrates. *Forensic Chemistry,* 23(100318), pp. 1-11.

Jasni, N. & Lajis, M., 2013. Surface Topography in Machining of AISI D2 Hardened Steel. *Applied Mechanics and Materials,* Volume 315, pp. 660-664.

Jenzen-Jones, N., 2015. Small Arms and Additive Manufacturing: An assessment of 3D-printed firearms, components, and accessories. In: G. M. B. King, ed. *Behind the Curve: New Technologies, New Control Challenges.* Geneva (CH): Small Arms Survey, pp. 43-74.

JEOL USA, Inc. , 2020. *A Guide to Scanning Microscope Observation.* [Online]
Available at: https://www.jeolusa.com/RESOURCES/Electron-Optics/Documents-Downloads/a-guide-to-scanning-microscope-observation
[Accessed 7th January 2024].

Jin, P. & Li, X., 2015. Correction of Image Drift and Distrotion in a Scanning Electron Microscopy. *Journal of Microscopy,* 260(3), pp. 1-13.

Joy, D. & Newbury, D., 2002. Low Voltage Scanning Electron Microscopy. *Cambridge University Press,* 10(2), pp. 22-23.

Kafle, A. et al., 2021. 3D/4D Printing of Polymers: Fused Deopsition Modelling (FDM), Selective Laser Sintering (SLS), and Stereolithography (SLA). *Polymers,* 13(18 (3101)), pp. 1-37.

Kalpakjian, S., Schmid, S. & Sekar, K., 2021. *Manufacturing Engineering and Technology.* 7th (SI) ed. Harlow (UK): Pearson Education Limited.

Kanaya, K. & Okayama, S., 1972. Penetration and Energy-Loss Theory of Electons in Solid Targets. *Journal of Physics D: Applied Physics,* 5(1), pp. 43-58.

Kaplan, J., Ling, S. & Cuellar, M., 2020. Public Beliefs about the Accuracy and Importance of Forensic Evidence in the United States. *Science & Justice,* Volume 60, pp. 263-272.

Kara, İ., 2022. The Relationship Between Gunshot-Residue Particle size and Botlzmann Distribution. *Forensic Science research,* 7(1), pp. 47-52.

Kara, I. et al., 2015. The Relationship Between the Surface Morphology and Chemical Composition of Gunshot Residue Patricles. *Journal of Forensic Sciences,* 60(4), pp. 1030- 1033.

Kara, I., Sarikavak, Y., Lisesivdin, S. & Kasap, M., 2016. Evaluation of Morphological and Chemical Differences of Gunshot Residues in Different Ammunitions Using SEM/EDS Technique. *Environmental Forensics,* 17(1), pp. 68-79.

Kara, İ. & Yalçinkaya, Ö., 2017. Evaluation of Persistance of Gunshot Residue (GSR) using Graphite Furnace Atomic Absorption (GFAAS) Method. *Bulgarian Chemical Communications,* 49(1), pp. 101-108.

Kesmez, Ö. et al., 2017. Fingerprint Resistant Coatings for Stainless Steel Substrates. *Progress in Organic Coatings,* Volume 112, pp. 51-56.

Khursheed, A., 2010. *Scanning Electron Microscope Optics and Spectrometers.* New Jersey (US), London (GB), Singapore (SG), Beijing (CN), Shanghai (CN), Hong Kong (HK), Taipei (TW), Chennai (IN): World Scientific.

Kim, K., Akase, Z., Suzuki, T. & Shindo, D., 2010. Charging Effects on SEM/SIM Contrast of Metal/Insulator System in Various Metallic Coating Conditions. *Materials Transactions,* 51(6), pp. 1080-1083.

Koehler, J., 2001. The Psychology of Numbers in the Courtroom: How to Make DNA-Match Statistics Seem Impressive or Insufficient. *Southern California Law Review,* 74(5), pp. 1275-1305.

Leikin, S. & Phillips, A., 2023. ICP-OES as a Viable Alterntive to ICP-MS for Trace Analysis: Meeting the Detection Limits Challenge. *Spectroscopy*, 1st October, pp. 7-13.

Liu, J., 2000. High-Resolution and Low-Voltage FE-SEM Imaging and Microanalysis in Materials Characterization. *Materials Characterization,* 44(4-5), pp. 353-363.

Li, X. et al., 2024. A Study on the Measurement of GSR with Bloodstains by ICP-MS. *Forensic Sciences Research,* 9(4), pp. 1-7.

Lucas, A., 1923. The Examination of Firearms and Projectiles in Forensic Cases. *Analyst,* 48(566), pp. 203-248.

Lucas, N. et al., 2016. A Study into the Distribution of Gunshot Residue Particles in the Random Population. *Forensic Science International,* Volume 262, pp. 150-155.

Margo, L., Shoemake, C., Inglott, A. & Azzopardi, L., 2015. Chemical Enhancement of Fingerprints on Various Porous and Non-porous Surfaces. *Indian Journal of Forensic Medicine & Toxicology,* 9(1), pp. 229-234.

Marshall, M. & Oxley, J., 2009. Explosives: The Threats and the Materials. In: J. O. M. Marshall, ed. *Aspects of Explosive Detection.* Amsterdam (NL), Oxford (GB): Elsevier Science, pp. 11-26.

Mavri, M., Fronimaki, E. & Kadrefi, A., 2023. Survey Analysis for the Adoption of 3D Printing Technology: Consumers' perspective. *Journal of Science and Technology Policy Management,* 14(2), pp. 353-385.

McTee, M. et al., 2025. Evaluating the Precision and Velocity of Factory vs. Handloaded Lead-free Ammunition. *Wildlife Society Bulletin,* 49(1), pp. 1-14.

Minzière, V. et al., 2022. The Relevance of Gunshot Residues in Forensic Science. *WIREs Forensic Science,* 5(1), pp. 1-26.

Minzière, V., Robyr, O. & Weyermann, C., 2023. Should Inorganic or Organic Gunshot Residues be Analysed First?. *Forensic Science International,* 348(111600), pp. 1-13.

Mohammed, A. & Abdullah, A., 2018. *Scanning Electron Microscopy (SEM): A review.* Băile Govora, International Conference on Hydraulics and Pneumatics - HERVEX.

Montgomery, D. & Runger, G., 2003. *Applied Statistics and Probability for Engineers.* 3rd ed. New York (US): John Wiley & Sons, Inc..

Moran, J. & Bell, S., 2014. Skin Permeation of Organic Gunshot Residue: Implications for Sampling and Analysis. *Analytical Chemistry,* 86(12), pp. 6071-6079.

Morgan, R., Meakin, G., French, J. & Nakhaeizadeh, S., 2019. Crime Recontruction and the Role of Trace Materials from Crime Scenes to Court. *WIREs Forensic Science,* 2(1), p. e1364.

Moule, E. et al., 2017. Silver-assisted Development and Imaging of Fingermarks on Non-porous and Porous Surfaces. *Internation Journal of MAss Spectrometry,* Volume 422, pp. 27-31.

M-Vac Systems, Inc., 2017. *Bardole DNA Collection Method.* [Online]
Available at: https://www.m-vac.com/why-mvac/research/bardole-dna-collection-method
[Accessed 3rd October 2024].

Nanakoudis, A., 2019. *SEM: Types of Electrons and the Information the Provide.* [Online]
Available at: https://www.thermofisher.com/blog/materials/sem-signal-types-electrons-and-the-information-they-provide
[Accessed 14th May 2025].

Nash, M., Maskall, J. & Hill, S., 2000. Methodologies for Determination of Antimony in Terrestrial Evironmental Samples. *Journal of Evironmental Monitoring,* 2(2), pp. 97-109.

Nasrazadani, S. & Hassani, S., 2016. Modern Analytical Techniques in Failure Analysis of Aerospace, Chemical, and Oil and Gas Industries. In: A. Makhlouf & M. Aliofkhazraei, eds. *Handbook of Materials Failure Analysis with Case Studies from the Oil and Gas Industry.* Amsterdam (NL), Boston (US), Heidelberg (DE), London (GB), New York (US), Oxford (GB), Paris (FR), San Diego (US), San Francisco (US), Singapore (SG), Sydney (AU), Tokyo (JP): Butterworth-Heinemann, pp. 39-54.

Nesbitt, G. & Wolten, R., 1980. On the Mechanism of Gunshot Residue Particle Formation. *Journal of Forensic Sciences,* 25(3), pp. 533-545.

Neumann, C. et al., 2016. Presenting Quantitative and Qualitative Information on Forensic Science Evidence in the Courtroom. *Chance,* 29(1), pp. 37-43.

Newbury, D. & Ritchie, N., 2013. Is Scanning Electron Microscopy/Energy Dispersive X-ray Spectrometry (SEM/EDS) Quantitative?. *The Journal of Scanning Microscopies,* 35(3), pp. 141-168.

Nitrera Technologies, Inc., 2025. *Nitriding Options (Q Vs QP Vs QPQ).* [Online]
Available at: https://www.nitrera.com/articles/nitriding-options
[Accessed 11th September 2025].

Noymer, A., 2008. Alpha, Significance Level of Test. *Encyclopedia of Survey Research Methods,* Volume 0, pp. 17-19.

Nunn, S., 2013. Touch DNA Collection Versus Firearm Fingerprinting: Comparing Evidence Production and Identification Outcomes. *Journal of Forensic Sciences,* 58(3), pp. 601-608.

O'Connell, J., 2021. *Non-Planar 3D Printing: All you need to know.* [Online]
Available at: https://all3dp.com/2/non-planar-3d-printing-simply-explained/
[Accessed 6th June 2025].

Ohring, M. & Kasprzak, L., 2015. Characterization and Failure Analysis of Materials and Devices. In: L. K. M. Ohring, ed. *Reliability and Failure of Electronic Materials and Devices.* Amsterdam (NL), Boston (US),

Heidelberg (DE), London (GB), New York (US), Oxford (GB), Paris (FR), San Diego (US), San Francisco (US), Singapore (SG), Sydney (AU), Tokyo (JP): Academic Press, pp. 611-664.

Olivella, M. et al., 2002. A Study of Sulfur Functionalilites in Fossil Fuels Using Destructive- (ASTM and Py-GC-MS) and Non-destructive- (SEM-EDX, XANES, and XPS) Techniques. *Fuel,* 81(4), pp. 405-411.

O'Neal, B., 2014. *Authorities Bust European Crime Network Taking Advantage of 3D Printing Technology for Credit Card Fraud*. [Online]
Available at: https://3dprint.com/17936/3d-print-crime/
[Accessed 4th April 2025].

Organisation of Scientific Area Committees (OSAC) for Forensic Science, 2020. *Standard Practice for Gunshot Residue.* [Online]
Available at:
https://www.nist.gov/system/files/documents/2020/03/20/OSAC%20GSR%20SC%20E1588%20for%20SAC.pdf
[Accessed 19 04 2026].

Organisation of Scientific Area Committees for Forensic Science, 2022. *Organization of Scientific Area Committees (OSAC) for Forensic Science*. [Online]
Available at: https://www.nist.gov/system/files/documents/2022/10/31/OSAC%202021-N-0019%20Stand%20Pract%20for%20the%20Documentation%20and%20Processing%20of%20Shooting%20Scenes_REGISTRY.pdf
[Accessed 27th September 2024].

Organisation of Scientific Area Committees, 2020. *Organization of Scientific Area Committees (OSAC) for Forensic Science.* [Online]
Available at:
https://www.nist.gov/system/files/documents/2020/05/22/OSAC%20GSR%20SEM%20ED%20X-ray%20spec.pdf
[Accessed 8th December 2024].

Oxford Instruments, 2026. *AZtecGSR.* [Online]
Available at: https://nano.oxinst.com/AZtecGSR
[Accessed 3rd 08 2026].

Oxford University Press, 2025. *Oxford English Dictionary*. [Online]
Available at: https://www.oed.com/dictionary/firearm_n?tab=meaning_and_use#4231653
[Accessed 9th January 2025].

Oyler, K., Mehta, N. & Cheng, G., 2015. *Overview of Explosive Initiators,* Picatinny Arsenal (NJ, US): U.S. ARMY ARMAMENT RESEARCH, DEVELOPMENT AND.

Pavlovich, S. & Garrison, K., 2023. An Exploratory Study of Topographical Signatures within 3D Fused Deopsition Modelling Using Polylactic Acid (PLA) Filament. *Forensic Science International,* 349(111740).

Pearlman, S., 2015. *AMMO*. [Online]
Available at: https://www.pearlmanphotography.com/#/ammo/
[Accessed 28th 10 2024].

Petraco, N. & Petraco, N., 2020. A Guide to the Analysis of Forensic Household Dust Specimens and Their Statistical Significance. In: R. Saferstein & A. Hall, eds. *Forensic Sccience Handbook.* Boca Raton, London, New York: CRC Press, pp. 201-244.

Podgornik, B., Kafexhiu, F., Nevosad, A. & Badisch, E., 2020. Influence of Surface Roughness and Phosphate Coating on Galling Resistance of Medium-grade Carbon Steel. *Wear,* Volume 446-447, pp. 1-9.

Pollard, M., Batt, C., Stern, B. & Young, S., 2007. *Analytical Chemistry in Archaeology*. Cambridge (GB), New York (US), Melbourne (AU), Madrid (ES), Cape Town (ZA), Singapore (SG), São Paulo (BR): Cambridge University Press.

Polovková, J., Šimonič, M. & Szegényi, I., 2015. Study of Gunshot Residues from Sitox Ammunition Containing Marking Substances. *Egyptian Journal of Forensic Sciences,* 5(4), pp. 174-179.

Press, W., Teukolsky, S., Vetterling, W. & Flannery, B., 1993. *Numerical Recipes in Fortran 77.* 2nd ed. Cambridge (UK), New York (US), Melbourne (AU): Cambridge University Press.

Prusa Polymers, 2022. *Technical Datasheet.* [Online]
Available at: https://prusament.com/wp-content/uploads/2022/10/PLA_Prusament_TDS_2021_10_EN.pdf
[Accessed 7th September 2025].

Rahman, H. et al., 2025. Practical Guide to Calculate Sample Size for Chi-square Test in Biomedical Research. *BMC Medical Research Methodology,* 25(144), pp. 1-4.

Ramsey, M., 2022. *Persistance of Touch DNA for Forensic Analysis,* Lexington (US): National Criminal Justice Reference Service.

Reba, I., 1966. Applications of the Coanda effect. *Scientific American,* 214(6), pp. 84-93.

Ribeiro, G., Tangen, J. & McKimmie, B., 2019. Beliefs about Error Rates and Human Judgment in Forensic Science. *Forensic Science International,* Volume 297, pp. 138-147.

Ritchie, N. et al., 2020. Proposed Practices for Validating the Performance of Instruments Used for Automated Inorganic Gunshot Residue Analysis. *Forensic Chemistry,* 20(100252), pp. 1-20.

Ritter, J., 2014. *Influence of Berdan and Boxer Primer Split-Hole Diameter on 7.62-mm Cartridge Performance,* Aberdeen: Army Reseearch Laboratory.

Romolo, F. & Margot, P., 2001. Identification of Gunshot Residue: a critical review. *Foresnic Science International,* Volume 119, pp. 195-211.

Roux, C. et al., 2015. The End of the (Forensic Science) World as We Know it? The Example of Trace Evidence. *Philosophical Transactions: Biological Sciences,* 370(1674), pp. 1-8.

Rudzitis, E. & Wahlgren, M., 1975. Firearm Residue Detection by Instrumental Neutron Activation Analysis. *Journal of Forensic Sciences,* 20(1), pp. 119-124.

Rusly, S. et al., 2024. A Green Stabiliser for Nitrate Ester-based Propellants: An overview. *Heliyon,* 10(21), pp. 1-22.

Rusly, S. et al., 2024. Stabiliser Selection and Formulation Strategies for Enhanced Stability of Single Base Nitrocellulose Propellants: A review. *Energetic Materials Frontiers,* 5(1), pp. 52-69.

Saferstein, R., 2015. *Criminalistics: An Introduction to Forensic Science.* Boston (US): Pearson Education Limited.

Saniman, M. et al., 2020. Tensile Characteristics of Low Density Infill Patterns for Mass Reduction of 3D Printed Polylactic Parts. *International Journal of Automotive and Mechanical Engineering,* 17(2), pp. 7927-7934.

Santos, A. et al., 2015. Firing Distance Estimation Based on the Analysis of GSR Distribution on the Target Surface Using ICP-MS- An experimental study with 7.65 mm x 17 mm Browning Pistol (.32 ACP). *Forensic Science International,* Volume 247, pp. 62-68.

Sauzier, G. et al., 2016. Optimisation of Recovery Protocols for Double-Base Smokeless Powder Residues Analysed by Total Vaporisation (TV) SPME/GC-MS. *Talanta,* Volume 158, pp. 368-374.

Schuirmann, D., 1987. A Comparison of the Two One-sided Tests Procedure and the Power Approach for Assessing the Equivalence of Average Bioavailability. *Journal of Pharmacokinetics and Biopharmaceutics,* 15(6), pp. 657-680.

Schwoeble, A. & Exline, D., 2000. *Current Methods in Forensic Gunshot Residue Analysis.* Boca Raton Fl, London UK, New York NY, Washington D.C: s.n.

Schyma, C. et al., 2024. The Muzzle to Target Distance- staining inside different parts of the firearm barrel. *International Journal of Legal Medicine,* Volume 138, pp. 1149-1156.

Serol, M., Ahmad, S., Quintas, A. & Família, C., 2023. Chemical Analysis of Gunpowder and Gunshot Residue. *Molecules,* 28(14), pp. 1-25.

Sheptycki, J. & Edwards, A., 2009. Guns, crime and social order. *Criminology & Criminal Justice,* 9(3), pp. 259-264.

Shrivastava, P., Jain, V. & Nagpal, S., 2021. Gunshot Residue Detection Technologies- a review. *Egyptian Journal of forensic Sciences,* 11(11).

Sig Sauer, 2025. *Sig Sauer Custom Works.* [Online]
Available at: https://www.sigsauer.com/sig-custom-works
[Accessed 30th January 2025].

Sinscow, T., 1997. *Statistics at Square One.* 9th ed. London (UK): BMJ Books.

Sivakumaran, I. & Alankaram, V., 2012. The Wear Characteristics of Heat Treated Manganese Phosphate Coating Applied to AlSi D2 Steel with Oil Lubricant. *Tribology in Industry,* 34(4), pp. 247-254.

Smiths Metal Centres, 2023. *EN8 Technical Datasheet.* [Online]
Available at: https://www.smithmetal.com/pdf/engineering/en8.pdf
[Accessed 7th September 2025].

Smooth-On, Inc., 2019. *Durometer Shore Hardness Scale.* [Online]
Available at: https://www.smooth-on.com/assets/pdf/durometer_chart.pdf
[Accessed 7th September 2025].

Stamouli, A. et al., 2021. Survey of Gunshot Residue Prevalence on the Hands of Individuals from Various Population Groups In and Outside Europe. *Forensic Chemistry,* 23(100308), pp. 1-8.

Sterzik, V. & Bohnert, M., 2016. Reconstruction of Crimes by Infrared Photography. *Internation Journal of Legal Medicine,* Volume 130, pp. 1379-1385.

Stoney, D. & Stoney, P., 2015. Critical Review of Forensic Trace Evidence Analysis and the Need for a New Approach. *Forensic Science International,* Volume 251, pp. 159-170.

Tao, X. & Chen, X., 2025. Create More and More Triboelectric Charges on Polymer Surface. *Fundamental Reasearch,* 5(4), pp. 1683-1687.

Tariq, Q. et al., 2022. Synthesis and Energetic Properties of Trending Metal-Free Potential Green Primary Explosives: A review. *ChemistrySelect,* 7(17), pp. (e202200017) 1-20.

The National Archives, 2026. *Crime and Policing Act 2026.* [Online]
Available at: https://www.legislation.gov.uk/ukpga/2026/20/section/44
[Accessed 2nd August 2026].

Thermo Fisher Scientific Inc., 2025. *Principles of Scanning Electron Microscopy.* [Online]
Available at: https://www.thermofisher.com/uk/en/home/materials-science/learning-center/applications/scanning-electron-microscope-sem-electron-column.html#:~:text=Scanning%20electron%20microscopes%20(SEMs)%20use,lenses%20in%20the%20electron%20column.
[Accessed 28th February 2025].

ThermoFisher Scientific, 2023. *Safety Data Sheet: Aluminium powder*. [Online]
Available at:
https://www.fishersci.co.uk/chemicalProductData_uk/wercs?itemCode=11463503&lang=EN
[Accessed 27th November 2024].

Torre, C., Mattutino, G., Vasino, V. & Robino, C., 2002. Brake Linings: A source of non-gsr particles containing lead, barium, and antimony. *Journal of Forensic Sciences,* 47(3), pp. 494-504.

Tozzo, P. et al., 2022. Touch DNA Sampling Methods: Efficacy Evaluation and Systematic reveiw. *International Journal of Molecular Sciences,* 23(15541), pp. 1-19.

Tri-Tech 3D, 2025. *The FDM Workhorse of Large-Scale 3D Printing*. [Online]
Available at: https://www.tritech3d.co.uk/3d-printers/fortus-900/?utm_source=google&utm_medium=cpc&utm_campaign=&utm_term=fortus%20900mc&utm_content=633771576474&device=c&matchtype=p&adposition=&network=g&placement=&gclid=CjwKCAiA-ty8BhA_EiwAkyoa3_GSF-M-9w8kRzpLZW7AutN
[Accessed 7th February 2025].

Tucker, W. et al., 2017. Gunshot Residue and Brakepads: Compositional and Morphological Considerations for Forensic Casework. *Forensic Science International,* Volume 270, pp. 76-82.

Tyler, G. & Yvon, J., 2003. *ICP-OES, ICP-MS, and AAS Techniques Compared*. [Online]
Available at:
https://www.horiba.com/fileadmin/uploads/Scientific/Downloads/OpticalSchool_CN/TN/ICP/ICP-OES__ICP-MS_and_AAS_Techniques_Compared.pdf
[Accessed 7th January 2025].

Ultimaker, 2022. *Ultimaker PLA Technical Data Sheet*. [Online]
Available at: https://www.plgglobal.co.uk/wp-content/uploads/2022/07/Ultimaker-PLA-TDS-v5.00.pdf
[Accessed 7th September 2025].

United Nations General Assembly, 2014. *Recent developments in small arms and light weapons manufacturing, technology and design and implications for the implementation of the Internation Instrument to Enable States to Identify and Trace, in a Timely and Reliable Manner, Illicit Small Arms ands,* New York: s.n.

Urbanski, T., 1964. *Chemistry and Technology of Explosives*. 1 ed. Oxford (GB): Pergamon Press.

Van Oorschot, R., Glavich, G. & Mitchell, R., 2014. Persistence of DNA Deposited by the Original User on Objects After Subsequent Use by a Second Person. *Forensic Science International: Genetics,* 8(1), pp. 219-225.

Vanini, G. et al., 2015. Multivariate Optimisation of ICP OES Instrumental Parameters for Pb/Ba/Sb Measurement in Gunshot Residues. *Microchemical Journal,* Volume 120, pp. 58-63.

Vanini, G. et al., 2014. Analysis of Gunshot Residues Produced by .38 Caliber Handguns Using Inductively Coupled Plasma- Optical Emission Spectroscopy (ICP-OES). *Microchemical Journal,* Volume 115, pp. 106-112.

Vermeij, E., Duvalois, W., Webb, R. & Koeberg, M., 2009. Morphology and Composition of Pyrotechnic Residues Formed at Different Levels of Confinement. *Forensic Science International,* Volume 186, pp. 68-74.

Vernon-Parry, K., 2000. Scanning Electron Microscopy: An introduction. *III-Vs Review,* 13(4), pp. 40-44.

Vogelsanger, V. et al., 2011. *Ballistic Shelf Life of Propellants for Medium and Small Calibre Ammunition-Influence of Deterrent Diffusion and Nitrocellulose Degradation.* Interlaken (CH), International Ballistics Society.

Wallace, J., 2018. *Chemical Analysis of Firearms, Ammunition, and Gunshot Residue.* 2nd ed. Boca Raton (US): CRC Press.

Welch, B., 1938. The Significance of the Difference Between Two Means when the Population Variances are Unequal. *Biometrika,* 29(3-4), pp. 350-362.

Werner, D., Berthod, R., Rhumorbarbe, D. & Gallusser, A., 2021. Manufacturing of Firearms Parts: Relevant sources of information and contribution in a forensic context. *WIREs Forensic Science,* 3(3), pp. 1-23.

West, E. & Meterko, V., 2015-16. Innocence Project: DNA Exonerations, 1989-2014: A Review of Data and Findings from the First 25 Years. *Albany Law Review,* 79(3), pp. 717- 795.

Wong, D., 2015. Section IX- Additive Manufacturing and Surface Technology- Additive Manufacturing-Rapid Prototyping, Tooling & Manufacturing. In: A. Nee, ed. *Handbook of Manufacturing Engineering and Technology.* London (GB), Heidelberg (DE), New York (US), Dordrecht (NL): Springer, pp. 2469-2585.

Yolhamid, M. et al., 2018. The Novel Usage of Nitrocellulose as a Propellant of 5.56mm Bullet. *Solid State Phenomena,* Volume 280, pp. 361-367.

Yoon, Y., Yon, M., Jung, S. & Gupta, S., 2019. *Development of Three-Nozzle Extrusion System for Conformal Multi-Resolution 3D Printing with a Robotic Manipulator.* Anaheim (US), ASME.

Yüksel, B. et al., 2016. GFAAS Determination of Antimony, Barium, and Lead Levels in Gunshot Residue Swabs: An Application in Forensic Chemistry. *Atomic Spectroscopy,* 37(4), pp. 164-169.

Zeichner, A. & Eldar, B., 2004. A Novel Method for Extraction and Analysis of Gunpowder Residues on Double-Side Adhesive Coated Stubs. *Journal of Forensic Sciences,* 49(6), pp. 1-13.

Zeichner, A. & Levin, N., 1993. Collection and Efficiency of Gunshot Residue (GSR) Particles from Hair and Hands Using Double-Side Adhesive Tape. *Journal of Forensic Sciences,* 38(3), pp. 571-584.

Zeichner, A., Levin, N. & Dvorachek, M., 1992. Gunshot Residue Particles Formed by using Ammunitions that have Mercury Fulminare Based Primers. *Journal of Forensic Science,* 37(6), pp. 1567-1573.

Zhou, W., Apkarian, R., Wang, Z. & Joy, D., 2007. Fundamentals of Scanning Electron Microscopy. In: W. Zhou & Z. Wang, eds. *Scanning Microscopy for Nanotechnology.* New York (US): Springer, pp. 1-40.

Zhu, S., Akehurst, S., Lewis, A. & Yuan, H., 2022. A Review of the Pre-Chamber Ignition System Applied on Future Low-Carbon Spark Ignition Engines. *Renewable and Sustainable Energy Reviews,* 154(111872), pp. 1-25.

Appendix 1: Data- Particle Size: Baseline

Metallic Baseline:

Range (µm)	M1a	M2a	M3a
<0	0	0	0
0-0.25	0	0	0
0.25-0.5	0	37	79
0.5-0.75	0	12	22
0.75-1	0	10	14
1-1.25	4	3	10
1.25-1.5	0	5	5
1.5-1.75	0	1	8
1.75-2	0	3	7
2-2.25	0	1	9
2.25-2.5	0	2	8
2.5-2.75	0	2	9
2.75-3	0	2	3
3-3.25	0	0	6
3.25-3.5	0	1	10
3.5-3.75	0	0	0
3.75-4	0	2	8
4-4.25	1	0	4
4.25-4.5	1	1	4
4.5-4.75	0	0	5
4.75-5	0	0	6
>5	1	34	161

Range (µm)	M1b	M2b	M3b
<0	0	0	0
0-0.25	0	0	0
0.25-0.5	0	39	365
0.5-0.75	0	13	57
0.75-1	0	6	45
1-1.25	5	2	25
1.25-1.5	0	1	13
1.5-1.75	0	2	14
1.75-2	0	3	8
2-2.25	4	2	11
2.25-2.5	0	2	5
2.5-2.75	0	1	11
2.75-3	0	1	3
3-3.25	1	0	10
3.25-3.5	0	2	7
3.5-3.75	0	0	0
3.75-4	0	0	11
4-4.25	0	0	1
4.25-4.5	0	0	2
4.5-4.75	0	0	4
4.75-5	2	0	3
>5	1	16	214

Polymer Baseline:

Range (µm)	P1a	P2a	P3a	P4a	P5a	P6a
<0	0	0	0	0	0	0
0-0.25	0	0	0	0	0	0
0.25-0.5	288	160	3502	349	993	0
0.5-0.75	336	159	3377	190	767	0
0.75-1	295	120	995	78	473	0
1-1.25	504	177	758	53	426	333
1.25-1.5	293	97	396	25	231	0
1.5-1.75	341	111	312	18	198	0
1.75-2	315	82	192	10	185	0
2-2.25	297	77	150	7	128	147
2.25-2.5	307	70	120	4	99	0
2.5-2.75	258	64	93	7	70	0
2.75-3	207	46	88	7	55	0
3-3.25	220	41	62	0	56	46
3.25-3.5	243	46	46	1	53	0
3.5-3.75	0	0	0	0	0	0
3.75-4	221	29	51	2	47	0
4-4.25	166	30	45	2	25	0
4.25-4.5	180	21	46	2	34	31
4.5-4.75	148	18	38	1	25	0
4.75-5	132	26	34	0	34	0
>5	3271	529	522	10	410	58

Range (µm)	P1b	P2b	P3b	P4b	P5b	P6b
<0	0	0	0	0	0	0
0-0.25	0	0	0	0	0	0
0.25-0.5	287	110	1849	346	678	0
0.5-0.75	297	127	1547	279	486	0
0.75-1	273	106	597	105	286	0
1-1.25	369	154	559	96	318	493
1.25-1.5	226	75	375	47	214	0
1.5-1.75	241	114	336	28	163	0
1.75-2	246	94	183	19	145	0
2-2.25	236	101	173	10	127	313
2.25-2.5	235	76	147	12	105	0
2.5-2.75	185	70	100	9	83	0
2.75-3	147	60	96	2	65	0
3-3.25	144	52	79	4	62	101
3.25-3.5	143	63	65	6	59	0
3.5-3.75	0	0	0	0	0	0
3.75-4	131	74	66	7	56	0
4-4.25	127	54	56	4	31	0
4.25-4.5	122	44	49	0	38	57
4.5-4.75	111	41	55	4	39	0
4.75-5	108	40	46	3	31	0
>5	2794	909	905	39	548	153

Appendix 2: Data- Particle Size: Experimental

Metallic:

Range (µm)	M1a	M3a	M4a	M5a	M6a	Average	Standard Deviation
0-0.25	0	0	0	0	0	0	0
0.25-0.5	1967	119	10	12	561	533.8	832.6918398
0.5-0.75	662	60	10	18	288	207.6	278.2639035
0.75-1	222	47	10	28	80	77.4	84.88698369
1-1.25	187	28	13	39	77	68.8	70.18689336
1.25-1.5	82	16	10	35	49	38.4	28.8669361
1.5-1.75	44	12	15	31	20	24.4	13.12630946
1.75-2	45	3	18	22	18	21.2	15.15585695
2-2.25	20	3	3	13	13	10.4	7.334848328
2.25-2.5	15	6	8	18	8	11	5.196152423
2.5-2.75	15	7	6	11	9	9.6	3.577708764
2.75-3	6	4	11	6	6	6.6	2.607680962
3-3.25	14	5	3	5	12	7.8	4.868264578
3.25-3.5	5	1	3	7	9	5	3.16227766
3.5-3.75	0	0	0	0	0	0	0
3.75-4	9	3	2	5	8	5.4	3.049590136
4-4.25	2	0	1	3	6	2.4	2.302172887
4.25-4.5	5	1	1	8	7	4.4	3.286335345
4.5-4.75	5	0	4	2	2	2.6	1.949358869
4.75-5	3	0	1	3	3	2	1.414213562

Range (µm)	M1b	M3b	M4b	M5b	M6b	Average	Standard deviation
0-0.25	0	0	0	0	0	0	0
0.25-0.5	139	6	1	2	96	48.8	64.55772611
0.5-0.75	58	0	1	1	38	19.6	26.87563953
0.75-1	27	0	0	0	17	8.8	12.55786606
1-1.25	18	2	0	0	17	7.4	9.262828942
1.25-1.5	15	0	1	0	7	4.6	6.503845017
1.5-1.75	9	0	0	3	5	3.4	3.78153408
1.75-2	11	0	0	0	4	3	4.795831523
2-2.25	1	0	0	1	3	1	1.224744871
2.25-2.5	6	0	1	0	0	1.4	2.607680962
2.5-2.75	1	0	1	0	1	0.6	0.547722558
2.75-3	2	0	0	1	4	1.4	1.673320053
3-3.25	5	0	0	0	0	1	2.236067977
3.25-3.5	0	0	0	0	1	0.2	0.447213595
3.5-3.75	0	0	0	0	0	0	0
3.75-4	1	1	0	0	3	1	1.224744871
4-4.25	0	0	0	1	1	0.4	0.547722558

4.25-4.5	2	0	0	0	1	0.6	0.894427191
4.5-4.75	0	0	0	0	0	0	0
4.75-5	0	1	0	0	0	0.2	0.447213595
>5	8	0	1	3	15	5.4	6.188699379

Polymer:

Range (µm)	P1a	P2a	P3a	P4a	P5a	P6a	P7a	P8a	average	Standard Deviation
0-0.25	0	0	0	0	0	0	0	0	0	0
0.25-0.5	31	65	270	0	30	11	30	91	66	87.37439965
0.5-0.75	40	114	366	0	39	6	52	162	97.375	121.4212708
0.75-1	33	79	259	0	41	7	56	137	76.5	85.54697957
1-1.25	78	93	337	454	78	10	143	282	184.375	155.2057966
1.25-1.5	51	82	251	326	53	11	108	203	135.625	111.6447651
1.5-1.75	61	68	212	320	53	26	96	189	128.125	101.968395
1.75-2	42	46	154	301	32	17	95	133	102.5	94.24436323
2-2.25	28	43	128	266	36	24	65	102	86.5	81.43007517
2.25-2.5	27	32	100	225	35	17	56	67	69.875	68.0932921
2.5-2.75	35	18	82	166	18	14	42	92	58.375	52.53009342
2.75-3	12	22	50	142	24	14	32	58	44.25	42.74091382
3-3.25	23	17	50	133	25	8	27	53	42	39.86047093
3.25-3.5	29	16	43	119	20	9	34	41	38.875	34.50646937
3.5-3.75	0	0	0	0	0	0	0	0	0	0
3.75-4	14	21	43	100	14	10	20	42	33	29.84244341
4-4.25	21	11	31	85	14	8	17	28	26.875	24.79307219
4.25-4.5	22	10	36	76	10	5	24	24	25.875	22.60491413
4.5-4.75	21	12	20	69	7	4	17	19	21.125	20.32196208
4.75-5	15	10	24	64	6	5	14	22	20	19.04130848
>5	416	118	378	911	178	112	153	342	326	265.7006909

Range (µm)	P1b	P2b	P3b	P4b	P5b	P6b	P7b	P8b	average	Standard Deviation
0-0.25	0	0	0	0	0	0	0	0	0	0
0.25-0.5	6	6	13	0	34	5	16	346	53.25	118.7491353
0.5-0.75	9	21	11	0	47	4	48	279	52.375	93.40225984
0.75-1	12	31	10	0	33	9	35	105	29.375	33.21332564
1-1.25	16	31	10	483	48	14	73	96	96.375	159.1701134
1.25-1.5	12	36	2	351	45	13	53	47	69.875	115.1377281
1.5-1.75	14	27	6	293	30	15	49	28	57.75	95.94604138
1.75-2	14	18	5	222	30	14	23	19	43.125	72.64087299
2-2.25	8	23	7	176	22	12	18	10	34.5	57.50527926
2.25-2.5	5	16	3	164	19	8	12	12	29.875	54.45689645
2.5-2.75	4	15	5	108	12	11	7	9	21.375	35.19308982
2.75-3	1	15	1	95	7	9	5	2	16.875	31.9214997
3-3.25	8	11	8	81	9	4	2	4	15.875	26.48685658
3.25-3.5	1	7	2	68	9	4	9	6	13.25	22.32071427
3.5-3.75	0	0	0	0	0	0	0	0	0	0
3.75-4	3	9	3	67	3	4	4	7	12.5	22.12948905

4-4.25	3	4	0	49	5	1	1	4	8.375	16.50919657
4.25-4.5	4	8	1	46	8	1	2	0	8.75	15.36926432
4.5-4.75	4	8	0	53	3	0	2	4	9.25	17.8625706
4.75-5	3	7	3	32	4	1	1	3	6.75	10.37510757
>5	50	59	28	684	44	27	39	39	121.25	227.6323791

Appendix 3: Data- Particle Chemistry: Baseline

Metallic:

Chemistry	M1a	M2a	M3a
Ba	0	0	0
Ba Al	0	3	194
Ba Sb	0	2	0
Ba Si Ca	0	0	1
Cu Zn	0	1	1
Pb	12	107	140
Pb Ba	0	0	3
Pb Sb	0	0	4
Sb	0	0	0
Sb Ba Pb	0	2	34
Sr	0	0	0

Chemistry	M1b	M2b	M3b
Ba	0	0	0
Ba Al	1	6	106
Ba Sb	0	0	0
Ba Si Ca	0	1	1
Cu Zn	1	0	0
Pb	1	81	678
Pb Ba	1	0	0
Pb Sb	1	0	3
Sb	1	0	0
Sb Ba Pb	0	1	20
Sr	0	0	0

Polymer:

Chemistry	P1a	P2a	P3a	P4a	P5a	P6a
Ba	**5**	**2**	**37**	**2**	**6**	**0**
Ba Al	**2497**	**511**	**1672**	**169**	**1090**	**277**
Ba Sb	**67**	**15**	**197**	**8**	**44**	**7**
Ba Si Ca	**556**	**51**	**21**	**4**	**35**	**0**
Cu Zn	**114**	**77**	**26**	**3**	**30**	**0**
Pb	**83**	**47**	**895**	**11**	**264**	**13**
Pb Ba	**113**	**31**	**399**	**3**	**126**	**12**
Pb Sb	**620**	**264**	**3738**	**292**	**1021**	**150**
Sb	**45**	**14**	**293**	**10**	**15**	**2**
Sb Ba Pb	**3912**	**889**	**3547**	**263**	**1677**	**154**
Sr	**0**	**0**	**0**	**0**	**0**	**0**
Sb Ba Pb Sn	**5**	**1**	**0**	**0**	**0**	**0**
Ti Zn Cu	**4**	**0**	**1**	**0**	**0**	**0**

Chemistry	P1b	P2b	P3b	P4b	P5b	P6b
Ba	4	**2**	**20**	**1**	**0**	**1**
Ba Al	2205	**948**	**1921**	**205**	**1061**	**586**
Ba Sb	51	**22**	**105**	**10**	**29**	**9**
Ba Si Ca	431	**89**	**28**	**0**	**26**	**4**
Cu Zn	96	**44**	**22**	**1**	**15**	**0**
Pb	75	**46**	**325**	**22**	**251**	**32**
Pb Ba	96	**38**	**220**	**11**	**124**	**24**
Pb Sb	510	**169**	**2452**	**436**	**767**	**233**
Sb	42	**12**	**109**	**7**	**15**	**7**
Sb Ba Pb	2910	**992**	**2080**	**326**	**1245**	**221**
Sr	1	**1**	**0**	**0**	**0**	**0**
Sb Ba Pb Sn	6421	**2363**	**7282**	**1019**	**3533**	**0**
Ti Zn Cu	0	**0**	**0**	**0**	**0**	**0**

Appendix 4: Data- Particle Chemistry: Experimental

Metallic:

Chemistry	1a	3a	4a	5a	6a
Ba	6	0	0	0	4
Ba Al	252	51	98	129	216
Ba Sb	38	3	1	2	21
Ba Si Ca	7	1	0	1	0
Cu Zn	10	5	0	1	6
Pb	809	140	20	50	162
Pb Ba	251	15	8	12	8
Pb Sb	1256	70	33	57	639
Sb	39	1	7	4	79
Sb Ba Pb	706	47	13	42	109
Sr	0	0	0	0	0

Chemistry	1b	3b	4b	5b	6b
Ba	0	0	0	0	0
Ba Al	2	0	1	0	13
Ba Sb	2	0	0	0	6
Ba Si Ca	0	0	0	0	0
Cu Zn	1	0	0	0	0
Pb	155	4	3	4	107
Pb Ba	60	5	1	6	9
Pb Sb	53	0	0	0	44
Sb	0	0	0	0	18
Sb Ba Pb	29	0	0	1	14
Sr	0	0	0	0	1

Polymer:

Chemistry	1a	2a	3a	4a	5a	6a	7a	8a
Ba	1	8	5	5	2	0	5	8
Ba Al	653	138	483	799	306	130	324	895
Ba Sb	13	19	26	26	11	11	12	34
Ba Si Ca	1	0	3	5	1	0	4	1
Cu Zn	19	3	23	88	18	19	37	25
Pb	63	354	485	534	102	11	82	61
Pb Ba	17	77	247	217	36	9	32	23
Pb Sb	124	182	783	1040	159	55	374	688
Sb	64	62	105	34	26	1	53	80
Sb Ba Pb	43	33	673	1008	51	81	157	271

Chemistry	1b	2b	3b	4b	5b	6b	7b	8b
Ba	0	1	0	3	1	2	2	1
Ba Al	103	135	35	1093	56	37	70	205
Ba Sb	3	3	2	27	8	3	5	10
Ba Si Ca	0	0	1	8	0	0	1	0

Cu Zn	4	6	0	123	5	7	17	1
Pb	16	102	13	496	63	17	50	22
Pb Ba	5	10	7	235	40	7	9	11
Pb Sb	19	73	14	524	79	43	156	436
Sb	19	11	2	31	12	7	41	7
Sb Ba Pb	7	10	43	431	147	32	47	326